BIDIRECTIONAL CIRCULAR RING ANTENNA USING TWO PROBES FOR POLARIZATION DIVERSITY

PANISA KEOWSAWAT

A THESIS SUBMITTED IN PARTIAL FULFILLMENT
OF THE REQUIREMENT FOR THE DEGREE OF
DOCTOR OF ENGINEERING IN ELECTRICAL ENGINEERING
FACULTY OF ENGINEERING
KING MONGKUT'S INSTITUTE OF TECHNOLOGY LADKRABANG
2009

KMITL 2009-EN-D-018-121

หัวข้อวิทยานิพนธ์	สายอากาศวงแหวนวงกลมแพร่กระจายคลื่นสองทิศทางที่ใช้โพรบสองโพรบสำหรับไดเวอร์ซิตีเชิงการโพลาไรซ์
นักศึกษา	นางสาวปาณิศา แก้วสวัสดิ์
รหัสนักศึกษา	45160310
ปริญญา	วิศวกรรมศาสตรดุษฎีบัณฑิต
สาขาวิชา	วิศวกรรมไฟฟ้า
พ.ศ.	2552
อาจารย์ที่ปรึกษาวิทยานิพนธ์	ศ.ดร.โมไนย ไกรฤกษ์
อาจารย์ที่ปรึกษาวิทยานิพนธ์ร่วม	ศ.ดร.จุนอิชิ ทาคาดะ

บทคัดย่อ

วิทยานิพนธ์นี้นำเสนอสายอากาศสองโพรบที่กระตุ้นวงแหวนวงกลมสำหรับระบบหลายอินพุตหลายเอาต์พุต สายอากาศถูกวิเคราะห์โดยใช้วิธีการเหนี่ยวนำของสนามแม่เหล็กไฟฟ้า โดยมีขั้นตอนในการออกแบบ คือ ขั้นแรก เลือกรัศมีที่เหมาะสมของวงแหวนจากการออกแบบสายอากาศโพรบเดี่ยว จากนั้น พิจารณาเลือกความยาวโพรบและความยาวของวงแหวนที่เหมาะสม จากสายอากาศแบบสองโพรบ ซึ่งขนาดของสายอากาศที่เหมาะสมคือ รัศมีวงแหวนเป็น 0.3 เท่าของความยาวคลื่น ความยาววงแหวนเป็น 0.3 เท่าของความยาวคลื่น และความยาวโพรบเป็น 0.25 เท่าของความยาวคลื่น นอกจากนี้ได้ปรับปรุงค่าการแยกระหว่างโพรบทั้งสองโดยวิธีปรับเลื่อนตำแหน่งของโพรบและด้วยวิธีใส่ขดลวดระหว่างโพรบทั้งสอง จากการศึกษาพบว่า สายอากาศสองโพรบที่มีขดลวดระหว่างโพรบทั้งสองมีคุณสมบัติดีกว่าสายอากาศแบบสองโพรบที่มีการเลื่อนตำแหน่งโพรบ จากนั้น ได้สร้างสายอากาศต้นแบบสำหรับใช้งานที่ความถี่ 5.2 กิกะเฮิรตซ์ แล้วนำไปวัดและเปรียบเทียบผลที่ได้กับผลการคำนวณทางทฤษฎี ซึ่งพบว่า ผลทั้งสองมีความสอดคล้องกัน ผลการวัดได้แสดงค่าการแยกของสายอากาศมีค่ามากกว่า 20 dB ในขณะที่ค่าการสูญเสียย้อนกลับของแรงดันมีค่าน้อยกว่า 2:1 ตลอดย่านความถี่ของเครือข่ายท้องถิ่นไร้สาย 5 กิกะเฮิรตซ์ สายอากาศมีแบบรูปการแพร่กระจายคลื่นแบบสองทิศทางด้วยค่าอัตราขยาย 4 dBi ในทิศทางที่ต้องการ คุณสมบัติหลายอินพุตหลายเอาต์พุตของสายอากาศที่นำเสนอได้ศึกษาในสภาพแวดล้อมบริเวณช่องทางเดินภายในอาคารด้วยวิธีการที่แตกต่างกันสองวิธี วิธีแรกเป็นวิธีที่สายอากาศที่นำเสนอถูกใช้เป็นสายอากาศทดสอบในระบบหลายอินพุตหลายเอาต์พุตโดยตรง ส่วนวิธีที่สองช่องสัญญาณในระบบหลายอินพุตหลายเอาต์พุตของสายอากาศถูกสร้างขึ้นใหม่จากพารามิเตอร์ของช่องสัญญาณจากการวัดแบบสองทิศทางโดยวิธีการกำหนดเฟสแบบสุ่ม ซึ่งผลการวัดที่ได้จากทั้งสองวิธีดังกล่าว แสดงให้เห็นว่าสายอากาศที่นำเสนอให้ความจุของช่องสัญญาณมากกว่าสายอากาศไดโพลแบบเดิมที่มีการโพลาไรซ์เป็นแบบแนวตั้งและวางห่างกันตามแนวนอนด้วยระยะ 1 เท่าของความยาวคลื่น นอกจากนี้ การปรับปรุงค่าการแยกของสายอากาศที่นำเสนอ มีผลให้ค่าความจุของช่องสัญญาณที่ได้จากการใช้สายอากาศนี้มีค่าเพิ่มขึ้นด้วย

Thesis	Bidirectional Circular Ring Antenna Using Two Probes for Polarization Diversity
Student	Ms. Panisa Keowsawat
Student ID.	45160310
Degree	Doctor of Engineering
Program	Electrical Engineering
Year	2009
Thesis Advisor	Prof. Dr. Monai Krairiksh
Thesis Co-advisor	Prof. Dr. Jun-ichi Takada

ABSTRACT

This thesis presents a two-probe excited circular ring antenna for the Multiple-Input Multiple-Output (MIMO) systems. The antenna was analyzed by using the induced emf method. First, an appropriate radius of the ring was chosen from a single probe antenna. Then, the appropriate probe length and ring length were considered from the two-probe antenna. The appropriate antenna parameters are a ring radius of 0.3λ, ring length of 0.3λ and probe length of 0.25λ. Moreover, the isolation between the two probes was improved by offsetting the position of two probes and by insertion of an inductor coil between the probes. From the study, the two-probe antenna with an inductor coil provides better performance than the two-probe offsetting antenna. The prototype antenna at the frequency of 5.2 GHz was fabricated and measured to compare with theoretical calculations which resulted in the same trend. Measurements illustrated that the isolation achieved was in excess of 20 dB while the VSWR was less than 2:1 over the 5 GHz indoor wireless local area network (WLAN). The bi-directional radiation pattern was achieved with 4 dBi gain in the desired direction. The MIMO performance of the proposed antenna was studied in the corridor environment by two different methods. The first method was the field test measurement in which the proposed antennas were used as the antennas under test in the MIMO systems. Second, the MIMO channels of the proposed antennas were reconstructed from the channel parameters from the double directional channel measurement by using the random phase method. The results from both methods show that the proposed antenna provides higher mutual information than the use of the 1λ horizontally spaced vertically polarized dipole array antennas. Moreover, the isolation improvement can increase the mutual information of the channel by using this proposed antenna.

ACKNOWLEDGEMENTS

This Thesis could not be completed without the invaluable help from many persons to whom I would like to express my appreciation.

First, I would like to give my grateful thank to my advisor, Professor Dr. Monai Krairiksh, for his helpful suggestions, advice and support during my study. I would like to give my appreciate to Professor Dr. Jun-ichi Takada of Tokyo Institute of Technology, Japan for his suggestions to my research and his support through National Information and Communications Technology (NICT) for my short-term research student in his laboratory. I would like to also thank Associated Professor Dr. Sompol Kosulvit and Assistant Professor Dr. Chuwong Phongcharoenpanich for their helpful discussions.

I would like to thank all of my colleagues in Wireless Communication Laboratory for their friendship and helpful. Moreover, I would like to thank members of Takada's Laboratory for their help in my measurement in Japan.

I would like to acknowledge the Thailand Research Fund (TRF) which provided financial assistance to the undertaken project through the Royal Golden Jubilee Ph.D. Program (Grant No. PHD/0067/2546).

Finally, I would like to express my appreciation to my parents for their patience, support and invaluable encouragement throughout the long period of my study.

Panisa Keowsawat

TABLE OF CONTENTS

TABLE OF CONTENTS (continued)

TABLE OF CONTENTS (continued)

LIST OF TABLES

LIST OF FIGURES

LIST OF FIGURES (continued)

CHAPTER 1

INTRODUCTION

1.1 Introduction

The multiple antennas at transmitting and receiving sides have been used for a long time in the wireless communication. It was extended from the use of the single pair antennas between the transmitter and receiver in the traditional communication or Single-Input Single-Output (SISO) system. The purpose of using multiple antennas is for increasing the quality of the communication. In 1980s, the multiple antennas at the receiver were used for the received diversity system or Single-Input Multiple-Output (SIMO) to mitigate the fading signal and hence improve the communication quality [1], [2]. With this approach, the communication quality can be increased since the receiver can always receive the signal. The simplest idea is that when the received signal from one antenna is very low, such as lower than the threshold, the switch will select to receive the signal from another antenna. Then, the communication can still be continued. It can also be said that the communication interval is increased by this receive diversity. There are many types of the diversity system, such as frequency diversity, temporal diversity, spatial diversity and antenna diversity. One of the most well-known diversity systems is the spatial diversity that uses the identical antenna placed at the different positions to receive the uncorrelated signal. In case of the antenna diversity, the different antennas are used instead to receive the uncorrelated signal. These different antennas use the different antenna characteristics for the diversity system, such as polarization diversity and pattern diversity. The advantage of the antenna diversity is its compact size since the different antenna characteristics can be packed together in one structure. For antenna diversity case, the extra space between the antennas is not necessary. However, in the cellular system, the use of the diversity at the mobile phones is not popular since it is more expensive, more power consumption and more complexity. Hence, the receive diversity is usually used in the uplink at the base station. Since the multiple antennas are already used at the base station, the motivation of using these multiple antennas for transmitting diversity or Multiple-Input Single-Output (MISO) system is motivated [3]. Additionally, because of the growth of the signal coding, the transmit diversity becomes popular and it motivates the use of the Multiple-Input Multiple-Output antennas in the communication

system. The difference between the receive diversity system and the MIMO system is that the same signals are transmitted and received in the diversity system, whereas the different signals or independent data are used in the MIMO systems. Consequently, in the diversity system case, the throughput (output in bits/s) is not increased.

The growing demand for wireless communication makes it important to determine the capacity limits of the underlying channels for these systems. These capacity limits dictate the maximum data rates that can be transmitted over wireless channel with small error probability. The mathematical theory of communication underlying channel capacity was proposed by Claude Shannon in the late 1940s [4]. This theory is based on the notion of mutual information between the input and output of a channel. In particular, Shannon defined channel capacity as the channel's mutual information maximized over all possible input distribution.

The most powerful usage of MIMO is the transmission of several parallel data streams to increase the capacity of the system, called spatial multiplexing. In this case, the different data streams are transmitted in parallel from the different transmit antennas and the multiple receive antenna elements are used for separating the different data streams at the receiver. The advantage of this method is that the data rate can be increased without requiring more spectra [5]–[7] which is highly beneficial for large data transmission such as multimedia data. The early reports of the MIMO system in [4]–[7] motivate many researches in the MIMO systems. Nowadays, the concept of MIMO radio channel is an interesting topic in communication research. MIMO is being considered for the third-generation cellular systems (W-CDMA), IEEE 802.16a (WMAN) and IEEE 802.11n of wireless local area networks (WLAN).

As mentioned above, parallel subchannels can be achieved from the spatially separated antenna elements of the arrays. It was found that by increasing the number of mobile antenna elements and the spacing between them, the capacity of such a system for a large angular-spread environment was increased [8]. Nevertheless, this large antenna spacing increases both size and cost of the equipment in the systems. In an environment of limited space, the MIMO system can be accomplished by utilizing the independence of the propagation paths of the two different polarizations [9]. In this case, the use of dual-polarized antennas for polarization diversity is suggested wherein two orthogonal polarizations can be provided in the same structure. Polarization diversity has been recommended as an attractive solution for obtaining parallel channels in MIMO systems [9]–[11]. The report of capacity increasing of around 10–20% from using polarization

diversity over single-polarization with spatially-separated elements is found in [12]. In addition, the combination of polarization diversity with spatial diversity or pattern diversity can enhance the decorrelation between communication links. Waldschmidt *et al.* [13] presented an extremely broadband, spiral and sinuous antenna by using the combination of pattern and polarization diversity. They also show that a system based on the combination of polarization and spatial diversity is best-suited for the situation where a trade-off between space and capacity has to be made. Getu and Andersen [14] proposed a compact MIMO cube antenna for indoor environment with wide angular spread. This antenna is made from 12 electric dipole antennas at the edges of a cube and uses space and polarization diversity techniques. Furthermore, Dong *et al.* [15] studied a trimonopole antenna structure with polarization diversity. This kind of antenna offers channel capacity that approaches the capacity of an uncorrelated MIMO Rayleigh channel. Moreover, it was shown that the increase in channel capacity is due mainly to polarization diversity, not pattern diversity.

In general, the MIMO antenna performance should be considered in the real MIMO environment. The performance of the MIMO systems that use different antennas can be measured in the real practical environment. The multiple orthogonal parallel transmission links maybe found using the singular value decomposition (SVD) of the MIMO channel matrix [7], [16]. However, if there are many investigated antennas, the assessing performance of the MIMO system by using generalized channel (channel without the effect of the transmitting and receiving antennas) are preferable since it can reduce the hard effort in the measurements. To assess the performance of MIMO systems in real propagation channel, accurate characteristics of the channel are required. There are a lot of attempts to simulate the behavior of the channel. The first method is based on the electromagnetic approach by computer modeling with the ray optical model [17], [18]. The second one is the statistical model that explains the statistic of the scatterers in the channel [19], [20]. However, since the complexity of reflection, scattering, diffraction etc., in real propagation environments can never be completely modeled by electromagnetic simulation in the first method and because of the simplicity of the statistical approaches in the second one, both models have to be verified by propagation measurements. The other approach is proposed that is the double directional channel measurement which the properties of the propagation channel are independent with the measurement antennas [21]. The double directional channel measurement can be deduced by using channel sounder [22] which is the measuring equipment to observe the time-varying multipath channel impulse response

(CIR). By using the double directional measurement, the parameters of the multipath can be found. These parameters in the path model are DoA (Direction of Arrival) at the receiver array, DoD (Direction of Departure) at the transmitter array, TDoA (Time Delay of Arrival), Doppler shift, and the complex polarimetric path weight matrix. These parameters can be estimated by using parametric estimation algorithms. Finally, the complete channel model can be regenerated by these extracted parameters, such as DoA, DoD, TDoA and polarimetric path weight matrix.

In addition to the MIMO performance, the antennas for the MIMO system should be designed to provide an appropriate radiation pattern and electrical characteristics. In general, an antenna for wireless communication may be intended either for directional or omnidirectional patterns [23], [24]. Recently, Kosulvit [25] has proposed a bidirectional antenna with a probe excited circular ring that is suitable for a long and narrow environment like a corridor or a tunnel. That antenna had a simple design and configuration. The electrical characteristics such as return loss and isolation are important for the antenna design. Some researchers reported the influence of mutual coupling on MIMO system which led ultimately to poor performance. For example, in [26], Waldschmidt analyzed the impact of mutual coupling on the capacity of an MIMO system with compact antenna array. It is also stated in [6] that the increase in mutual coupling associated with reduced antenna spacing causes problems for achieving high capacity. It appears in [27] that the capacity result of the antenna system degrades at close antenna separation in case of wideband systems. It implies that isolation of the MIMO antenna should be maximized to obtain high capacity performance. For a compact antenna structure, isolations of higher than 20 dB between two antenna elements are acceptable [23], [28].

1.2 Purpose and the Scope of the Thesis

In this thesis, a modified bidirectional circular ring antenna equipped with two-probe excited ring is proposed for the 5 GHz WLAN (5.15-5.25 GHz) of IEEE 802.11n indoor communication. This bidirectional antenna is suitable for using in a longitudinal area, such as in the corridor. The proposed antenna is based on the circular ring antenna that is excited by a single probe in [25]. The attractive properties of the antenna in [25] are simple structure with the bidirectional radiation pattern and ease of fabrication. It also has moderate directivity (7 dBi at 1.9 GHz) and wide impedance bandwidth. The antenna

configuration and antenna design are shown in Chapter 2. To gain insight into the antenna parameters, the induced emf method is used in the analysis of the design and in the development of the real antenna, and an equivalent circuit is used to determine the impedance characteristics of the antenna. The fields at the aperture were derived from the fields inside the ring by using Green function. The process of antenna design was as follows: first, the parameters of a single probe antenna were chosen to obtain a suitable ring radius. Then, the parameters of a two-probe antenna that yield suitable probe length and ring length were determined. The design that yielded suitable antenna parameters with maximum isolation and accepted return loss was identified. In Chapter 3, the improvement of the isolation between the two probes of the antenna is illustrated. The isolation is enhanced by offsetting the position of the two probes and by insertion of an inductor coil between them. Finally, a prototype antenna designed to operate at the center frequency of 5.2 GHz was fabricated and tested. In Chapter 4, the MIMO Theory and the mutual information calculation based on the SVD approach are shown. In this thesis, the MIMO performance of the proposed antenna is evaluated with two methods. The first method is the direct measurement of channel matrix in practical corridor environment and the second one is by using the result of double directional channel measurement in the corridor. The direct MIMO performance measurements of the proposed antennas are also described in Chapter 4 whereas the double directional channel measurement is described in Chapter 5. In Chapter 5, the multipath parameters including polarimetric path weight matrix, DoD at the transmitting site, DoA at the receiving site, and path delay are extracted from the sounding measurement data by using the high resolution program (RIMAX) [29]. Depolarization of signal was studied in terms of cross polarization power ratio (*XPR*) [30], [31]. Angular power spectrum and angular spread of incoming signal in a corridor environment were also investigated. The extracted parameters of the discrete multipaths were calculated with the random phase and the radiation pattern of investigated antenna to create the complete propagation channel. The different channel matrices with the different antennas were investigated. Here, the MIMO performance of the proposed bidirectional dual-polarized antenna and the 1λ horizontally spaced vertically polarized dipole array antennas (dipole array antennas) were compared in both Chapter 4 and 5. Finally, the conclusion and discussion were drawn in Chapter 6.

CHAPTER 2

A TWO-PROBE EXCITED CIRCULAR RING ANTENNA

2.1 Introduction

In this chapter, a structure of the proposed two-probe excited circular ring antenna is described. The analysis and design of a two-probe excited circular ring antenna are also presented in this chapter. The analysis was done by using the induced emf method. The impedance characteristics of the antenna were analyzed by using an equivalent circuit. The antenna design is aimed to obtain the desired antenna characteristics, i.e., bidirectional radiation pattern, VSWR of less than 2:1 and maximum isolation. These characteristics can be obtained by adjusting the parameters: ring radius (a) and ring length (d) of the antenna. The design process was as follows: first, a suitable radius of the ring was chosen for a single probe antenna. Then, the suitable probe length and ring length were determined for the two-probe antenna. Finally, isolation between the two probes was considered. Moreover, in case of two-probe antenna, the electrical characteristics of the antenna, such as radiation pattern and input impedance, are also simulated by using Numerical Electromagnetic Code 2 (NEC2) to confirm the theory. As a result, ring radius, ring length and probe length that provide the desired antenna characteristics are chosen to fabricate the prototype antenna.

2.2 Antenna Configuration and Analysis

2.2.1 Antenna Configuration

The circular ring antenna proposed in [25] has only one excited probe. To construct the dual-polarized antenna from the circular ring antenna in [25], another probe needs to be added and it should be perpendicular to the conventional probe to provide the cross polarization.

A two-probe excited circular ring antenna consists of two linear electric probes. The probes have length l and their feeding points are positioned at $(r=a,\ \theta=\pi/2,\ \phi=\phi_1')$ and $(r=a,\ \theta=\pi/2,\ \phi=\phi_2')$. Probe 1 is on $+x$-axis $(\phi_1'=0^o)$; it provides horizontal polarization. Probe 2 is on the $+y$-axis $(\phi_2'=90^o)$ and provides vertical

polarization. The difference between probe angles is $\Delta\phi$. The probes are surrounded by a circular ring antenna with ring radius a and ring length d. The electromagnetic fields propagate from the ring in both z and $-z$ directions. The field is radiated from the two apertures at the ends of the ring in the plane $z = -d/2$ and $z = d/2$, as shown in Fig. 2.1.

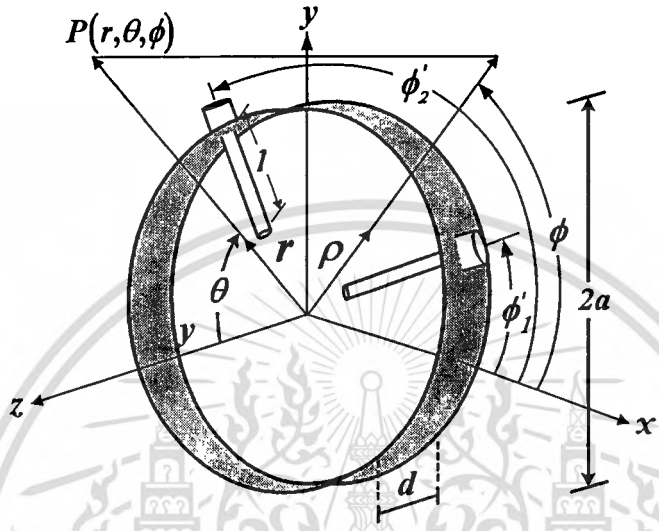

Fig. 2.1 Configuration of the two-probe excited circular ring antenna

2.2.2 Input Impedance and VSWR

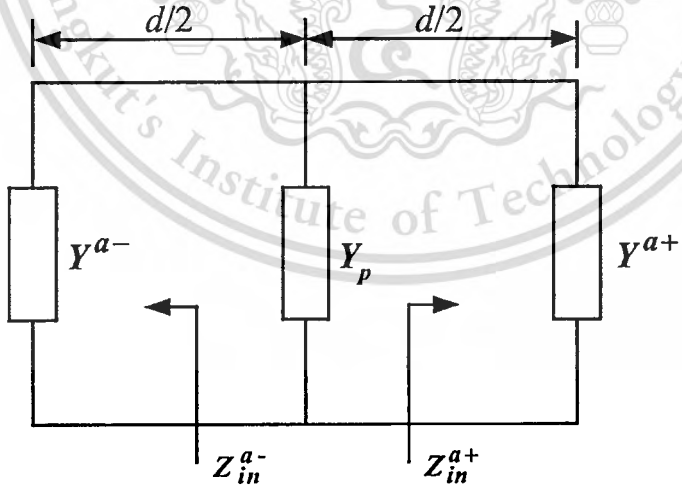

Fig. 2.2 Equivalent circuit of the probe excited ring antenna

From the antenna configuration shown in Fig. 2.1, its equivalent circuit diagram is illustrated in Fig. 2.2. The input impedance of the antenna is calculated from the shunt circuit parameters. These parameters are the admittance of the probe and the admittance of the two

apertures, neglecting the reflections and the mutual coupling from the two apertures. Precisely, the input impedance of the antenna is the inverse of the total admittance of the equivalent circuit.

Induced emf method was used to calculate the self and mutual impedances of the antennas because it was easy to obtain design parameters from the closed form mathematical expressions used in the method [32]. To calculate the self impedance at the feeding probe, the tangential electric field components on the surface of the wire had to be expressed as closed form in equation (2.1) below. Its derivation is shown in the appendix. Sinusoidal current distribution was assumed along the probe length. Under these conditions, the input impedance at the feeding probe (Z_p) could be expressed as

$$Z_p = \frac{j\omega\mu_0}{I_m}\sum_{m=0}^{\infty}\sum_{n=1}^{\infty}\left[\begin{array}{l} c_\zeta m^2 \cos\left[m(\phi-\phi')\right]\int_{a-l}^{a}\frac{J_m(\zeta\rho)}{\rho}\sin[k(\rho-a+l)]E_{a,TE}\begin{cases} e^{-jk_\zeta(z-z')}; z>z' \\ e^{-jk_\zeta(z'-z)}; z<z' \end{cases} d\rho \\ +c_\xi\frac{k_\xi^2}{\kappa_\xi^2}\cos\left[m(\phi-\phi')\right]\int_{a-l}^{a}\frac{\partial J_m(\xi\rho)}{\partial\rho}\sin[k(\rho-a+l)]E_{a,TM}\begin{cases} e^{-jk_\xi(z-z')}; z>z' \\ e^{-jk_\xi(z'-z)}; z<z' \end{cases} d\rho \end{array}\right] \quad (2.1)$$

where I_m is the maximum current which is equal to unity and $k=\omega\sqrt{\mu\varepsilon}$. ζ and ξ correspond to the transverse electrical mode (TE) and transverse magnetic mode (TM), respectively. They are defined as $\zeta = q_{mn}/a$ and $\xi = p_{mn}/a$ respectively, where q_{mn} and p_{mn} are the eigenvalues for different m and n. These values are tabulated in [33] and [34]. J_m is the Bessel function of the first kind of order m. The primed and unprimed coordinates represent the location of source and the observation point, respectively.

The admittance of the probe is equal to the inverse of the input impedance Z_p. Note that the electric field in equation (A1) in the appendix cannot be used to find the impedance at the feeding probe directly since this equation is not valid at $z=z'$; therefore, interpolation techniques [35] were used to find the impedance at the probe position $z = 0$.

The aperture admittance Y_a was calculated by using equation (2.2) below [36].

$$Y_a = \frac{1}{V^2}\int_0^{2\pi}\int_0^{a}\left(\bar{E}_t^a \times \bar{H}_t^a\right)\cdot\hat{a}_z\ \rho d\rho d\phi, \quad (2.2)$$

By substituting $\vec{E}_t^a$ and $\vec{H}_t^a$, the tangential electric and magnetic fields at the aperture respectively, from equation (A1) to (A4), Y_a can be expressed

$$Y_a = \frac{1}{V^2}\int_0^{2\pi}\int_0^{a}\left[\left[\begin{array}{l} -j\omega\mu_0\sum_{m=0}^{\infty}\sum_{n=1}^{\infty}\left[\begin{array}{l} c_\zeta m^2\frac{J_m(\zeta\rho)}{\rho}\cos\left[m(\phi-\phi')\right]E_{a,TE}\begin{cases} e^{-jk_\zeta(z-z')}; z>z' \\ e^{-jk_\zeta(z'-z)}; z<z' \end{cases} \\ +c_\xi\frac{k_\xi^2}{\kappa_\xi^2}\frac{\partial J_m(\xi\rho)}{\partial\rho}\cos\left[m(\phi-\phi')\right]E_{a,TM}\begin{cases} e^{-jk_\xi(z-z')}; z>z' \\ e^{-jk_\xi(z'-z)}; z<z' \end{cases} \end{array}\right] \\ \sum_{m=0}^{\infty}\sum_{n=1}^{\infty}\left[\begin{array}{l} c_\zeta\frac{k_\zeta}{\kappa_\zeta}\left(jm^2k\right)\frac{J_m(\zeta\rho)}{\rho}\cos\left[m(\phi-\phi')\right]H_{a,TE}\begin{cases} -e^{-jk_\zeta(z-z')}; z>z' \\ +e^{-jk_\zeta(z'-z)}; z<z' \end{cases} \\ +c_\xi\frac{k_\xi}{\kappa_\xi}\left(jk\right)\frac{\partial J_m(\xi\rho)}{\partial\rho}\cos\left[m(\phi-\phi')\right]H_{a,TM}\begin{cases} -e^{-jk_\xi(z-z')}; z>z' \\ +e^{-jk_\xi(z'-z)}; z<z' \end{cases} \end{array}\right] \end{array}\right]\cdot \right. \\ \left. -\left[\left[\begin{array}{l} -j\omega\mu_0\sum_{m=0}^{\infty}\sum_{n=1}^{\infty}\left[\begin{array}{l} c_\zeta m\frac{\partial J_m(\zeta\rho)}{\partial\rho}\sin\left[m(\phi-\phi')\right]E_{a,TE}\begin{cases} e^{-jk_\zeta(z-z')}; z>z' \\ e^{-jk_\zeta(z'-z)}; z<z' \end{cases} \\ +c_\xi m\frac{k_\xi^2}{\kappa_\xi^2}\frac{J_m(\xi\rho)}{\rho}\sin\left[m(\phi-\phi')\right]E_{a,TM}\begin{cases} e^{-jk_\xi(z-z')}; z>z' \\ e^{-jk_\xi(z'-z)}; z<z' \end{cases} \end{array}\right] \\ \sum_{m=0}^{\infty}\sum_{n=1}^{\infty}\left[\begin{array}{l} c_\zeta\frac{k_\zeta}{\kappa_\zeta}\left(jmk\right)\frac{\partial J_m(\zeta\rho)}{\partial\rho}\sin\left[m(\phi-\phi')\right]H_{a,TE}\begin{cases} -e^{-jk_\zeta(z-z')}; z>z' \\ +e^{-jk_\zeta(z'-z)}; z<z' \end{cases} \\ +c_\xi\frac{k_\xi}{\kappa_\xi}\left(jmk\right)\frac{J_m(\xi\rho)}{\rho}\sin\left[m(\phi-\phi')\right]H_{a,TM}\begin{cases} -e^{-jk_\xi(z-z')}; z>z' \\ +e^{-jk_\xi(z'-z)}; z<z' \end{cases} \end{array}\right] \end{array}\right]\cdot \right. \\ \left. \cdot\hat{a}_z\ \rho d\rho d\phi, \right. \end{array}\right] \tag{2.3}$$

where V is the voltage across the aperture. Since the input impedance of the antenna is taken to be the reciprocal of the shunt admittances, the transformation of these admittances at the ends of both apertures can be carried out (i.e. from $z=\pm d/2$ along the ring length to the probe position z = 0) by using the transmission line equation [37]. The transformation is conducted only for the case that the optimal ring length yielded a single mode distribution. The total input admittance can be determined by the relationship below

$$Y_{in_{total}} = Y_{in}^{a-} + Y_p + Y_{in}^{a+}, \tag{2.4}$$

where the superscript $a-$ and $a+$ are the positions of the aperture in $z < z'$ and $z > z'$ directions, respectively.

Finally, the input impedance can be obtained from the inverse of equation (2.4)

$$Z_{in_{total}} = \left[Y_{in_{total}} \right]^{-1}. \tag{2.5}$$

In this thesis, the characteristic impedance of the antenna is evaluated in term of VSWR. Their relationship can be expressed as follows [38]

$$\text{VSWR} = \frac{1+|\Gamma|}{1-|\Gamma|}, \tag{2.6}$$

where $\Gamma = \dfrac{Z_{in} - Z_0}{Z_{in} + Z_0}$ and Z_0 is the characteristic impedance of the transmitter or receiver. It is equal to 50 Ω in this work.

2.2.3 Mutual Impedance and Isolation

When one antenna is placed near another antenna, its input impedance can be calculated by adding the mutual impedance with the self impedance (input impedance without another antenna) and it is called driving point impedance [32]. The mutual impedance (referring to the input current I_{1i} of antenna 1) is

$$Z_{mutual} = Z_{21i} = -\frac{1}{I_{1i} I_{2i}} \int_{l} \vec{E} \cdot \vec{I} \, dl, \tag{2.7}$$

where $\vec{E}$ is the electric field component radiated by antenna 1 parallel to antenna 2 and $\vec{I}$ is the current distribution along antenna 2. For the proposed antenna, $\vec{E}$ is expressed by equation (A1) in the appendix and $\vec{I}$ is assumed to be a sinusoidal current distribution where $I_{1i} = I_{2i} = I_m \sin(kl)$. Hence,

$$Z_{mutual} = \frac{j\omega\mu_0}{I_m^2 \sin^2(kl)}$$

$$\sum_{m=0}^{\infty}\sum_{n=1}^{\infty}\left[\begin{array}{l} c_\zeta m^2 \cos\left[m(\phi-\phi')\right]\int_{a-l}^{a}\frac{J_m(\zeta\rho)}{\rho}\sin\left[k(\rho-a+l)\right]E_{a,TE}\begin{Bmatrix}e^{-jk_\zeta(z-z')}\\ e^{-jk_\zeta(z'-z)}\end{Bmatrix}d\rho \\ +c_\xi\frac{k_\xi^2}{\kappa_\xi^2}\cos\left[m(\phi-\phi')\right]\int_{a-l}^{a}\frac{\partial J_m(\xi\rho)}{\partial\rho}\sin\left[k(\rho-a+l)\right]E_{a,TM}\begin{Bmatrix}e^{-jk_\xi(z-z')}\\ e^{-jk_\xi(z'-z)}\end{Bmatrix}d\rho \end{array}\right] \quad (2.8)$$

Therefore, the admittance of the mutual impedance can be calculated from the inverse of the mutual impedance. Note that Z_{mutual} in equation (2.8) is calculated from interpolation techniques since the electric field in equation (A1) in the appendix is not valid at the feeding probe position $z = 0$.

To find the aperture admittance (Y_a), the expression in equation (2.2) can be used where E_t^a and H_t^a are the tangential electric and magnetic fields at the aperture, taken from the electric and magnetic field component radiated by antenna 1 parallel to antenna 2. The total admittance can also be found by using (2.4). Finally, the total mutual impedance can be obtained from the inverse of the total admittance.

Isolation of the antenna can be computed as follows, as in [38],

$$\text{Isolation (dB)} = -20 \log |S_{21}| \quad (2.9)$$

where

$$S_{21} = \frac{2Z_{21}'}{\Delta} \quad (2.10)$$

$$\Delta = \left(z_{11}' + 1\right)\left(z_{22}' + 1\right) - z_{12}' z_{21}' \quad (2.11)$$

$$z_{ij}' = \frac{Z_{ij}}{Z_0} \quad , i=1, 2 \text{ and } j=1, 2 \quad (2.12)$$

and Z_0 is the characteristic impedance of the feeding coaxial cable (assumed to be 50 Ω). Z_{11} and Z_{22} are driving point impedances at probe 1 and probe 2, respectively. Z_{21} and Z_{12} are mutual impedances from probe 1 to probe 2 and from probe 2 to probe 1, respectively. Since the antennas are identical, $Z_{11} = Z_{22}$ and $Z_{21} = Z_{12}$.

As seen in the expressions of the antenna's input impedance and mutual impedance, it is clear that both of them are dependent on ring radius a, ring length d, probe length l and the angle between the two probes $\Delta\phi$.

2.2.4 Higher Modes

Before further investigation, the effect of higher modes on the impedance of the antenna should be determined. So far, only the dominant mode (TE_{11}) is considered as the propagation mode in the waveguide, but there also exist higher modes affecting the antenna impedance since it is calculated at the feeding probe. As an example, the input impedance at the feeding probe of an antenna that has a ring radius of 0.3λ, a ring length of 0.2λ, and a probe length of 0.25λ is determined for the purpose of illustrating the effect of higher modes. Note that the shortest ring length is 0.2λ which is the width of an SMA connector. Since the number of modes is large when the ring length is small, the number of modes obtained from the shortest ring length is used as a representative for those of other ring lengths.

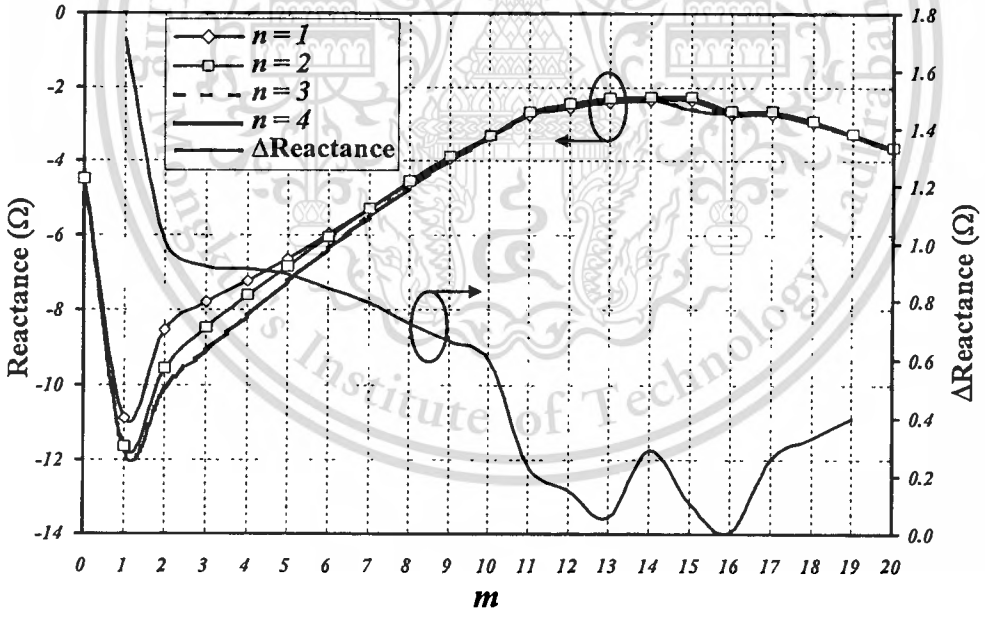

Fig. 2.3 Impedance of the antenna for different m and n values ($a = 0.3\lambda$, $d = 0.2\lambda$, $l = 0.25\lambda$)

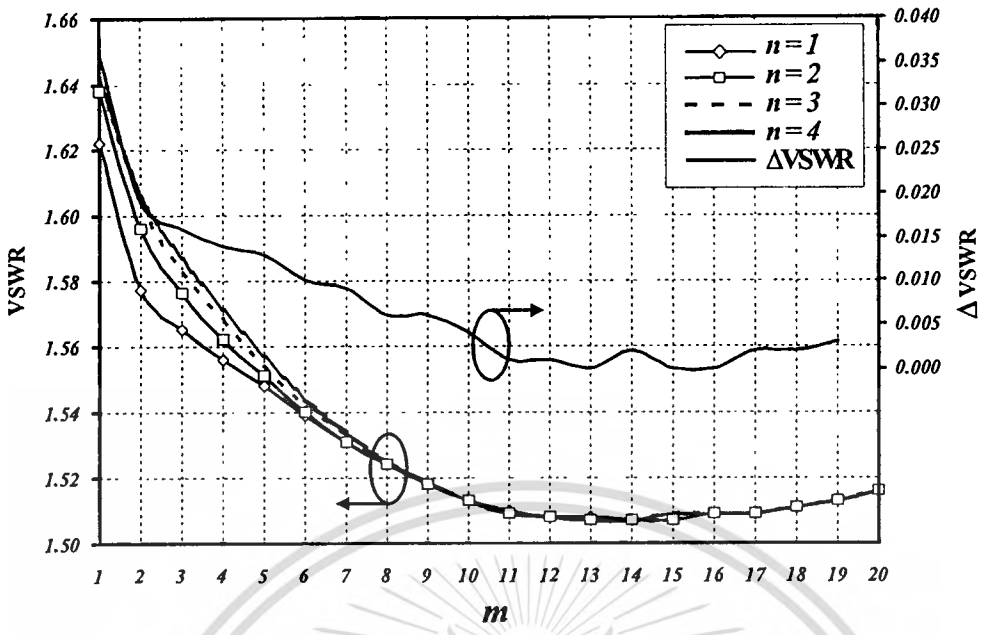

Fig. 2.4 VSWR of the antenna for different m and n values ($a = 0.3\lambda$, $d = 0.2\lambda$, $l = 0.25\lambda$)

Figure 2.3 shows the total impedances from each mn modes with the one from the lower mode. Since resistance is equal to 33.30 Ω for all cases, only the reactance values are shown in this figure. Because m affects the impedance of the antenna more significantly than n, we choose the case $n = 4$ to study the effect of m on the impedance. The differences between the impedances of m and m+1 values, with $n = 4$ modes, are shown in Fig. 2.3. It is clear that the impedance of the antenna does not converge (ΔReactance $\neq 0$) when m and n increase, as can be seen in this figure. The impedance seems to converge at $m = 13$, but ΔReactance increases again at $m = 14$. This kind of fluctuation is observed again as m increases. On the other hand, when the impedance in terms of VSWR is considered, shown here in Fig. 2.4, the high fluctuation is not obvious. Please note that only the VSWR at the feeding probe is considered and that it starts from $m = 1$ because it is equal to infinity at $m = 0$, where there exists only the reactance term. When only the cases where the variation of VSWR is less than 0.005 is considered, the first case is at $m = 11$ and $n = 4$. The VSWR is 1.509 there. The difference between this VSWR value and that of $m = 12$ and $n = 4$ is 0.001. Moreover, the differences between the VSWR values of any pairs of m and m+1 modes are always lower than 0.005 as m increases beyond 11. Therefore, the values of $m = 11$ and $n = 4$ are chosen for our calculation. Additionally, the impedances of the TE and TM modes have also examined. It is found that the dominant mode, TE_{11}, had the most significant effect on the impedance of the antenna, and the higher modes, TE_{21}, TM_{11}, TM_{01} and TM_{21}, also showed some influences.

2.3 Antenna Design

2.3.1 Single Probe Antenna

In this study, the adjacent higher mode is TE_{21}. To allow only the dominant mode to propagate along the waveguide, the ring radius of the waveguide was precisely chosen to cutoff the TE_{21} higher mode. The ring radius (a) was chosen under the criterion cited in [25] and [33] as

$$0.293\lambda < a < 0.486\lambda \tag{2.13}$$

where λ is the wavelength of the operating frequency.

Because Kosulvit's study [25] stated that directivity performance of the antenna degrades when ring radius is larger than 0.4λ, ring radii of 0.3λ and 0.34λ is chosen. Even though ring radius of 0.3λ is suggested [25], a larger ring radius is more interesting because of its higher obtainable directivity. Figure 2.5 shows the VSWR of the antenna as a function of probe length, calculated for two ring radii, and four ring lengths. The probe lengths investigated from 0.15λ to 0.29λ and 0.15λ to 0.33λ.; the ring radii chosen were 0.3λ and 0.34λ; and the ring lengths were 0.2λ , 0.3λ , 0.4λ , and 0.5λ. The frequency is fixed at 5.2 GHz. The ring length is limited to 0.5λ since the directivity of the antenna decreases rapidly with longer ring length and bidirectional pattern would not be obtained, according to Kosulvit's study [25].

Note that these VSWR results were the same for both probe 1 and probe 2 since they are identical according to the reciprocity theorem. From Fig. 2.5, it is evident that for both ring radii, the longer the feeding probe, the better the VSWR, and larger ring radius yielded higher VSWR. For instance, the VSWRs obtained from the antenna with ring radius of 0.34λ were higher than 2, for all probe lengths and ring lengths. Consequently, ring radius of 0.3λ was chosen for further investigation, not only for the reason just mentioned, but because waveguides with this dimension were widely available commercially.

When ring radius was 0.3λ and probe length was 0.27λ, almost all ring lengths yielded the lowest VSWRs, except for ring length of 0.2λ where the lowest VSWR was obtained at probe length of 0.25λ. It can also be seen that VSWR decreased as ring length increased. Finally, ring length of 0.5λ yielded the absolute lowest VSWR. To sum up, the chosen single probe antenna possessed the following parameters: ring radius of 0.3λ, ring

length of 0.5λ and probe length of 0.27λ. These optimal ring and probe dimensions differed from those reported in [25] as the latters were chosen to provide maximum directivity.

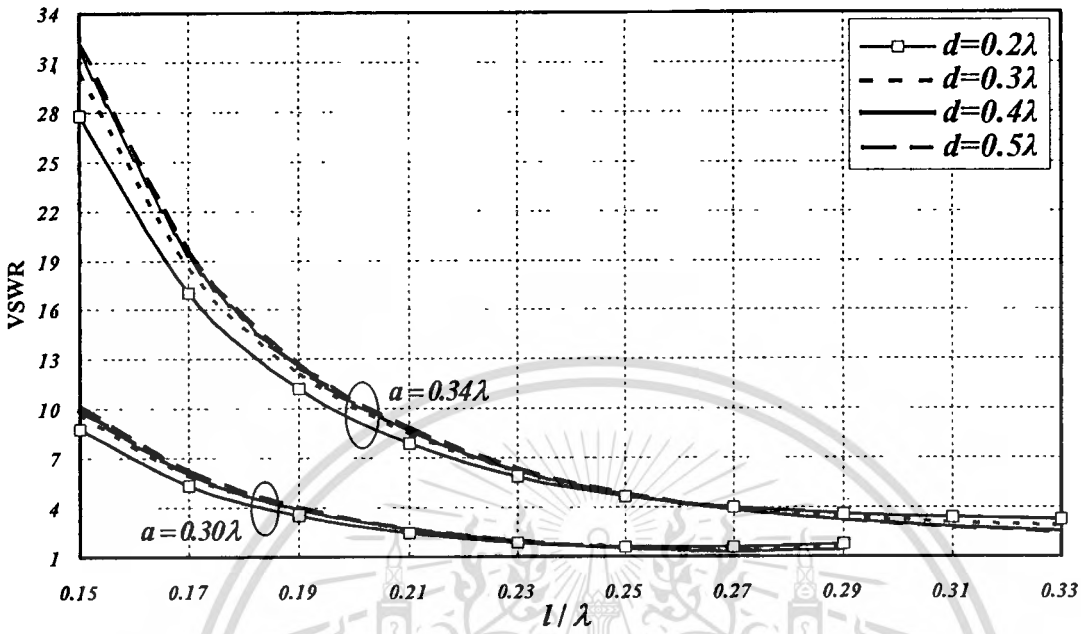

Fig. 2.5 VSWR for various probe lengths: ring radius of 0.30λ and 0.34λ (f = 5.2 GHz)

2.3.2 Two-Probe Antenna

In this section, the impedance characteristics of the antennas with two-probe excited ring is considered. For these antennas, both the VSWR of each antenna and the isolation between the two antenna ports were objects to concern, and since ring length and probe length also have a significant impact on the two-probe antenna performance, their variations were of interest.

To achieve a suitable probe length for a two-probe antenna, VSWR has to be trade-off with isolation. A maximum isolation of more than 20 dB with minimum VSWR less than 2:1 was aimed for in this study.

Fixing the radius at 0.3λ, the angle between the two probes at 90°, and the operating frequency at 5.2 GHz, VSWR and isolation of the antenna were plotted, in Fig. 2.6, as a function of probe length for various ring lengths. Note that the isolation results were applicable for both the isolation of probe 1 from probe 2 and that of probe 2 from probe 1 since they are identical according to the reciprocity theorem. It was found that the shorter the feeding probe, the higher the VSWR and isolation. Feeding probe length shorter than 0.23λ yielded VSWR higher than 2. Therefore, if isolation higher than 20 dB and VSWR less

than 2 were intended for, probe length of 0.25λ was a good choice. Even though probe length of 0.23λ provided 1 dB higher isolation, its VSWRs were approximately 2 for all ring lengths, so it is not the best choice. It can be seen that the variations of VSWR and isolation were in opposite direction. The probe length that achieved desirable VSWR yielded undesirable isolation.

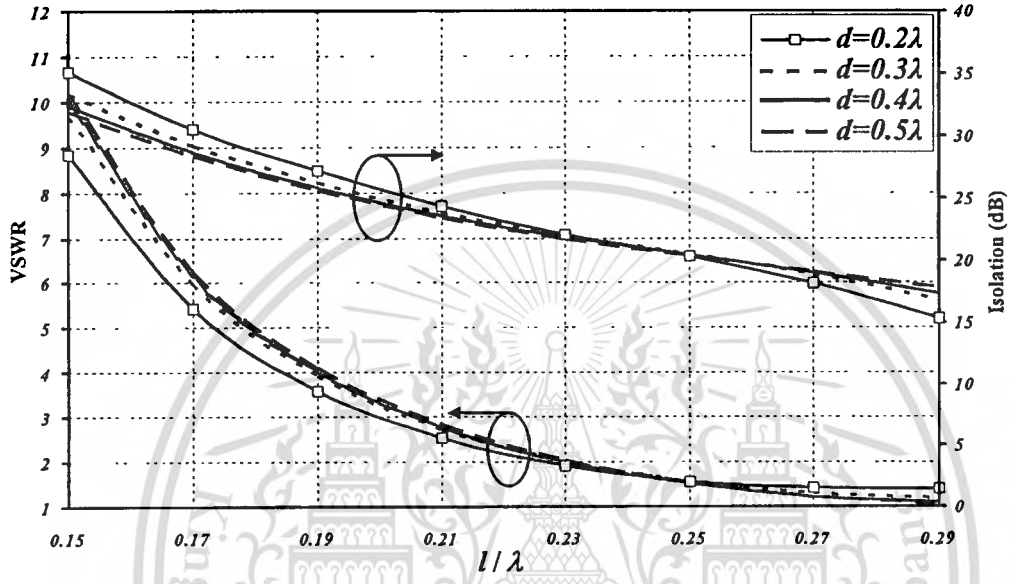

Fig. 2.6 VSWR and isolation of the antenna with varying probe length ($a = 0.3\lambda$, $\Delta\phi = 90°$, f = 5.2 GHz)

Figure 2.7 shows the VSWR and isolation of the antenna as a function of the angle between the two probes for different ring lengths with probe length fixed at 0.25λ and operating frequency fixed at 5.2 GHz. It is evident that larger angle between the two probes provided higher VSWR, while maximum isolation was achieved at the angle of 90° where the two-probe antenna produced orthogonal polarizations. The isolation were higher than 20 dB for all ring lengths at this angle. VSWR increased enormously when the angle between the two probes was larger than 90°. The isolation at these angles were small since the probes produced nearly the same polarization. Lastly, high mutual coupling between the two probes was also observed.

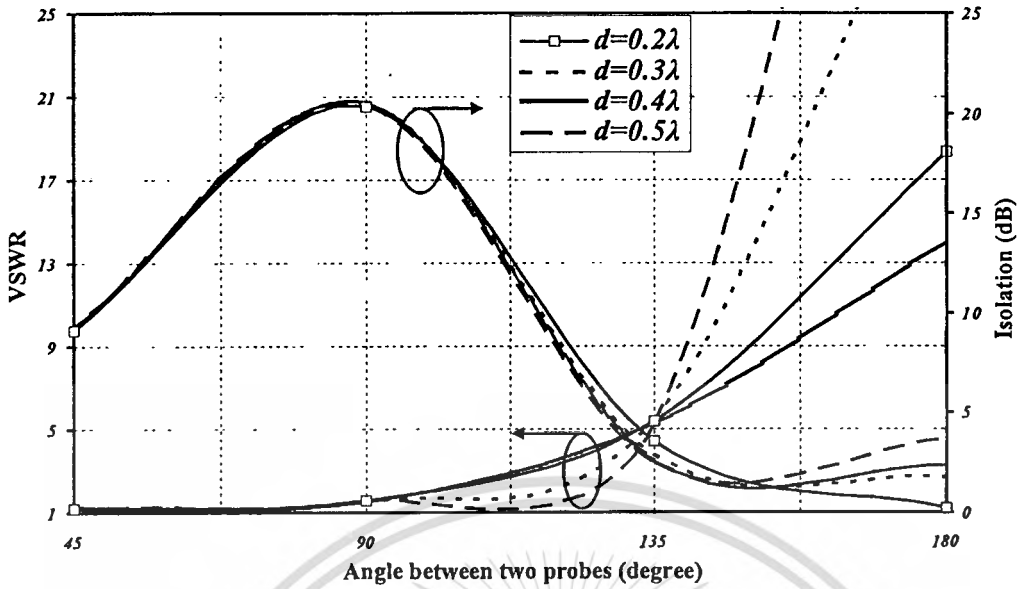

Fig. 2.7 VSWR and isolation of the antenna with varying angle between the two probes (a = 0.3λ, l = 0.25λ, f = 5.2 GHz)

Figure 2.8 shows VSWR and isolation of the antenna as functions of frequency for different ring lengths when the probe length is fixed at 0.25λ and the angle between the two probes is 90°. The frequency range spanned the frequencies of 5.1 GHz to 5.3 GHz. The start frequency was set at 5.1 GHz since the cut-off frequency of this particular ring radius was 5.08 GHz. This frequency range was chosen to study because it is the operating range of the 5 GHz indoor WLAN, i.e. 5.15 - 5.25 GHz. The results obtained were as follow: the VSWRs of the antenna were less than 2 and the isolation were approximately 20 dB within the operating band for all ring lengths. At the center frequency of 5.2 GHz, ring length of 0.3λ provided maximum isolation. Therefore, it can be concluded that ring radius of 0.3λ, ring length of 0.3λ, probe length of 0.25λ, and the angle between the two probes of 90° were to be used for two-probe excited circular ring antenna. Note that its resonance frequency was not at 5.2 GHz since the probe length that provided maximum isolation was chosen.

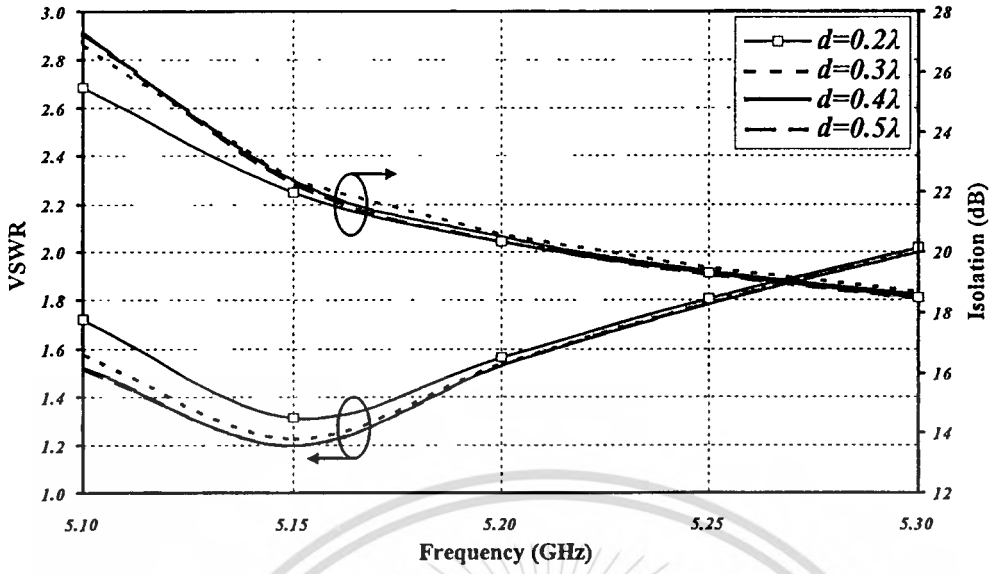

Fig. 2.8 VSWR and isolation of the antenna at various frequencies ($a = 0.3\lambda$, $l = 0.25\lambda$, $\Delta\phi = 90°$)

2.3.3 Simulation by Numerical Electromagnetics Code 2 (NEC2)

To confirm the antenna design by the analysis, the Numerical Electromagnetics Code 2 (NEC2) based on the Method of Moments (MoM) simulation program is used. By using NEC2 program, the antenna structure is modeled by small wire grids. The segment length of each wire should be less than 0.1λ [39]. However, at the probe of the antenna, the segment length can be finely divided to 0.01λ to obtain the accurate input impedance. The two probes are excited by a voltage gap feed. At the probe base, the two diagonal wires are added to support high current density according to the suggestion in [39]. The lossy wire grid is used to model brass with conductivity of 2.56×10^7 S/m since it is used to fabricate the prototype antenna. The wire radius is equal to the radius that provides the equivalent wire grid surface area to the real surface area [39], [40]. By using NEC2 program, the VSWR and isolation are studied when the ring radius and the ring length of the antenna are varied. As same as the simulation, the length of the two probes is identical and equals 0.25λ.

The contour plot in Fig. 2.9 is the result at the center frequency (5.2 GHz) of the operating band with respect to the ring radius and the ring length of the antenna. Since the probe length is fixed at 0.25λ, the ring radius should be larger than 0.25λ to avoid the contact between the probe and the ring. Then, the investigated ring radius started at 0.3λ. In addition, the ring length should be larger than 0.10λ since the ring becomes only a wire when the ring length is too small. By using NEC2, the radiation pattern of the antenna can be obtained.

Then, the radiation pattern is also considered for the bidirectional radiation pattern. Here, the ring radius of 0.30λ–1λ and the ring length of 0.10λ–1λ are investigated.

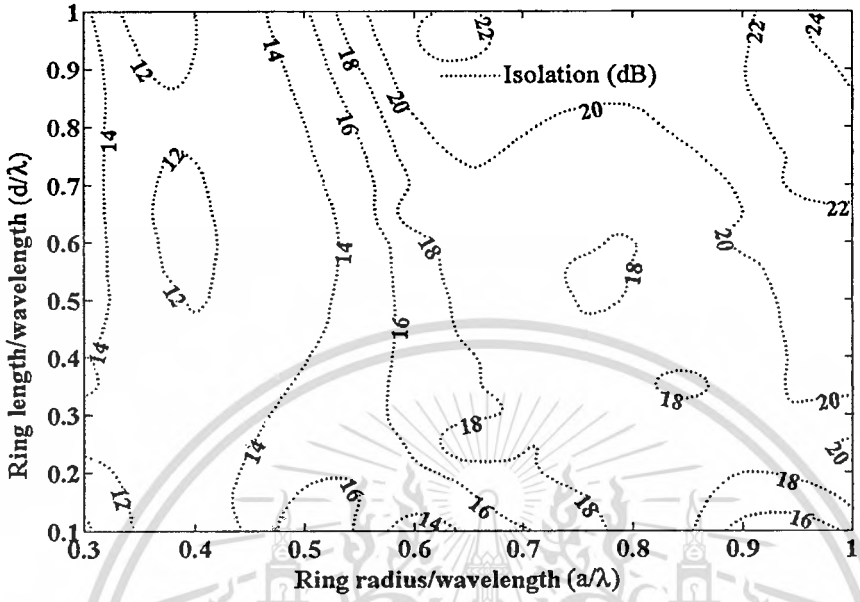

Fig. 2.9 Contour plot of the isolation of the antenna with respect to the ring radius (a) and the ring length (d)

Only the contour plot of isolation is shown here since the VSWR is less than 2:1 for all cases. From the result in Fig. 2.9, the isolation can be maximized by extending the ring radius and ring length. The enlarged ring radius provides good isolation since the gap between the two probes is widen. However, the antennas with an enlarged ring radius provide the main beam in the undesired direction. Their main beams do not point along the corridor and their radiation patterns are also not the bidirectional radiation pattern. This result is also mentioned in [25]. The beams of these antennas point toward the opposite side of the excited probe that causes loss of the transmission power in the undesired direction. In addition, the enlarged ring length makes the circular ring antenna become the circular waveguide. As a result, the gain in the desired directions of the antenna becomes small due to the ohmic loss in the waveguide. The dimension of the antenna with the appropriate gain (higher than 2.15 dBi) and the bidirectional radiation pattern comprises of 0.30λ–0.50λ ring radius and 0.10λ–0.50λ ring length (shaded area). Unfortunately, these interesting antennas have small isolation (12-16 dB). It can be noted that the difference of the isolation between the calculation and simulation can be observed. The isolation from NEC2 is lower than that from the calculation. This difference is maybe from the aperture coupling effect that is omitted in the analysis

calculation.

When the trade off between VSWR and isolation is considered, the parameter of 0.30λ ring radius and 0.30λ ring length is obtained. These parameters are identical to the calculation result and it can confirm the accuracy of the theory. Finally, the antenna parameters for the prototype antenna are shown in Table 2.1 and the prototype antenna is illustrated in Fig. 2.10.

Table 2.1 Dimensions of the prototype antenna

Antenna Parameters	**Physical Dimension at f = 5.2 GHz**
Ring radius (a)	0.3λ (1.73 cm)
Ring length (d)	0.3λ (1.73 cm)
Probe length (l)	0.25λ (1.44 cm)
Angle between two probes ($\Delta\phi$)	90°
Probe diameter	1 mm

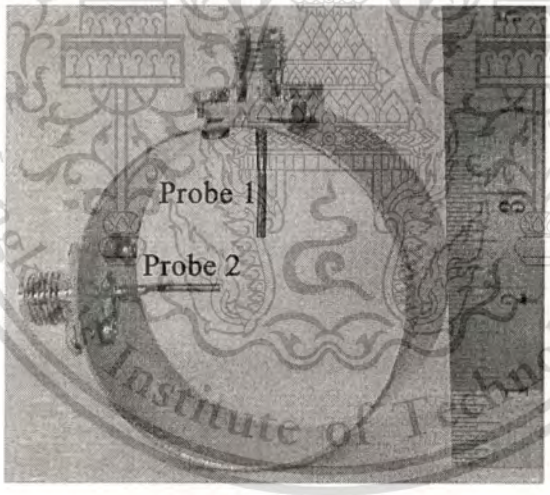

Fig. 2.10 Prototype antenna

2.3.4 Measurement Results

The prototype antenna is fabricated to validate the theory. The VSWR and isolation of the antenna as functions of probe length, are considered between the theoretical calculations and actual measurements from the prototype antenna, are shown in Fig. 2.11. The results show good agreement between the calculated and measured VSWRs when probe length is longer than 0.19λ. However, calculated and measured isolation differed quite

significantly. The calculated isolation was 10 dB higher than that of the measured one due to the omission of the reflection and mutual coupling effect between the two apertures in the calculation. This result is as same as the result that mentioned in NEC2 simulation result. The calculation results reach the higher isolation value than that of the simulation and measurement results. On the other hand, good agreement between calculated and measured VSWRs was observed because the impedance of the antenna depended mainly only on probe length, according to Kosulvit's explanation [25]. The differences between the calculated and measured VSWRs and isolation were 6.5% and 44.7%, respectively, for the probe length of 0.25λ at the fixed frequency of 5.2 GHz. These results were not perfect; nevertheless, they exhibited the same trend that can be confirmed that the proposed design principles were reliable. Since the prototype antenna was fabricated by using brass, the antenna efficiency due to the conduction and dielectric losses is equal 0.78.

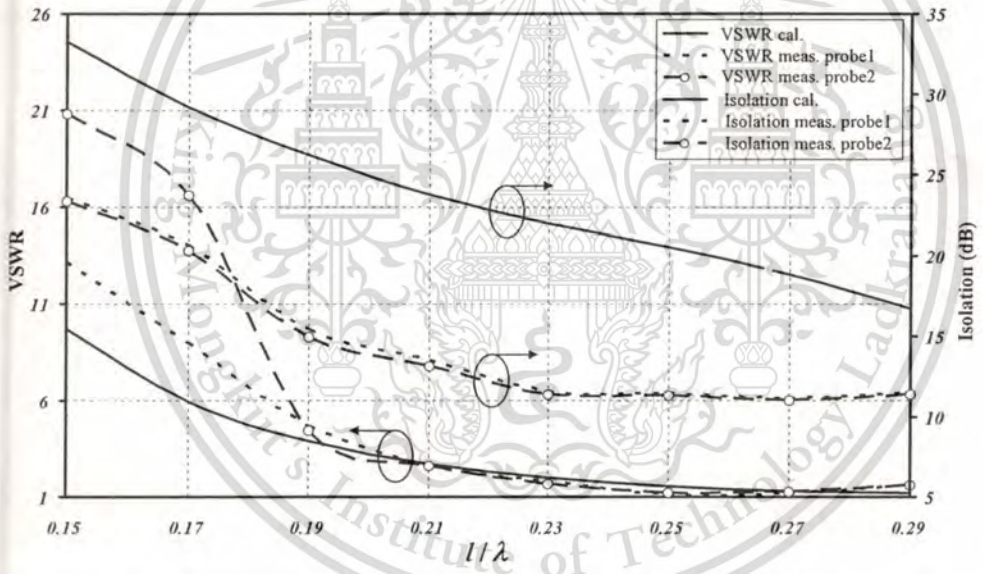

Fig. 2.11 Calculated and measured VSWR and isolation of the antenna with varying probe length ($a = 0.3\lambda$, $\Delta\phi = 90°$, $f = 5.2$ GHz)

2.4 Conclusion

A two-probe excited circular ring antenna is proposed. The antenna configuration and design are described. The analysis was done by using the induced emf method. The accuracy of the analysis is confirmed by the same trend result from the NEC2 program. The antenna parameters that are ring radius of 0.3λ, ring length of 0.3λ and probe length of 0.25λ is concluded from the study. These parameters are used to construct the prototype antenna and used for further study in the next chapter.

CHAPTER 3

A TWO-PROBE ANTENNA WITH AN ISOLATION IMPROVEMENT

3.1 Introduction

In chapter 2, the two-probe antenna parameters can be achieved. Even though the VSWR is acceptable, the isolation can not meet the requirement. The study in [41] shows that the increase of the angle between the two probes can improve the isolation. However, in this thesis, the angle between two probes is fixed to 90° to provide the orthogonal polarization. Hence, the isolation of the antenna is improved by offsetting the position of the two probes and by insertion the inductor coil between two probes in this chapter. These approaches can improve the isolation of the antenna higher than 20 dB.

3.2 Two-Probe Antenna with Probes Offsetting

3.2.1 Antenna Design

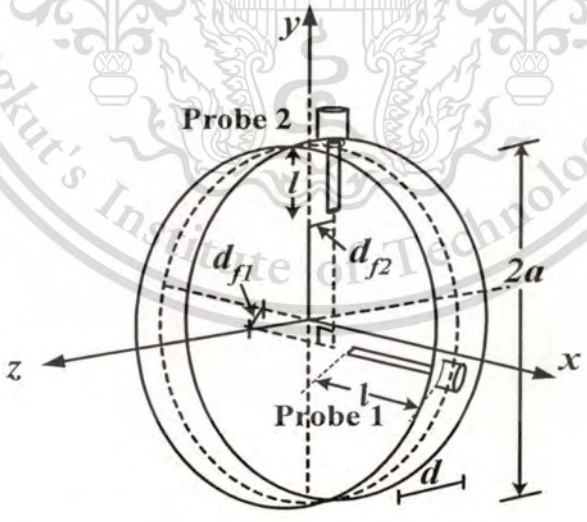

Fig. 3.1 Structure of the two-probe antenna with probe offsetting

To improve the isolation, the change of the positions of the two probes is employed (offset probe). The change of the positions of the two probes can reduce the influence between the two probes because they are not placed in the same plane. It is similar to changing the position of the antenna elements from the side-by-side

configuration to the parallel in echelon configuration according to the effect of the element configuration on the mutual coupling in [32]. When the offset probe antenna is considered, the offset distances (d_{f1} and d_{f2}) are identical and are equal to $d/4$ with respect to the normal probe position ($x = 0$ plane) as shown in Fig. 3.1. This offset distance is the maximum distance that the connector of the feed probe can be placed on the ring of the prototype antenna. In this case, the antenna is simulated by using NEC2 program.

At this offset distance, the isolation between two probes is maximized. The isolations of the antenna with the offset probes are shown in Fig. 3.2. After offsetting two probes, the isolations of the antennas are increased. The same trends of the results are achieved as the conventional two-probe antenna in Chapter 2. The increase of the ring radius and ring length provides good isolation with non-bidirectional radiation pattern. The dimensions of ring radius and ring length in the shaded area are still interesting. The isolations in this shaded area are 12–20 dB.

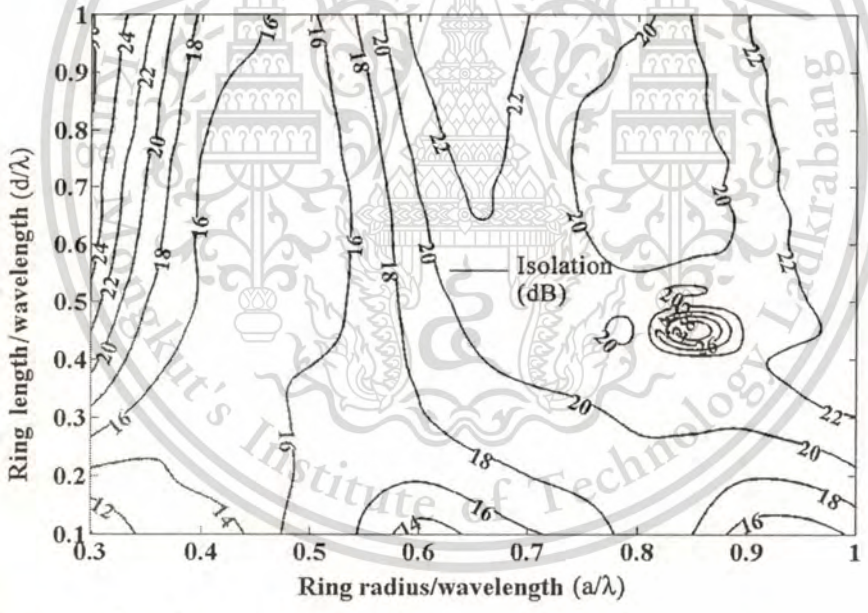

Fig. 3.2 Contour plot of the isolation of the antenna with respect to the ring radius (a) and the ring length (d) when $d_{f1} = d_{f2} = d/4$

The antenna with 0.30λ ring radius and 0.30λ ring width provides the highest gain in the desired directions. This antenna has the isolation of 20.7 dB. Higher isolation can be achieved from other antenna dimensions with the non-bidirectional pattern. Finally, in this thesis, the ring radius of 0.30λ and the ring width of 0.30λ are used to fabricate the prototype antenna of the two-probe offsetting antenna as shown in Fig. 3.3.

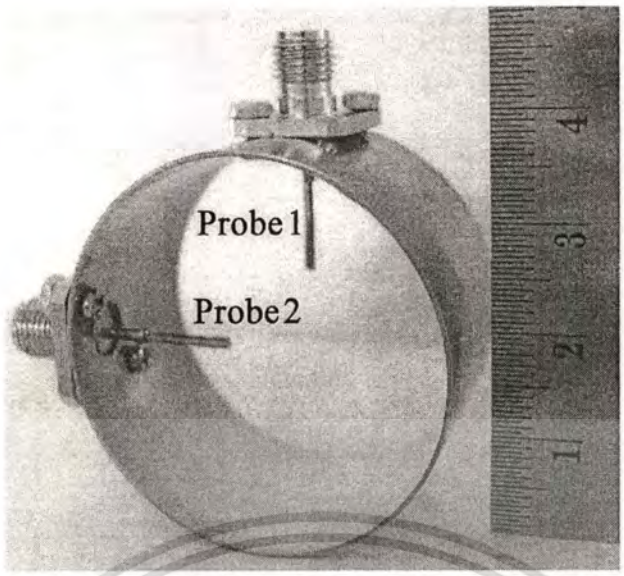

Fig. 3.3 Prototype of two-probe antenna with probe offsetting

3.2.2 Measured VSWR and Isolation

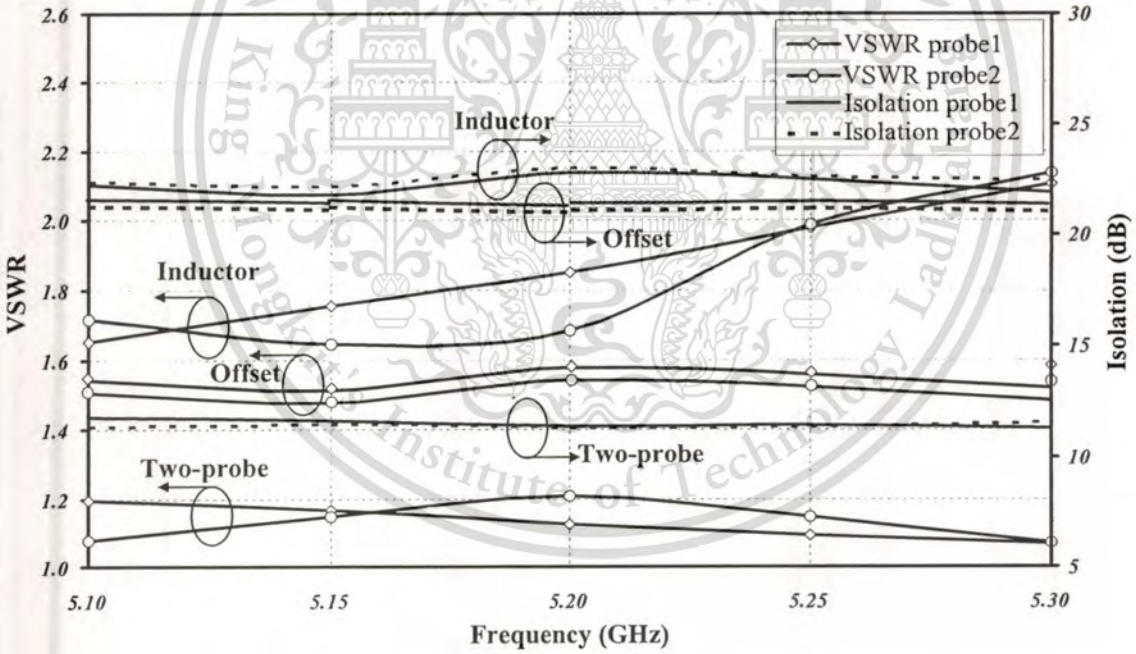

Fig. 3.4 Measured VSWR and isolation of the antennas

Figure 3.4 shows measured VSWR and isolation of the conventional two-probe antenna (two-probe antenna) and the offset probe antenna (offset) over 5.1–5.3 GHz band. It can be observed that the VSWR of the offset probe antenna is higher than that of the conventional two-probe antenna. In addition, these VSWR are less than 2:1 all over the band. In contrast, the isolation of the offset probe antenna is 8 dB higher than that of the conventional two probe antenna.

3.2.3 Radiation Pattern and Gain

The measured radiation patterns of the offset antennas are shown in Fig. 3.5. When probe 1 is excited, probe 2 is terminated with 50 Ω load and vice versa when probe 2 is excited. From Fig. 3.5 the antenna has bidirectional radiation pattern along the *x*-axis. In this measurement, the transmitting antenna is a monopole on a ground plane that has the center frequency of 5.2 GHz and the receiving antenna is the prototype of the proposed antenna. The separation between the transmitting and receiving antennas is 52 cm which can cover the far field distance for both transmitting and receiving antennas. The measurements were processed in a small anechoic chamber in the laboratory.

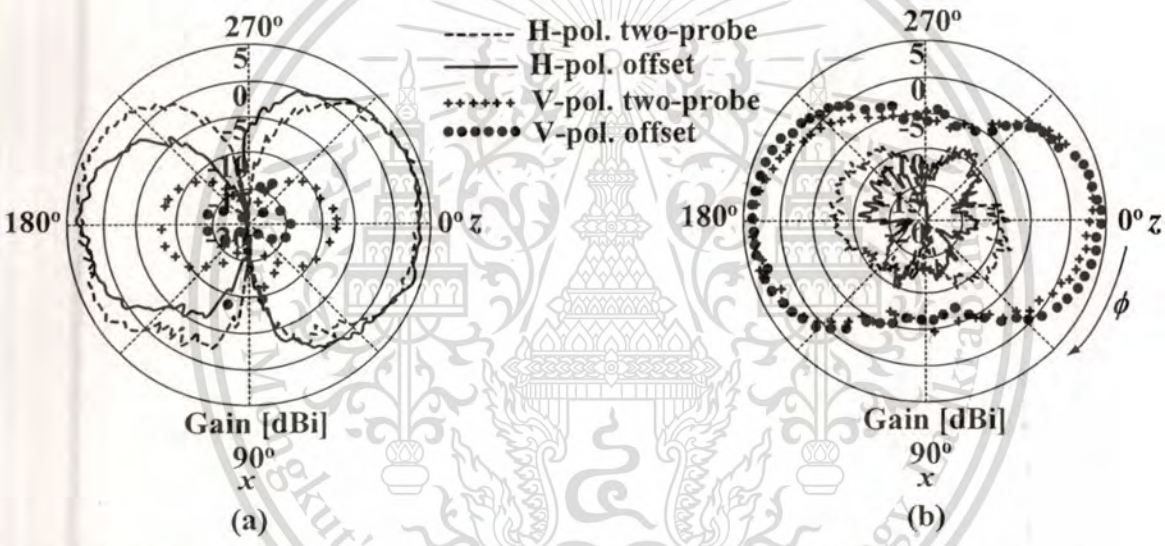

Fig. 3.5 Radiation patterns of the two-probe and offset probe antennas (a) Probe 1 is excited and probe 2 is terminated (b) Probe 2 is excited and probe 1 is terminated

When probe 1 is excited, the dominant polarization is horizontal polarization and the minor polarization is vertical polarization and vice versa when probe 2 is excited. The significant effect of probe offset can be seen from the radiation pattern of the horizontal polarization in Fig. 3.5(a). The HPBW of the radiation patterns toward the +*z*-axis and the –*z*-axis are different. In Fig. 3.5(b), the radiation patterns of the vertical polarization for the two-probe and offset probe antennas are almost identical. The highest gain of the vertical polarization is approximately 4 dBi toward the ±*z*-directions for both the two-probe and the offset probe antennas whereas the horizontal polarization radiation patterns between the two-probe and the offset probe antennas are different. The radiation

patterns of the offset probe antenna are not symmetrical due to the offset position of the probes. The difference between the vertical polarization level and the horizontal polarization level is higher than 10 dB in the maximum gain direction .

3.3 Two-Probe Antenna with an Inductor Coil

3.3.1 Antenna Design

According to the analysis result in section 2.3.2, the impedance, VSWR and isolation at 5.2 GHz are summarized in Table 3.1.

Table 3.1 Impedance, VSWR, and isolation of the two-probe antenna at the frequency of 5.2 GHz

Characteristics	Results
Input impedance(Ω)	32.63+j4.94
Mutual impedance(Ω)	0-j6.44
VSWR	1.54
Isolation (dB)	20.56

From the mutual impedance values in Table 3.1, the antenna possessed capacitive reactance that originated from mutual interaction between the two probes. This effect was also confirmed by the measured impedance of the prototype antenna that was fabricated in Chapter 2 as shown in Table 3.2. To cancel this effect, an air-core inductor coil was inserted between the feeding probes to create a resonance circuit with inductive reactance. This approach was confirmed by the simulation in NEC2 that resulted the decreasing of mutual impedance and then, the increasing of the isolation. This LC series resonance circuit provided high impedance, blocking the current flow from one probe to the other. The air-core inductor coil was made from the copper wire that has radius of 0.5 mm with 4 turns and provided the coil total length of 3 mm. However, it could not create a perfect, infinite impedance, resonance circuit from this coil because of the following reasons: 1) the inserted inductor coil could not produce pure inductance at high frequencies because of the frequency-dependent wire resistance; and 2) the adjacent turns of the coil exhibited a parasitic capacitance effect. The characteristic of the coil was measured by the network analyzer with the result of small inductive reactance at 5.2 GHz. The self resonant frequency of the coil was not occurred at the operating frequency

because of the reasons that mentioned above. Therefore, the isolation between the two probes of the antenna was not infinite, but the resonance circuit constructed still significantly reduced the current at the end of feeding probes, improving the isolation. In the next section, the experimentally-measured effect of this inductor coil on VSWR, isolation, and radiation pattern of the antenna will be discussed.

A prototype antenna was fabricated with the parameters shown in Table 2.1. Photographs of the antenna with and without inductor coil are shown in Fig. 3.6. The VSWR and isolation of the antenna with inductor coil are also compared to those without the coil (conventional two-probe antenna). Lastly, the radiation patterns and gains of these two antenna configurations were reported.

(a) (b)

Fig. 3.6 Photographs of the proposed antenna (a) without an inductor coil (b) with an inductor coil

3.3.2 Measured VSWR and Isolation

As can be seen from the results in Fig. 2.11, the isolation of the real antenna is lower than that of the theoretical one. The same trend can be observed in Table 3.2 in terms of mutual impedance, i.e. the mutual impedance of the real antenna has a higher capacitive reactance than that of the calculated one because of the omission of the reflection and the mutual coupling between the two apertures. Consequently, the prototype antenna is designed to utilize an inductor coil with higher inductive reactance. A suitable inductor coil was chosen to resonate with the capacitive reactance of the two-probe antenna. The inductance value was approximated by using an expression for an air-core inductor coil reported in [38]. After insertion of the inductor coil, it was clear, as can be seen in Table 3.2, that the mutual impedance of the antenna was effectively

reduced. The capacitive reactance of the antenna was reduced as expected, and so enhances the isolation.

Table 3.2 Impedance, VSWR, isolation, and gain of the two-probe antenna at the frequency of 5.2 GHz

Parameters	Two-probe		Offset	With L
	Cal.	Meas. ant.1, ant.2	Meas. ant.1, ant.2	Meas. ant.1, ant.2
Input impedance (Ω)	32.63+j4.94	57.19-j21.15, 33.39-j14.51	54.28-j17.12 52.15-j12.78	85.10-j21.82, 33.38-j20.60
Mutual impedance (Ω)	0-j6.44	8.07-j24.86, 6.06-j25.44	7.15-j22.18 7.08-j23.29	6.31-j5.68, 6.09-j5.67
VSWR	1.54	1.44, 1.43	1.55, 1.54	1.84, 1.88
Isolation (dB)	20.56	11.36, 11.36	20.89, 20.56	22.79, 22.98
Gain (dBi)	4.12 (NEC2)	3.94, 3.95	3.99, 4.02	4.23, 4.30

In Fig. 3.4, a comparison between the measured VSWRs and isolation of antennas with inductor coil and without inductor coil is shown. These parameters are shown as functions of frequency. It can be seen that the VSWR of the proposed antenna with inductor coil was slightly high. It was higher than that of the proposed antenna without an inductor coil. On the other hand, the isolation of the antenna with inductor coil is 11 dB higher than that without. Since the VSWR of the antenna with inductor coil was less than 2:1, but the isolation provided by the coil was higher than 20 dB observed over the desired bandwidth (5.15-5.25 GHz), choosing the antenna with inductor coil seemed to be a good design trade-off.

3.3.3 Radiation Pattern and Gain

Even after a reasonable trade-off between VSWR and isolation had been achieved, the influence of the inserted inductor coil on the radiation pattern of the proposed antenna still had to be investigated. Figure 3.7 shows the radiation patterns of the antenna with and without an inductor coil.

Figure 3.7 shows that bidirectional radiation patterns were achieved for both of the antenna configurations. When probe 1 was excited and probe 2 was terminated with

50 Ω load, the antenna radiated horizontal polarization as major component and vertical polarization as minor component, as shown in Fig. 3.7(a) and vice versa when probe 2 was excited and probe 1 was terminated, as shown in Fig. 3.7(b). From both figures, it can be seen that the major components of the antenna with and without an inductor coil were the same while their minor components were slightly different. The insertion of inductor coil degraded the cross polarization component of the antenna. Lastly, the gain of both kinds of antenna were approximately 4 dBi in both ±z-directions.

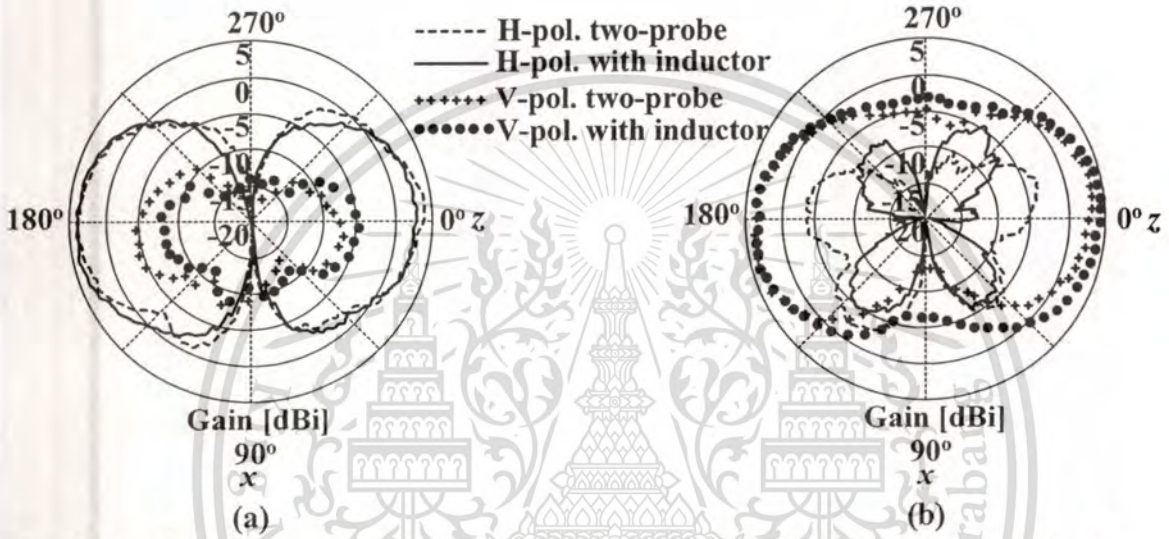

Fig. 3.7 Radiation patterns of the antennas with and without inductor coil (a) Probe 1 is excited and probe 2 is terminated (b) Probe 2 is excited and probe 1 is terminated

When two-probe antenna with probe offsetting and two-probe antenna with an inductor coil are compared, their VSWRs, isolations and the radiation patterns are considered. From Fig. 3.4 and Table 3.2, the measured VSWR of the antenna with inductor coil is higher than that of the offset antenna. However, both have the VSWR less than 2:1. When the isolation is investigated, the antenna with inductor coil provides 2 dB isolation higher than that of the offset antenna. In addition, when the radiation pattern is also considered from Figs. 3.5 and 3.7, the antenna with inductor coil is more suitable since it has symmetrical bidirectional pattern. Because of the offsetting of two probes in offset antenna, its radiation pattern is not symmetry. In conclusion, since the VSWR of the two-probe with inductor coil antenna is less than 2:1, the isolation is higher than 20 dB over the desired bandwidth (5.15-5.25 GHz), and the radiation pattern is a bidirectional pattern that is symmetry, the two-probe antenna with inductor coil seemed to be a suitable antenna for using in MIMO communication.

3.4 Conclusion

In this chapter, isolation of two-probe antenna was improved by offsetting the position of two probes and by inserting the inductor coil. When the criteria of VSWR less than 2 and maximized isolation are considered, the two-probe antenna with an inductor coil provides better performance than the two-probe offsetting antenna. For the further study of MIMO performance, the two-probe antenna with an inductor coil is used to evaluate.

CHAPTER 4
MIMO DIRECT MEASUREMENT AND MUTUAL INFORMATION RESULTS

4.1 Introduction

In this chapter, the systems with multiple antennas at the transmitter and receiver are considered, which are commonly referred to as Multiple-Input Multiple-Output (MIMO) systems. In MIMO systems, multiplexing exploits the structure of the channel gain matrix to obtain independent signaling paths that can be used to send independent data. Indeed, the initial excitement about MIMO was motivated by the pioneering work of Winters [42], Foschini [5], Foschini and Gans [6], and Teletar [7] predicting remarkable spectral efficiencies for wireless systems with multiple transmit and receive antennas. In this chapter, a MIMO theory are examined and its advantage are describe. Then, the direct measurements of the channel matrix of the proposed antennas are measured in the practical indoor environment. The mutual information results from the MIMO systems using the proposed antennas are compared with those from the system using dipole array antennas.

4.2 Fundamental of Multiple-Input Multiple-Output

4.2.1 Narrowband MIMO Model

In this section, a narrowband MIMO channel is considered. A narrowband point-to-point communication system of M_t transmit and M_r receive antennas is shown in Fig. 4.1. This system can be represented by the following discrete-time mode:

$$\begin{bmatrix} y_1 \\ \vdots \\ y_{M_r} \end{bmatrix} = \begin{bmatrix} h_{11} & \cdots & h_{1M_t} \\ \vdots & \ddots & \vdots \\ h_{M_r1} & \cdots & h_{M_rM_t} \end{bmatrix} \begin{bmatrix} x_1 \\ \vdots \\ x_{M_t} \end{bmatrix} + \begin{bmatrix} n_1 \\ \vdots \\ n_{M_r} \end{bmatrix} \tag{4.1}$$

or simply as $\mathbf{y} = \mathbf{Hx}+\mathbf{n}$. Here $\mathbf{x}$ represents the M_t-dimensional transmitted signal, $\mathbf{n}$ is the M_r-dimensional noise vector, $\mathbf{y}$ is the M_r-dimensional received signal and $\mathbf{H}$ is the $M_r \times M_t$ matrix of channel gains h_{ij} representing the gain from transmits antenna j to receive antenna i.

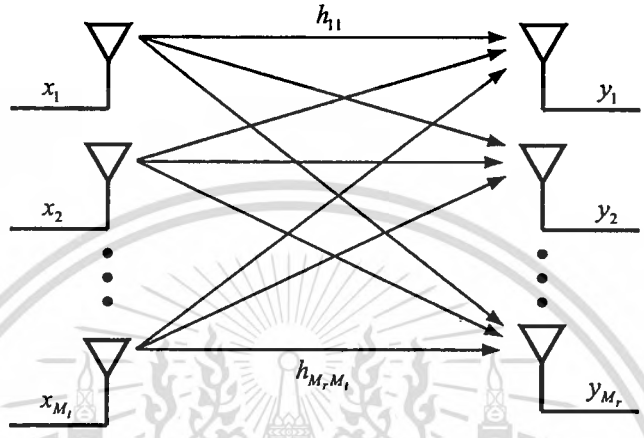

Fig. 4.1 MIMO systems

4.2.2 Parallel Decomposition of the MIMO Channel

When both the transmitter and receiver have multiple antennas, the performance gain called multiplexing gain is offered. The multiplexing gain of a MIMO system results from the fact that a MIMO channel can be decomposed into a number $R_{\mathbf{H}}$ of parallel independent channels. Because $R_{\mathbf{H}}$, the rank of matrix $\mathbf{H}$, can not exceed the number of columns or rows of $\mathbf{H}$, it follows that $R_{\mathbf{H}} \leq \min(M_t, M_r)$. If $\mathbf{H}$ is full rank, which is referred to as a rich scattering environment, then $R_{\mathbf{H}} = \min(M_t, M_r)$. Other environments may lead to a low-rank $\mathbf{H}$: a channel with high correlation among the gains in $\mathbf{H}$ may have rank 1. By multiplexing independent data onto these independent channels, an $R_{\mathbf{H}}$ -fold increase in data rate can be obtained in comparison with a system with just one antenna at the transmitter and receiver. This increased data rate is called the multiplexing gain. In this section, the approach to obtain independent channels from a MIMO system is described.

Consider a MIMO channel with $M_r \times M_t$ channel gain matrix $\mathbf{H}$. Let $R_{\mathbf{H}}$ denotes the rank of $\mathbf{H}$, for any matrix $\mathbf{H}$, its singular value decomposition (SVD) can be obtained as [7], [16]

$$\mathbf{H}=\mathbf{U}\Sigma\mathbf{V}^{\mathbf{H}} \quad (4.2)$$

where

$$\Sigma = diag\left(\sigma_1,\ldots,\sigma_{R_\mathbf{H}}\right) \in R^{M_r \times M_t} \; ;\sigma_1 \geq \sigma_2 \geq \ldots \geq \sigma_{R_\mathbf{H}} \geq 0 \tag{4.3}$$

$$\mathbf{U} = \left[\mathbf{u_1},\ldots,\mathbf{u_m}\right] \in C^{M_r \times M_r} \tag{4.4}$$

$$\mathbf{V} = \left[\mathbf{v_1},\ldots,\mathbf{v_m}\right] \in C^{M_t \times M_t} \tag{4.5}$$

The $M_r \times M_r$ matrix $\mathbf{U}$ and the $M_t \times M_t$ matix $\mathbf{V}$ are unitary matrices which imply that $\mathbf{U^H U}=\mathbf{I}_{Mr}$ and $\mathbf{V^H V}=\mathbf{I}_{Mt}$. Σ is $M_r \times M_t$ diagonal matrix of singular values $\{\sigma_i\}$ of $\mathbf{H}$. These singular values have the property that $\sigma_i = \sqrt{\lambda_i}$ for λ_i that is the i th largest eigenvalue of $\mathbf{HH}^H$ and $\mathbf{H}^H\mathbf{H}$, and $R_\mathbf{H}$ of these singular value are nonzero.

The parallel decomposition of the channel is obtained by defining a transformation on the channel input and output $\mathbf{x}$ and $\mathbf{y}$ via transmit precoding and receiver shaping [43]. In transmit precoding the input $\mathbf{x}$ to the antenna is generated by a linear transformation on input vector $\tilde{\mathbf{x}}$ as $\mathbf{x} = \mathbf{V}\tilde{\mathbf{x}}$. Receiver shaping performs a similar operation at the receiver by multiplying the channel output $\mathbf{y}$ by $\mathbf{U}^H$, as shown in Fig. 4.2.

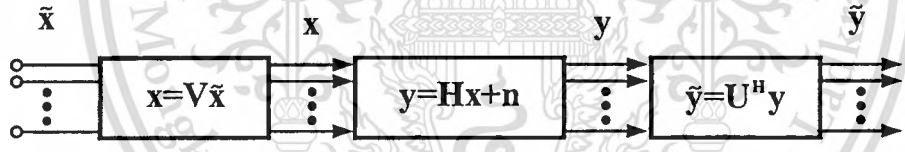

Fig. 4.2 Transmit precoding and receiver shaping

The transmit precoding and receiver shaping transform the MIMO channel into $R_\mathbf{H}$ parallel Single-Input Single-Output (SISO) channels with input $\tilde{\mathbf{x}}$ and output $\tilde{\mathbf{y}}$, since from the SVD we have

$$\begin{aligned}
\tilde{\mathbf{y}} &= \mathbf{U}^H\left(\mathbf{Hx}+\mathbf{n}\right) \\
&= \mathbf{U}^H\left(\mathbf{U}\Sigma\mathbf{V}^H\mathbf{x}+\mathbf{n}\right) \\
&= \mathbf{U}^H\left(\mathbf{U}\Sigma\mathbf{V}^H\mathbf{V}\tilde{\mathbf{x}}+\mathbf{n}\right) \\
&= \mathbf{U}^H\mathbf{U}\Sigma\mathbf{V}^H\mathbf{V}\tilde{\mathbf{x}}+\mathbf{U}^H\mathbf{n} \\
&= \Sigma\tilde{\mathbf{x}}+\mathbf{n}
\end{aligned} \tag{4.6}$$

where $\tilde{\mathbf{n}} = \mathbf{U}^H \mathbf{n}$. Note that multiplication by a unitary matrix does not change the distribution of the noise, then $\mathbf{n}$ and $\tilde{\mathbf{n}}$ are identically distributed in the Additive White Gaussian Noise (Noise) channel. Thus, the transmit precoding and receiver shaping transform the MIMO channel into $R_{\mathbf{H}}$ parallel independent channels, where the i th channel has input $\tilde{x}_i$, output $\tilde{y}_i$, noise $\tilde{n}_i$, and channel amplitude gain σ_i. Note that these σ_i are related because they are all functions of $\mathbf{H}$, but since the resulting parallel channels do not interfere with each other, it can be said that the channels with these gains are independent-linked. This parallel decomposition is shown in Fig. 4.3. By sending independent data across each of the parallel channels, the MIMO channel can support $R_{\mathbf{H}}$ times the data rate of a system with just one transmit and receive antenna, leading to a multiplexing gain of $R_{\mathbf{H}}$. Note, however, that the performance on each one of the channels will depend on its gain σ_i.

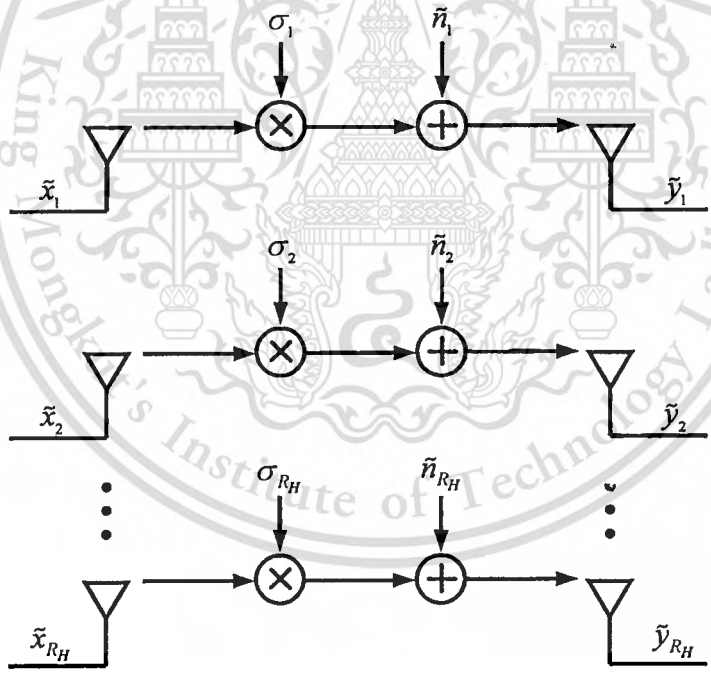

Fig. 4.3 Parallel decomposition of the MIMO channel

4.2.3 MIMO Channel Capacity

The mathematical theory of communication underlying channel capacity was pioneered by Claude Shannon in the late 1940s [4]. This theory is based on the notion of mutual information between the input and output of a channel. In particular, Shannon defined channel capacity as the channel's mutual information maximized over all possible input distributions. Capacity equals the maximum data rate that can be transmitted over the channel with arbitrarily small error probability. Capacity versus outage defines the maximum rate that can be transmitted over the channel with some nonzero outage probability. The capacity of a MIMO channel is an extension of the mutual information formula for a SISO channel. In general, the fading channel capacity with channel fade level information at both the transmitter and receiver is achieved when the transmitter adapts it power, data rate, and coding scheme to channel variation. The optimal power allocation in this case is a "water-filling", where power and data rate are increased when channel conditions are favorable and decreased when channel conditions are not favorable. However, in this thesis, the optimal power allocation water filling is not assumed. Then, the maximized mutual information of the capacity is not yielded. The channel's mutual information results are achieved. This mutual information is the mutual information for equal power allocation and it is optimum if the transmitter does not know the channel state information (CSI).

For an M_t -transmit M_r -receive antenna system of the uniform power transmission, mutual information $I(\mathrm{X}:\mathrm{Y})$ is given by

$$I(\mathbf{X};\mathbf{Y}) = B\log_2 \det\left[I_{M_r} + \frac{\rho}{M_t} HH^H \right] \tag{4.7}$$

where $\rho = P/\sigma^2$. P_i is the transmission power of each channel, σ_0^2 is noise power and B is the bandwidth.

Using the SVD of **H**, we can express this as [7], [16]

$$I(\mathrm{X};\mathrm{Y}) = \sum_{i=1}^{R_H} B\log_2(1+\gamma_i), \text{ bits/s} \tag{4.8}$$

where $\gamma_i = \sigma_i^2 \rho$.

To consider the mutual information over the frequency spectrum,

$$\frac{I(\mathbf{X};\mathbf{Y})}{B} = \sum_{i=1}^{R_H} \log_2(1+\gamma_i), \quad \text{bits/s/Hz} \tag{4.9}$$

$$\frac{I(\mathbf{X};\mathbf{Y})}{B} = \sum_{i=1}^{R_H} \log_2\left(1+\sigma_i^2 \frac{P_i}{\sigma_0^2}\right), \text{ bits/s/Hz} \tag{4.10}$$

Usually, the MIMO channel mutual information reported by most of the existing studies was investigated under a constant received power condition and assumed transmission power control [6], [8], [9]. However, in order to evaluate the effect of antenna gain on mutual information, power allocation was not used in this calculation. In this thesis, the channel matrix **H** should be the real matrix in the propagation environment including the part of antenna and propagation loss. Power in each channel and noise power were calculated from the transmitted power levels and the noise floor of the receiver according to IEEE Std 802.11a [44] which the transmission power control is not considered. For the 5.15 to 5.25 GHz band, the total maximum output power was equal to 40 mW. Since each transmitter transmitted an independent data stream of power, power in each channel equals 20 mW or 13 dBm. According to IEEE Std 802.11a, the noise figure of the receiver was equal to 10 dB, noise power was equal to -91 dBm over the 20 MHz bandwidth. Finally, by using power in each channel, noise power and eigenvalues, mutual information was obtained. From the value of the above power in each channel and noise power, the calculated Signal to Noise Ratio (SNR) was 104 dB which was rather high from the SNR used in an optimal power allocation system. However, these power in each channel and noise power are actually used in WLAN IEEE 802.11a. This SNR value was calculated without the consideration of the propagation loss since this effect was already included in the matrix **H**. In the calculation of mutual information of the proposed antenna and the dipole array antennas, the same values of power in each channel and noise power were used.

4.3 Measurement Procedure

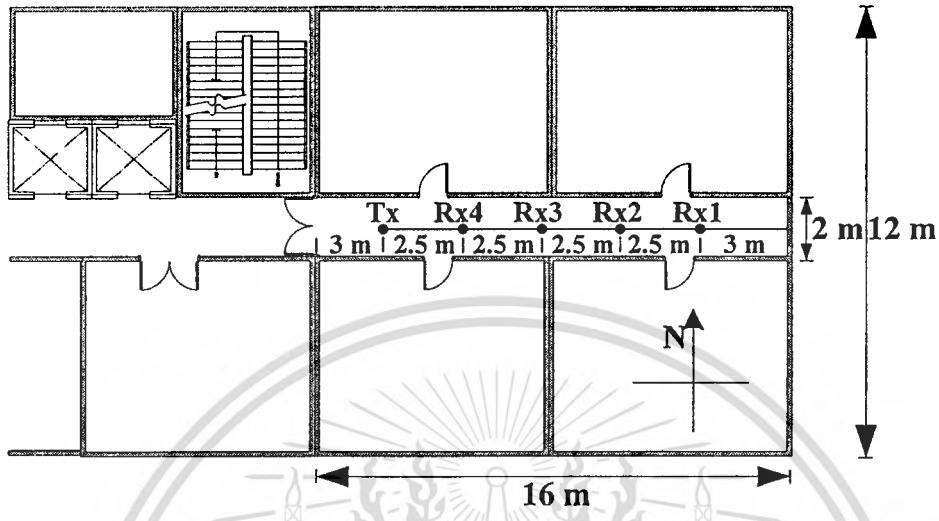

Fig. 4.4 Layout of the measured floor

The MIMO channel measurement data of the proposed antenna was conducted in a corridor on the 10th floor of the Krom Luang Naradhiwas Rajanagarindra building, King Mongkut's Institute of Technology Ladkrabang as shown in Fig. 4.4. There are laboratory rooms with thick glass windows and wooden doors along both sides of the corridor. The experiment was not extended into the office room since the bidirectional radiation pattern of the proposed antenna is expected to cover only the service area in corridor. The width of the corridor is 2 m and the length is 16 m. The ceiling is 3 m above the floor. Wideband measurements were performed in the range of 4.8 GHz to 6.2 GHz which corresponds to the frequency bandwidth of the proposed circular ring antenna. This frequency bandwidth was also limited by the bandwidth of the amplifier and the switch that were used in the measurement. The channel is considered as wide-sense stationary (WSS) within this bandwidth and measurements were conducted in such a way that both transmitter and receiver were fixed at one location when the 801 frequency samples were recorded. These samples are treated as different channel realizations to draw cumulative distribution function (CDF). The transmitting antenna was installed at the center of the ceiling in the corridor marked as Tx in Fig. 4.4. The receiving antenna with a height of 1.5 m from the floor was installed on a tripod at the center of the floor. All the locations represent Line-of-Sight (LoS) scenarios where the transmitter and receiver separation was

varied from 10 m to 2.5 m corresponding to Rx1 to Rx4 in Fig. 4.4. At Rx1, the receiving antenna was 3 m away from one end of the corridor where the other end of the corridor is a glass door that was opened during the measurement. This glass door opens to the elevator hall and leads to another corridor on the opposite side of the building.

Eight sets of Tx-Rx antennas were utilized. The first four sets used the same kind of antennas for Tx and Rx namely: two-probe antenna, offset probe antenna, inductive coil antenna and the dipole array antennas. The next three sets used the dipole array antennas as the Rx with the other antenna as Tx. The dipole antenna with a center frequency of 5.2 GHz was used as the element of the 1λ horizontally spaced vertically polarized dipole array antennas. This dipole array antennas represents both the conventional transmitting antenna at the access point and the receiving antenna at the user terminal. Although in practical WLAN communications, the bidirectional dual-polarized antenna is proposed to be used at the access point and the dipole array antennas is usually used at the user terminal, the used of bidirectional dual-polarized antennas at both transmitting and receiving sides is also studied to investigate the MIMO channel characteristics by using these antennas. The corridor environment, transmitter and receiver antennas are illustrated in Figs. 4.5 to 4.10.

Fig. 4.5 Corridor environment

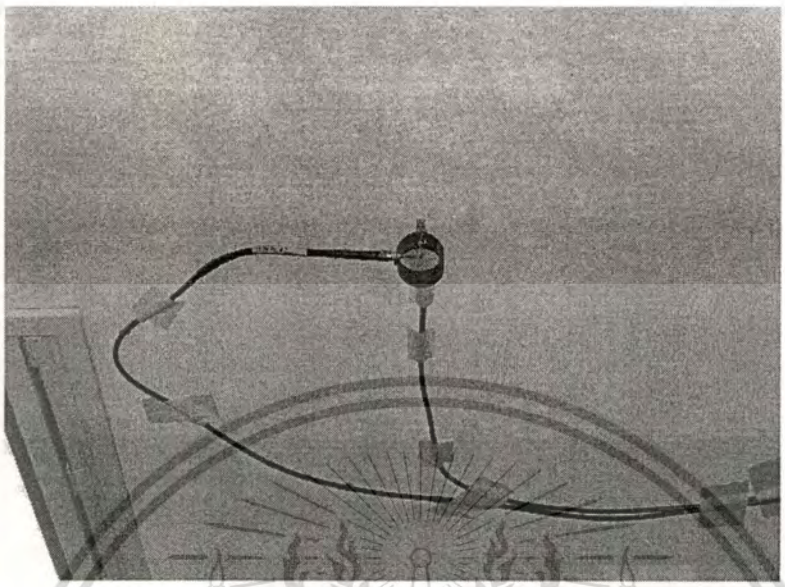

Fig. 4.6 Circular ring antenna on the ceiling for the transmitter

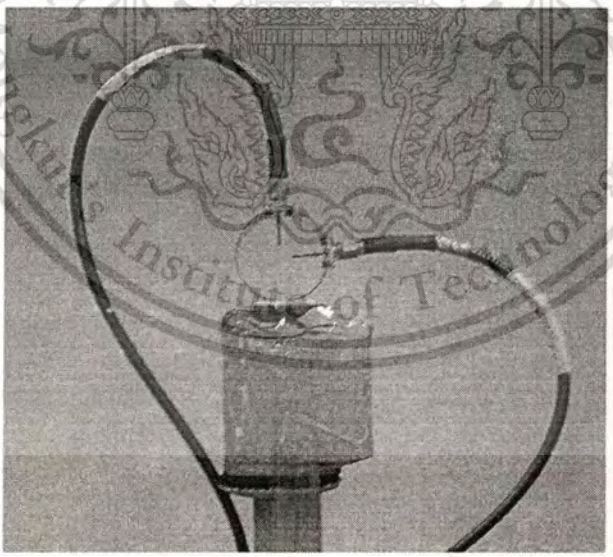

Fig. 4.7 Circular ring antenna on the floor for the receiver

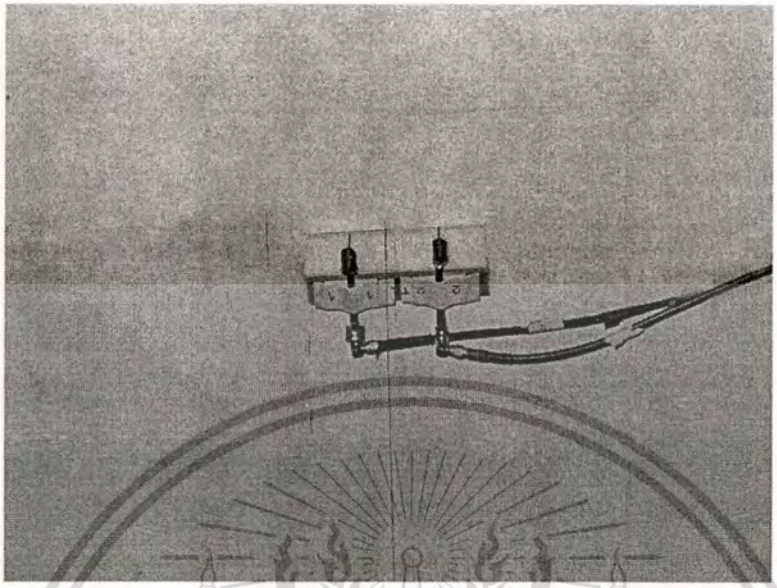

Fig. 4.8 Dipole array antennas on the ceiling for the transmitter

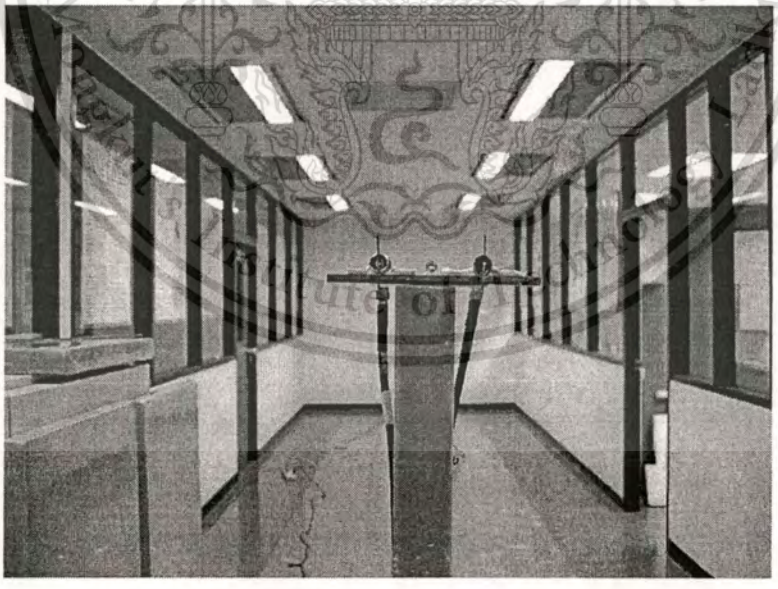

Fig. 4.9 Dipole array antennas on the floor for the receiver (Note: see the wall behind the receiver)

Fig. 4.10 Transmitting and receiving antennas in corridor environment

The wideband signal with 10 dBm of power from port 1 of a network analyzer was amplified by a power amplifier to transmit 20 dBm of power for all measurements. A switch was used for selecting the element of the transmitting antenna just as a switch was also used for selecting the receiving element of the antenna. A low noise amplifier (LNA) amplified the received signal from the antenna by 5 dB gain before sending it to port 2 of the network analyzer. The diagram of the equipment set-up in the measurement is shown in Fig. 4.11. The S_{21} was measured in this measurement and the effects of the transmission lines, switches and amplifiers were compensated by the offline calibration. During the measurement, when the transmitting switch selects element 1 of the transmitting antenna, the receiving switch would select element 1 then element 2 of the receiving antenna. During this time, the unused antenna ports are connected to the switch ports via the transmission lines which yield the same result as connecting the unused antenna ports with the 50 Ω loads. After recording the data, the transmitting switch will change to select element 2 of the transmitting antenna and the receiving switch again, selects element 1 then element 2 of the receiving antenna. During the measurement, the movement of people was not allowed to keep the channel static.

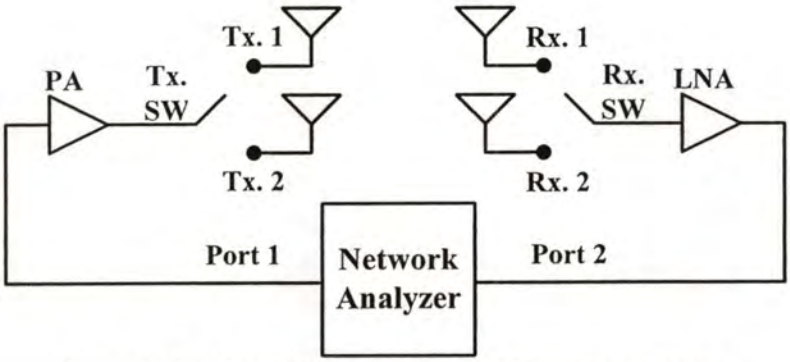

Fig. 4.11 Mutual information measurement set-up

4.4 Mutual Information Results

The mutual information results at 10% outage probability of different antenna setup from 4 points of the measurement are shown in Table 4.1 and Table 4.2. The mutual information performances of the two-probe antenna, offset probe antenna, and two-probe antenna with inductive coil which have different isolation between the two probes are discussed.

From Table 4.1 and Table 4.2, the mutual information from the use of the two-probe antenna is higher than that of the dipole array antennas. Moreover, the antennas that improve the isolation, i.e. offset probe antenna and two-probe antenna with inductive coils, have the higher mutual information than the two-probe antenna without isolation improvement. It can be concluded that the improvement of the isolation can increase the mutual information of the MIMO systems.

Table 4.1

Comparison of 10% outage mutual information (bits/s/Hz) for same antennas as the transmitter and the receiver

Antenna	Rx1	Rx2	Rx3	Rx4
Two-probe	41.66	42.91	46.86	49.84
Offset probe	42.39	44.20	47.13	49.39
Inductive coil	43.77	45.55	48.86	52.38
Dipole Array	38.62	40.29	43.90	44.47

In Table 4.1, at point 1, the use of the two-probe antenna with an inductive coil yields the highest mutual information of 43.77 bits/s/Hz and is 5.15 bits/s/Hz or 13.34% higher than the use of the dipole array antennas. The offset probe antenna provides a higher mutual information than the two-probe antenna. The mutual information at the measured point is increased when the distance between the transmitter and the receiver is decreased, that is the mutual information of point 2 is higher than that of point 1 and maximum mutual information occurs at point 4. This effect is due to the higher receiver signal when the receiver approaches closer to the transmitter. The difference of the mutual information between the measured points is approximately 1–4 bits/s/Hz.

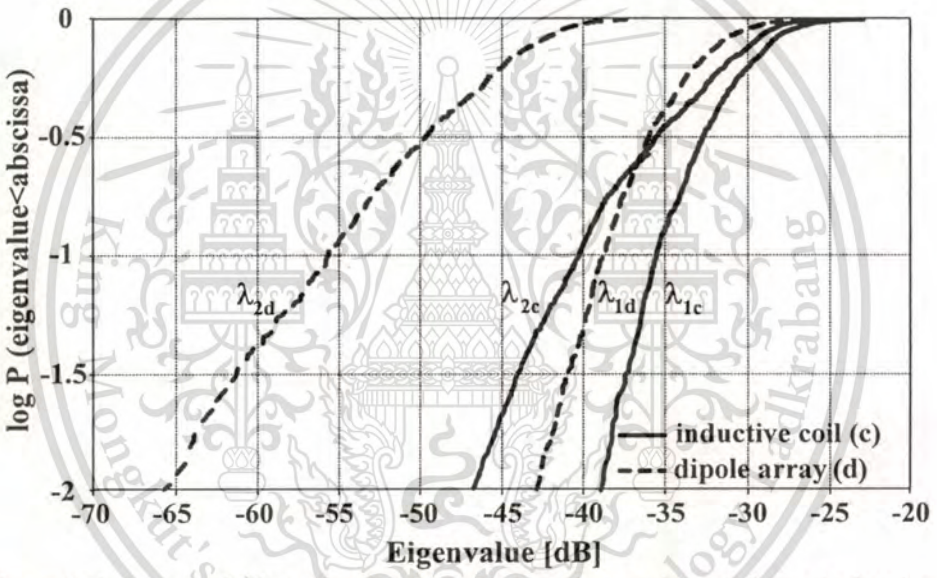

Fig. 4.12 Cumulative probability distribution of the eigenvalues of the inductive coil antenna and the dipole array antennas at Rx1

Fig. 4.12 shows the empirical cumulative distribution function (CDF) of the eigenvalues of the MIMO channels that use the same antennas at both transmitting and receiving sides. The use of the two-probe antenna with inductive coil for both transmitting and receiving antennas are compared with that of the dipole array antennas. λ_{1c} and λ_{2c} are the first and second eigenvalues of the two-probe antenna with inductive coil, respectively whereas λ_{1d} and λ_{2d} are the first and second eigenvalues of the dipole array antennas, respectively. There are two points that should be discussed from Fig. 4.12. First, both eigenvalues of the two-probe antenna with inductive coil (λ_{1c} and λ_{2c}) are in

the same level of amplitude whereas the eigenvalues of the dipole array antennas have a large gap between them. The 10% outage probability of λ_{1c} and λ_{2c} of the two-probe antenna with inductive coil are -35.57 dB and -40.67 dB, respectively whereas the λ_{1d} and λ_{2d} of the dipole array antennas are -38.84 dB and -55.67 dB, respectively. It can be concluded that the use of the bidirectional dual-polarized antenna provides two strong uncorrelated channels whereas the use of the dipole array antennas provides only one significant channel in the corridor environment. This result is already a well-known advantage of the dual-polarized antenna that usually provides two uncorrelated channel regardless of the environment. The large gap between the eigenvalues of the dipole array antennas has an effect on the mutual information when compared with the maximal condition under which all the eigenvalues are equal in case of dual-polarized antenna. The mutual information comparison between the dual-polarized antenna and copolarized configuration can be found in [12] that the dual-polarized antenna provides higher mutual information than the copolarized elements. Second, from the result in Fig.4.12, it can be observed that λ_{1c} of the two-probe antenna with inductive coil is 3.33 dB higher than λ_{1d} of the dipole array antennas. This value is the same value of the difference between the gain of the two-probe antenna with inductive coil and dipole array antennas. However, this result has a small influence on the final mutual information results. Consequently, since λ_{1c} and λ_{2c} of the two-probe antenna with inductive coil are higher than λ_{1d} and λ_{2d} of the dipole array antennas, the mutual information of the two-probe antenna with inductive coil is higher than that of the dipole array antennas. Moreover, at the other Rx positions, the mutual information results of the two-probe antenna with inductive coil are higher than those of the dipole array antennas. These results can confirm the advantage of using this proposed antenna in the corridor environment. The mutual information results of the two-probe antenna with inductive coil and dipole array antennas correspond to the results in Fig. 4.12 are shown in Table 4.1 together with the mutual information of different antenna configurations.

Table 4.2

Comparison of 10% outage mutual information (bits/s/Hz) for different antennas as the transmitter and dipole array antennas as the receiver

Tx Antenna (Rx Antenna:Dipole Array)	**Rx1**	**Rx2**	**Rx3**	**Rx4**
Two-probe	38.74	40.40	43.99	44.53
Offset probe	38.88	41.05	44.19	44.85
Inductive coil	40.60	42.22	45.05	46.54

In Table 4.2, the dipole array antennas is used at the receiving side as the user terminal antenna and the proposed bidirectional dual-polarized antennas are used at the transmitting side as the access point antenna. All of the results show a higher mutual information by using the proposed antenna at the access point than by using the dipole array antennas at the access point as in the case of traditional communications. This result confirms the interesting view of using this proposed antenna as the access point antenna in WLAN systems. The use of the two-probe antenna with inductive coil as the transmitting antenna provides the highest mutual information of 40.60 bits/s/Hz which is 2 bits/s/HZ or 5.18% higher than the use of the traditional dipole array antennas. Note that the mutual information results in Table 4.2 are increased when the distance between the transmitter and receiver is decreased.

From Table 4.1 and Table 4.2, the mutual information from the use of the two-probe antenna is higher than that of the dipole array antennas. Moreover, the antennas that improve the isolation, i.e. offset probe antenna and two-probe antenna with inductive coils, have the higher mutual information than the two-probe antenna without isolation improvement. It implies that the improvement of the isolation can increase the mutual information of the MIMO system. Specifically, the mutual information of the antenna can be improved by 2 bits/s/Hz from the inductive coil technique. For example, in Table 4.1, the use of the two-probe antenna with inductive coil antenna as the transmitting and the receiving antennas has the mutual information of 2.11 bits/s/Hz or 5.06% higher than the use of the two-probe antenna as the transmitting and the receiving antennas.

4.5 Conclusion

In this chapter, the basic of the MIMO communications and mutual information of the MIMO channel based on the SVD approached are describes. The appropriate mutual information can be achieved with the compact structure of the proposed two-probe excited circular ring antenna. Because of the dual polarization and the higher antenna gain, the use of the proposed antenna provides higher mutual information, by 3 bits/s/Hz, than the use of the 1λ horizontally spaced vertical polarization dipole array antennas in the corridor environment. Especially, the use of the two-probe antenna with an inductive coil as the transmitting and receiving antennas provides the highest mutual information result. The independent two parallel channels can be observed for the proposed dual-polarized antenna. Inserting the inductive coil between the two probes can improve the isolation and the mutual information performance of the proposed antenna.

CHAPTER 5
DOUBLE DIRECTIONAL CHANNEL MEASUREMENT AND MUTUAL INFORMATION RESULTS

5.1 Introduction

In this chapter, the double directional channel measurement in a corridor is presented. Multipath parameters including polarimetric path weight matrix, DoD, DoA, and path delay are extracted from the sounding measurement data. Depolarization of signal was studied in terms of cross polarization power ratio (*XPR*) [30], [31]. Angular power spectrum and angular spread of incoming signal in a corridor environment were also investigated. The extracted multipath parameters can be used in combination with the directivity of any assessed antennas to create a complete channel model like the evaluation approach in [45]. Consequently, the mutual information that corresponds to these channel responses can be obtained. Here, the mutual information of a MIMO system with two-probe antenna, offset probe antenna, two-probe antenna with inductive coil and 1λ horizontally-spaced vertically-polarized dipole array antennas are compared with each other.

5.2 Double Directional Channel Measurement

Double directional channel measurement directly describes the properties of the physical multipath propagation channel. Ideally, such measurements are independent of the properties associated with the measurement antennas. This representation models the channel in wave number space according to the directional impulse response $M(\mathbf{k},\mathbf{k}',t)$ where $\mathbf{k}$ and $\mathbf{k}'$ are vectors associated with receive and transmit wave number (direction), t is time, and single polarization has been assumed. Assuming only far-field propagation mechanisms, $\mathbf{k}$ and $\mathbf{k}'$ are unit vectors in the propagation direction, with wave propagation at the speed of light. For simplicity, the fields at the receiver are typically modeled as a discrete set of plane-wave according to

$$M(\mathbf{k},\mathbf{k}',t) = \sum_{l=1}^{L} \gamma_l e^{j\phi_l} \delta(t-\tau_l)\delta(\mathbf{k}-\mathbf{k}_l)\delta(\mathbf{k}'-\mathbf{k}'_l) \quad (5.1)$$

where $\delta(\bullet)$ is the Dirac delta function, and the lth multipath component has amplitude γ_l that is equal $\gamma^{pp}, \gamma^{pq}, \gamma^{qp}$, and γ^{qq} that are complex polarimetric path weights for the different transmitting and receiving polarizations, phase ϕ_l, TDoA τ_l, DoA $\mathbf{k}_l$, and DoD $\mathbf{k}'_l$. Intuitively, each multipath component corresponds to a plane wave arriving at a specific time and directions at the receiver due to energy launched in a specific transmit direction. When the true channel behavior is well presented by (5.1), the multipath parameters maybe measured using conventional beamforming, basis matching techniques, or parametric estimation algorithms such as Estimation of Signal Parameters by Rotational Invariance Techniques (ESPRIT).

The estimated data can then be used to access the MIMO performance for any desired transmit/receive antenna configuration as well as for local movement of the arrays within this environment. This post-measurement flexibility is not possible with direct measurement of **H**, since in that case the antennas become part of the measured channel.

5.3 Measurement Procedure

This section describes the corridor channel measurement campaign that conducted on the 3rd floor of the south 6 building, Tokyo Institute of Technology, Japan. The layout and photograph are shown in Fig. 5.1. The width of the corridor is 2 m and the length is 64 m, with lecture rooms along both sides. The wall along the corridor and between the rooms were made of reinforced concrete with wooden office doors. The floor was rubber sheets on concrete and the ceiling was covered with metal grid (approximately 50 cm gap between the metal grid and the concrete layer). The height of the corridor was 2.45 cm. There were metal pipes between concrete layer and metal grid. A wideband measurement was performed in the 5 GHz band where the center frequency is 4.5 GHz with bandwidth of 120 MHz. using the Medav RUSK-Fujitsu MIMO channel sounder [22]. The periodic multi-frequency test signal used in the measurement had a repetition period of 0.8 μs and a bandwidth of 120 MHz. The measurement was based on MIMO channel with a polarimetric rectangular array antenna as the transmitting antenna (Tx) and a stacked uniform polarimetric circular patch array antenna as the receiving antenna (Rx). For every position in the measurements, the transmitting antenna height is 180 cm and the receiving

antenna height is 115 cm. The transmitted power in all measurements was fixed at 30 dBm and the time interval of the MIMO switch was 1 ms. Because the transmitting power was restricted by the transmission license, the Tx and Rx were separated only at a maximum distance of 26 m. All of the locations measured represented the Line-of-Sight (LoS) scenarios where the Tx-Rx separation varied from 26 m to 16 m. These separations corresponded to Rx1 to Rx4 in Fig. 5.1. The Tx was fixed at the location marked as "Tx" in Fig. 5.1. It should be noted that there was an emergency door 5 m behind the Tx. The Rx azimuth equals 0° was pointing at the Tx at all locations. For all measurements, dual-polarized elements were used in both transmitting and receiving array antennas to obtain a polarization matrix of the environment. The complex frequency responses were computed on-line and stored into the sounder's hard disk for subsequent off-line post-processing. At each point in the measurement, 500 snapshots were taken. During the measurement, people were not allowed to move around in order to keep the channel static. The Tx and Rx antennas were de-embedded from the channel response for estimation of the parameters. In order to obtain a correct extraction of the multipath parameters, the Tx and Rx had to be properly synchronized in time and frequency. This was done by connecting the Tx and Rx units via optical fibers. Moreover, the effect of signal propagation through the cable and the signal processing delays were eliminated by doing back-to-back calibration. The complex frequency response data from the sounding measurement was processed off-line by using the RIMAX algorithm [29], a multi-dimensional maximum likelihood algorithm, to extract the multipath parameters.

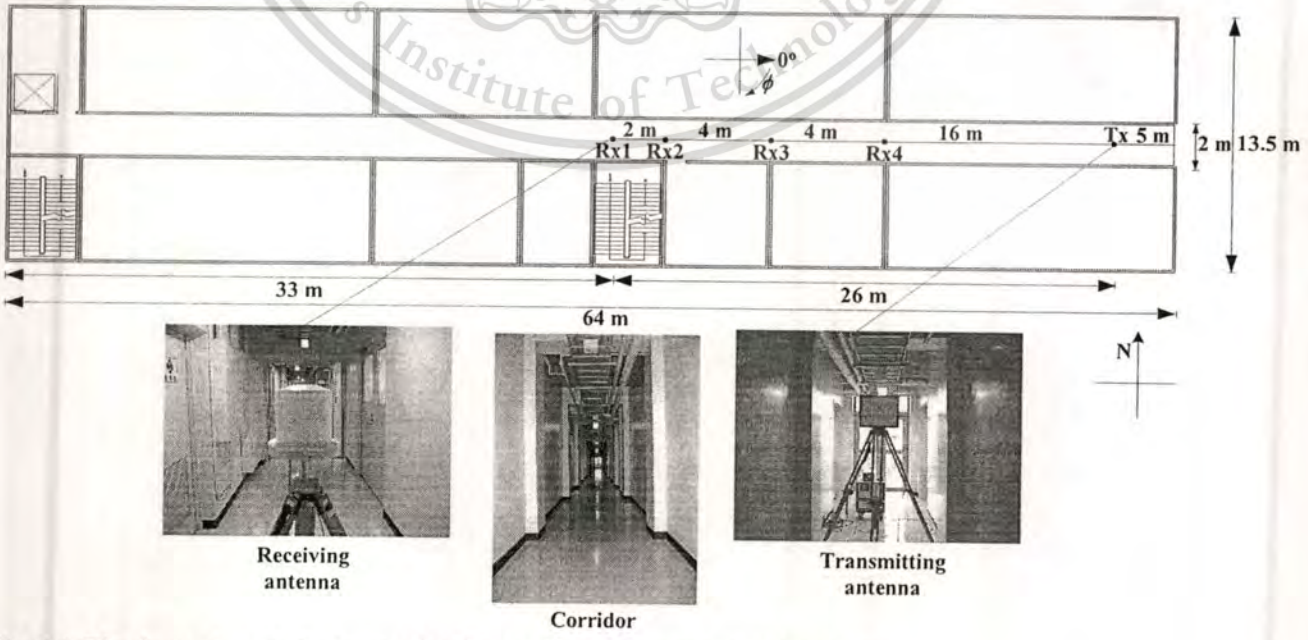

Fig 5.1 The layout and photograph of sounding measurement location

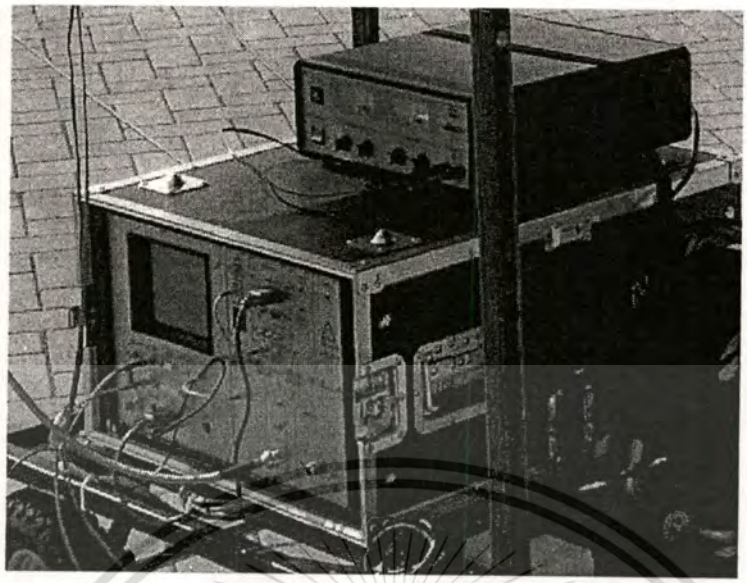

Fig 5.2 RUSK Fujitsu transmitter unit (Tx)

Fig 5.3 RUSK Fujitsu receiver unit (Rx)

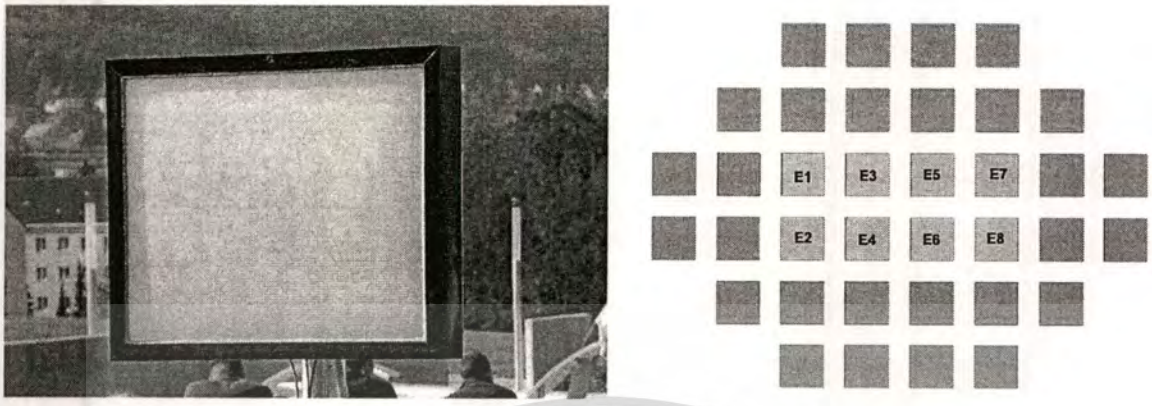

Fig 5.4 Transmitting antenna: Polarimetric rectangular array (PURA) (a) antenna (b) element assignment

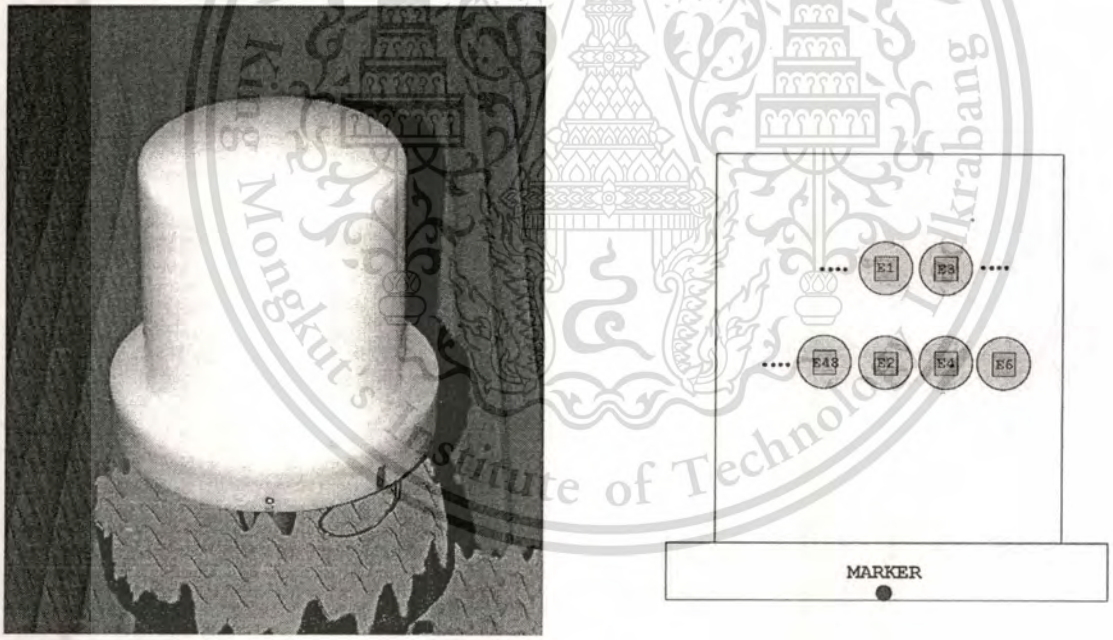

Fig 5.5 Receiving antenna: Stacked polarimetric uniform circular patch array (SPUCPA) (a) antenna (b) element assignment

5.4 Data Extraction

RIMAX algorithm [29] is an offline processing for MEDAV RUSK MIMO channel sounding measurements. This algorithm is used to estimate radio channel parameters from channel sounding measurement based on MATLAB™ function. RIMAX

uses two components to model the radio channel between transmitter and receiver. One component is the ray-optical model which describes the radio channel by superposition of a finite sum of concentrated (specular-alike) propagation paths. The second component describes the contribution of distributed diffuse scattering to the radio channel [29]. Depend on the detail of the measurements, the algorithm can estimates the four coefficients of the polarimetric path weight matrix, the azimuth and elevation at the TX-site, azimuth and elevation at the RX-site, the path delay, and the Doppler-shift of the specular components. The RIMAX estimates the parameter by using the maximum likelihood parameter estimators SAGE and a gradient based method GRAD. The RIMAX algorithms are applied to enhance the resolution of the channel that is usually limited by the available measurement aperture in the space-frequency-time domain by fitting an appropriate data model to the measured data. This resolution is only limited by the SNR, the measurement device calibration error, and the limited validity of the data model [29].

The RIMAX program is running under Windows and Linux. The machine should have at least 1 GB RAM. An example: 193 frequency bins × 16 Tx ports × 16 Rx ports × 3 snapshots for Doppler estimation and around 70 path 3000 snapshots will need around 1 week on a P4 2GHz 1Gbyte RAM. RIMAX can also run as a background service. The core algorithm is a maximum likelihood estimator. The objective is to find parameters for the propagation path model and the dense multipath component, such that the remainder is small and contains only white noise. The estimator minimizes the weighted difference between the channel observation and the reconstructed radio channel. The channel is reconstructed using the propagation path parameters. For the optimal weighting of the difference between measurement and estimated channel model, the estimated distribution of the Dense Multipath Component (DMC) is used. The RIMAX algorithm determines the number of propagation paths for each channel snapshot. The decision is made on the reliability of the determined propagation path parameters. The reliability is measured as the ratio between estimated propagation path power and the variance of this estimated power. A path is considered reliable if the certainty of the parameters is higher than their uncertainty. The user has to provide the necessary information to reconstruct the radio channel, the main information is about the antenna arrays. Furthermore, some information how to interpret the channel measurements is needed.

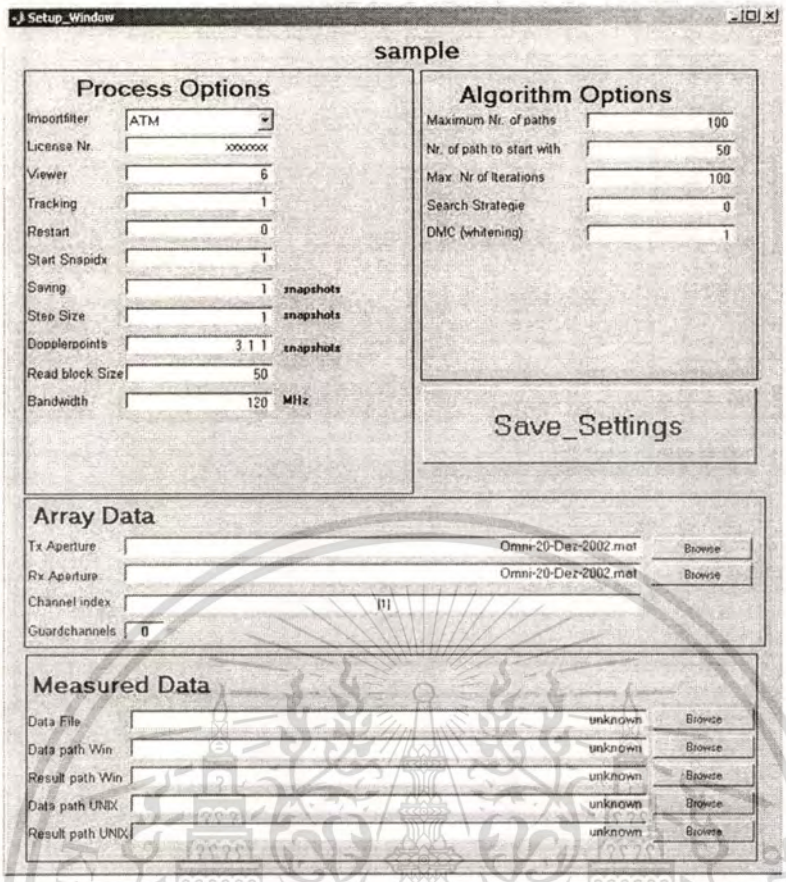

Fig 5.6 The user interface of RIMAX program

5.5 Channel Characteristics Result

To investigate the depolarization of the signal in the corridor environment, the cross polarization power ratio (*XPR*) [30], [31] term of each detected path is used. The centroid of the cross polarization power ratio (*XPRC*) and the spread of the cross polarization power ratio (*XPRS*) were calculated at each measured point and used to evaluate the depolarization of the environment as follow.

$$XPR_V = \left(\left| \frac{\gamma^{\mathrm{pp},k}}{\gamma^{\mathrm{qp},k}} \right|^2 \right) \tag{5.2}$$

$$XPR_H = \left(\left| \frac{\gamma^{\mathrm{qq},k}}{\gamma^{\mathrm{pq},k}} \right|^2 \right) \tag{5.3}$$

where XPR_V and XPR_H are the cross polarization power ratio and the $\gamma^{\mathrm{pp}}, \gamma^{\mathrm{pq}}, \gamma^{\mathrm{qp}}$, and γ^{qq} are complex polarimetric path weights for the different

transmitting and receiving polarizations. The first and second subscripts indicate the polarization at the receiver and transmitter ends, respectively, where p and q are the vertical and horizontal polarizations. k is the index of the detected paths.

In this thesis, the centroid of the cross polarization power ratio (*XPRC*) and the spread of the cross polarization power ratio (*XPRS*) are calculated at each measured point for evaluating the depolarization of the environment. The *XPRC* can be presented as

$$XPRC_V = \frac{\sum_{k=1}^{K} XPR_{V,k} \cdot P_{V,k}}{\sum_{k=1}^{K} P_{V,k}} \tag{5.4}$$

$$XPRC_H = \frac{\sum_{k=1}^{K} XPR_{H,k} \cdot P_{H,k}}{\sum_{k=1}^{K} P_{H,k}} \tag{5.5}$$

where

$$P_{V,k} = \left|\gamma_{\mathrm{pp},k}\right|^2 + \left|\gamma_{\mathrm{qp},k}\right|^2 \tag{5.6}$$

$$P_{H,k} = \left|\gamma_{\mathrm{qq},k}\right|^2 + \left|\gamma_{\mathrm{pq},k}\right|^2 \tag{5.7}$$

and *XPRS* can be obtained from

$$XPRS_V = \sqrt{\frac{\sum_{k=1}^{K} \left(XPR_{V,k} - XPRC_V\right)^2 \cdot P_{V,k}}{\sum_{k=1}^{K} P_{V,k}}} \tag{5.8}$$

$$XPRS_H = \sqrt{\frac{\sum_{k=1}^{K} \left(XPR_{H,k} - XPRC_H\right)^2 \cdot P_{H,k}}{\sum_{k=1}^{K} P_{H,k}}} \tag{5.9}$$

where K is the total number of estimated paths.

Table 5.1 Angular spread, *XPRC*, *XPRS*, and Front-to-Back ratio (F/B).

Rx	$XPRC_V$ [dB]	$XPRC_H$ [dB]	$XPRS_V$ [dB]	$XPRS_H$ [dB]	Angular Spread		F/B [dB]
					Front	Back	
Rx1	-0.3	-1.8	6.7	7.2	3.8°	4.2°	30.0
Rx2	2.6	-0.9	4.8	5.5	1.2°	3.2°	31.3
Rx3	5.7	2.3	3.4	3.8	1.1°	2.9°	37.8
Rx4	7.2	6.5	2.3	2.1	0.9°	2.7°	42.5

The *XPRC* and *XPRS* results are shown in Table 5.1. The $XPRC_V$ results of vertical polarization were mainly positive except at Rx1 where there was depolarization. As for the results of the $XPRC_H$ of horizontal polarizations, depolarizations could be observed at Rx1 and Rx2 but there were no depolarizations at Rx3 and Rx4. The *XPRS* of 2 to 7 dB could be observed in both polarizations. The angular spreads at the front of the receiver in the corridor environment, shown in Table 5.1, varied from 0.9° to 3.8°. In this small angular spread environment, the separation between the dipole array antennas is very large to achieve the uncorrelated channel, i.e. 10-20λ. This result shows the advantage of the proposed dual polarized antenna that can have a compact size with the independent channel. This result agreed well with the measurement reported in [46]. These *XPRC* and angular spread had an influence on the mutual information of the investigated antennas. The discrete azimuth angular power spectrums at Rx1 for vertical and horizontal polarizations are shown in Figs. 5.7(a) and (b), respectively. They have bidirectional patterns which were similar to the shape of the corridor. Hence, it can be concluded that a bidirectional radiation pattern antenna is suitable for this environment. The directions of significant paths, i.e. paths with high path gain, were in the azimuth direction of 0° and 180°. The nearly 180° path was the transmission path whose signals passed over the receiver and then reflected back from the wall behind it. As shown in Table 5.1, the result on F/B, which are the ratios of the incoming signal in the 0° direction to the incoming signal in the 180° direction, shows that the signal strength in the front direction was significantly strong at all points measured. The measured discrete angular power spectrums at Rx2, Rx3, and Rx4 were similar to those in Fig.5.7 and so not illustrated.

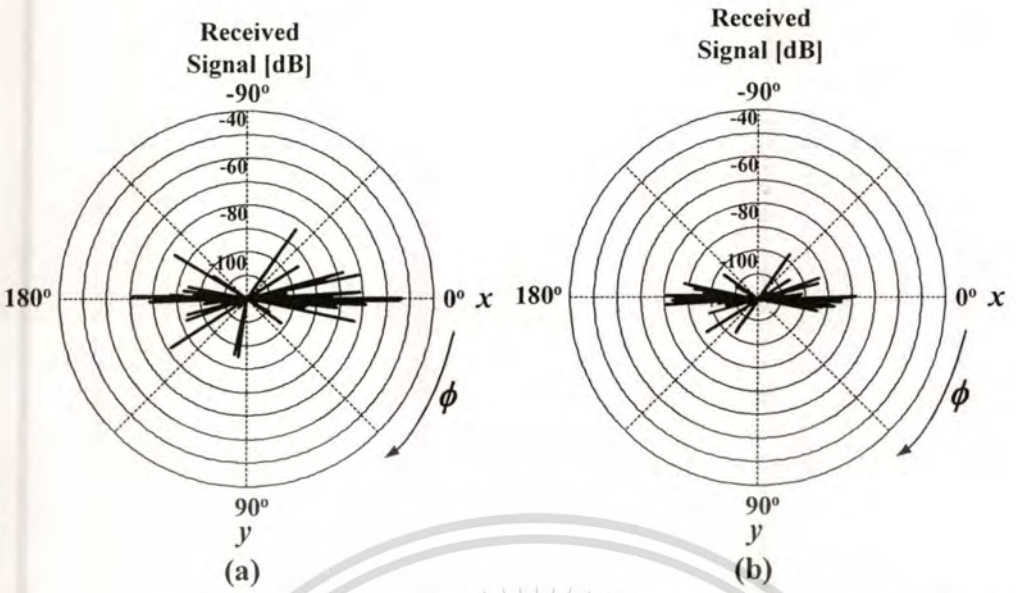

Fig 5.7 Received angular power spectrums at Rx1 (a) Vertical Polarization (b) Horizontal Polarization.

5.6 Mutual Information Calculation

Since mutual information is a random variable that depends on instantaneous channel, the Cumulative Distribution Function (CDF) of mutual information can be obtained from measurements with slightly displaced arrays or with temporally-varied scatterer arrangement. However, these complex measurement techniques can be replaced by a simple evaluation method that requires only a single measurement (single snapshot) of the channel [45]. This method uses the fact that different realizations of the channel are generated as the phases of multipath components change. These phases are uniformly distributed random variables that occur when the transmitter, receiver, or scatterers move in the channel. These adding random phases can be used to compute the impulse responses at the antenna elements, and at different frequencies that create different realizations, even though the channel sounding measurement was conducted at the center frequency of 4.5 GHz. The transfer function of a 2×2 MIMO system with single polarization is shown in [45]. However, for a 2×2 MIMO system with dual-polarized antennas at both ends, the different realizations of the transfer function of the different polarized transmitting and receiving antennas are

$$\mathbf{H}(t,\tau) = \iiint\int \bar{\mathbf{E}}_{\mathrm{R}}(\Omega_{\mathrm{R}}) \cdot \bar{\bar{\Gamma}}(t,\tau,\Omega_{\mathrm{R}},\Omega_{\mathrm{T}}) \cdot \bar{\mathbf{E}}_{\mathrm{T}}^{H}(\Omega_{\mathrm{T}}) \mathrm{d}\Omega_{\mathrm{R}} \mathrm{d}\Omega_{\mathrm{T}}$$

$$= \sum_{l=1}^{L} \begin{bmatrix} e_{R\theta 1}(\Omega_{Rl}) & e_{R\varphi 1}(\Omega_{Rl}) \\ e_{R\theta 2}(\Omega_{Rl}) & e_{R\varphi 2}(\Omega_{Rl}) \\ \vdots & \vdots \\ e_{R\theta N}(\Omega_{Rl}) & e_{R\varphi N}(\Omega_{Rl}) \end{bmatrix} \begin{bmatrix} \gamma_l^{\mathrm{pp}} & \gamma_l^{\mathrm{pq}} \\ \gamma_l^{\mathrm{qp}} & \gamma_l^{\mathrm{qq}} \end{bmatrix} \cdot \begin{bmatrix} e_{T\theta 1}^{*}(\Omega_{Tl}) & e_{T\theta 2}^{*}(\Omega_{Tl}) & \cdots & e_{T\theta N}^{*}(\Omega_{Tl}) \\ e_{T\varphi 1}^{*}(\Omega_{Tl}) & e_{T\varphi 2}^{*}(\Omega_{Tl}) & \cdots & e_{T\varphi M}^{*}(\Omega_{Tl}) \end{bmatrix}. \tag{5.10}$$

l is the index of estimated paths and L is the total number of estimated paths. $\bar{\bar{\Gamma}}$ is the different path weights which are complex polarimetric path weights $\gamma^{\mathrm{pp}}, \gamma^{\mathrm{pq}}, \gamma^{\mathrm{qp}}$, and γ^{qq} for the different transmitting and receiving polarizations. It is noted that $\gamma^{\mathrm{pp}}, \gamma^{\mathrm{pq}}, \gamma^{\mathrm{qp}}$, and γ^{qq} stay unchanged when the antenna elements were considered. $\bar{E}_R$ and $\bar{E}_T$ are the complex radiation patterns of the receiving and transmitting antennas, respectively. $\Omega = (\theta, \varphi)$ where θ and φ are the azimuth and elevation directions. τ is the delay different multipath number k. Finally, the mutual information of channel matrix **H** can be calculated using the approach in Chapter 4.

5.7 Mutual Information Results

Two sets of Tx-Rx antennas are calculated in this section. The first ones are the two-probe antenna, offset probe antenna, two-probe antenna with inductive coil and the dipole array antennas at both the Tx and Rx ends. The last ones are the two-probe antenna, offset probe antenna, two-probe antenna with inductive coil at the Tx and dipole array antenna at the Rx as in Chapter 4.

The mutual information of the proposed antenna and the dipole array antennas at 10% outage probability and at all measurement points are shown in Table 5.2 and Table 5.3. In Table 5.2, at Rx1, the proposed bidirectional dual-polarized antenna provided higher mutual information than the dipole array antennas did due to the corresponding radiation pattern with the angular power spectrums. In addition, there was the depolarization of the vertical polarization at Rx1 where the transmitted vertical polarization signals turned into a horizontal polarization in this corridor environment. Hence, the receiving vertical polarization dipole array antennas received cross

polarization. At other Rx positions (Rx2, Rx3 and Rx4) the mutual information from the dual-polarized antenna was higher than that from the dipole array antennas since the average angular spread at these Rx positions was very small. The performance of spatially-spaced MIMO systems degrades when their incoming signal angular spread is small such as in a line-of-sight environment [47], [48]. Mutual information increases as the distance between the transmitter and the receiver decreases due to stronger received signal as the receiver approaches the transmitter as same as the results in Chapter 4. It should be pointed out that bidirectional dual-polarized antenna is suitable for a corridor environment where the angular spread is small and depolarization exists.

Table 5.2

Comparison of 10% outage mutual information (bits/s/Hz) for same antennas as the transmitter and the receiver

Antenna	Rx1	Rx2	Rx3	Rx4
Two-probe	30.2	31.2	32.1	36.0
Offset probe	31.3	32.6	33.3	36.8
Inductive coil	31.7	33.5	34.6	37.2
Dipole array	18.0	18.3	18.7	19.2

Moreover, the antennas that improve the isolation, i.e. offset probe antenna and two-probe antenna with inductive coil, have the higher capacity than the two-probe antenna without isolation improvement. It shows that the improvement of the isolation can increase the mutual information of the MIMO systems as the results in Chapter 4. In Table 5.2, at Rx1, the use of the two-probe antenna with an inductive coil yields the highest mutual information of 31.7 bits/s/Hz and it is 13.7 bits/s/Hz or 76.1% higher than the use of the dipole array antenna. In addition, the offset probe antenna provides higher mutual information than the two-probe antenna.

From Table 5.3 when the receiving antenna is the dipole array antenna, the use of the two-probe antenna with an inductive coil provides the highest mutual information of 28.2 bits/s/Hz at Rx1 and this results is higher than the use of the dipole array antenna at both Tx and Rx. It implies that the use of the proposed bidirectional dual-polarized antenna at both Tx and Rx is more preferable in this corridor environment.

Unfortunately, the mutual information results in this chapter and Chapter 4 can not be directly compared to validate the mutual information calculations since the measurement environment are different. The different values of the mutual information can be observed because of the different environment properties, for example, the length of the corridor. However, the trend of the mutual information results with respect to the distance between Tx and Rx can be investigated. The eigenvalues of the proposed antenna can be obtained from the SVD approach as mention in Chapter 4.

Table 5.3

Comparison of 10% outage mutual information (bits/s/Hz) for different antennas as the transmitter and dipole array antennas as the receiver

Tx Antenna (Rx Antenna:Dipole Array)	**Rx1**	**Rx2**	**Rx3**	**Rx4**
Two-probe	26.4	27.1	27.9	28.5
Offset probe	26.6	28.3	29.1	30.2
Inductive coil	28.2	29.5	30.2	31.0

5.8 Conclusion

This chapter presents the results of double directional channel measurements in a corridor environment by channel sounder. Channel properties, especially polarization, in a corridor are determined from *XPRC*, *XPRS*, angular spread and angular power spectrum. The obtained channel multipath parameters, i.e. DoA, DoD, TDoA and polarimetric path weight are calculated with antenna directivity to produce MIMO channel model of arbitrary antenna. Then, mutual information of arbitrary antenna in a corridor environment can be investigated. It can be observed that the reflection along the corridor established the small spread of the incoming signal. Measurement results exhibit the bidirectional shape of the received angular power spectrum. It was found that depolarization of both vertical and horizontal polarizations should be concerned in installing the antenna in the corridor. For instance, traditional dipole antenna may be installed with tilt angle to achieve good communication performance when distance between Tx and Rx is in excess of 20 m. A dual polarized antenna is a good candidate to resolve depolarization of vertical polarization in the corridor environment. Furthermore,

the bidirectional antenna is suitable for the bidirectional angular power spectrum in the corridor environment. It was illustrated that the proposed antenna provides 70% higher mutual information than the dipole array antennas over the same SNR value. It is noted that this result is for 2×2 array antenna; however, the result maybe different for larger array. This increased mutual information enhances data rate in high-speed modern wireless communications.

CHAPTER 6

CONCLUSIONS AND DISCUSSIONS

A bidirectional circular ring antenna using two probes for polarization diversity is proposed for the MIMO systems. The antenna comprises of a circular ring that is excited by two perpendicular probes. The antenna design and antenna characteristics are presented in Chapter 2. The analysis was done by using the induced emf method and the impedance characteristics of the antenna were analyzed by using an equivalent circuit. The analysis was validated by using NEC2 simulation. The design process was as follows: First, a suitable radius of the ring was chosen for a single probe antenna. Then, the suitable probe length and ring length were determined for the two-probe antenna. The antenna parameters that are ring radius of 0.3λ, ring length of 0.3λ and probe length of 0.25λ is concluded from the study. The isolation between the two probes was enhanced by offsetting the position of two probes and by insertion of an inductor coil between the probes in Chapter 3. When the criteria of VSWR less than 2 and maximized isolation are considered, the two-probe antenna with an inductor coil provides better performance than the two-probe offsetting antenna. The operational characteristics of the prototype antenna at the frequency of 5.2 GHz were measured and compared with theoretical calculations. It was evident that the analysis and measurement results were in reasonable agreement. Measurements showed that the isolation achieved was in excess of 20 dB while the VSWR was less than 2:1. Bidirectional pattern was satisfactorily accomplished. The maximum gain was approximately 4 dBi in the desired direction. In addition to the satisfied antenna characteristics, the appropriate mutual information can be achieved with the proposed bidirectional circular ring antenna. The mutual information calculation based on the SVD approach was described in Chapter 4. The mutual information of this proposed antenna was considered in two methods. The first one was the direct field measurement in the corridor environment that was shown in Chapter 4. The 10% outage probability mutual information of the MIMO systems was considered. The results showed that the use of the proposed antenna provided higher mutual information, by 3 bits/s/Hz, than the use of the 1λ horizontally spaced vertical polarization dipole antennas. Especially, the use of the two-probe antenna with an inductive coil as the transmitting and receiving antennas provided the highest capacity result. The independent two parallel

channels could be observed for the proposed dual-polarized antenna. It can be concluded that inserting the inductive coil between the two probes can improve the isolation and the mutual information performance of the proposed antenna. The other method based on the double directional channel measurement by using the channel sounder and RIMAX high resolution algorithm is shown in Chapter 5. By this method, the channel characteristics of the corridor, such as polarimetric path weight matrix, DoA, DoD and TDoA, that is not affected by the transmitted and received antennas can be obtained. The MIMO channel of the proposed antenna can be calculated from this measured channel by using the random phase technique. In addition to the mutual information result of the antenna, the channel characteristics of the environment can also be obtained by using this technique. Moreover, the attempt of the measurement is reduced since only one of the channel measurements can be used for all transmitting and receiving antenna. However, the channel sounder equipment is very expensive and it uses complicated algorithm to extract the channel characteristics results from the channel measurement. From this method, the mutual information of MIMO system that use the proposed antenna was 12 b/s/Hz higher than that of the other MIMO system equipped with traditional 1λ horizontally-spaced vertically-polarized dipole array antennas. There is the depolarization of the vertical polarization transmission that degraded the mutual information of the dipole array antennas in this environment. The angular spread of the incoming signals at the receiver ranged from 0.9° to 3.8° depending on the distance between the transmitter and the receiver. Unfortunately, the results in Chapter 4 and Chapter 5 can not be compared since they are measured in the different environment. However, the inline results can be observed such as, the higher mutual information results of the proposed antenna than that of the dipole array antennas, the increasing of the mutual information results when the distances between the transmitter and receiver are decreased. From the above antenna characteristics and mutual information results in this thesis, the two-probe antenna can be a promising antenna for use in the high data rate communication such as in the MIMO system.

In this thesis, the reflections and the mutual coupling between two apertures for the inside and outside the ring are neglected, these resulted in the large different between the calculated and measured isolation. To evaluate these effects on the calculation results, the further calculations that include all of these effects should be considered. In addition, the result in Chapter 3 shows the influence of the inductor coil orientation on the

impedance of the antenna. However, since the aim of the isolation improvement is realized in this thesis, the effect of the inductor coil on the near field antenna characteristics should be concerned in the further study. As the aforementioned above, the increase of isolation between the antenna elements can increase the mutual information performance of the MIMO systems. Even though the bidirectional circular ring antenna using two probes yields the accepted isolation result, the isolation should be improved to gain the mutual information in the communication. There are some approaches to improve the isolation, for example, change the diameter of the probe or change the feeding structure. Moreover, the validation of mutual information results from the double directional measurement with the direct field test measurement is also preferable. However, these topics are left for further study.

REFERENCES

[1] R. G. Vaughan and J. B. Andersen, "**Antenna diversity in mobile communications**," IEEE Trans. Veh. Technol., Vol. VT-36, pp. 149–172, Nov. 1987.

[2] R. G. Vaughan, "**Polarization diversity in mobile communications**," IEEE Trans. Veh. Technol., Vol. VT-39, pp. 177–186, Aug. 1990.

[3] S. Alamouti, "**A simple transmit diversity technique for wireless communications**," IEEE J. Sel. Areas Commun., pp. 1451–1458, October 1998.

[4] C. E. Shannon, "**A mathematical theory of communication**," Bell Syst. Tech. J., Vol. 27, pp. 379–423, 623–656, Oct. 1948.

[5] G. J. Foschini, "**Layered space-time architecture for wireless communication in fading environments when using multi-element antennas**," Bell System Tech J., pp. 41–59, Autumn 1996.

[6] G. J. Foschini and M. J. Gans, "**On limits of wireless communications in a fading environment when using multiple antennas**," Wireless Pers. Commun., Vol. 6, pp. 311–335, Mar. 1998.

[7] I. E. Teletar, "**Capacity of multi-antenna Gaussian channels**," AT&T Bell Laboratories, Murray Hill, NJ, Tech. note, 1996.

[8] K. Sulonen, P. Suvikunnas, L. Vuokko, J. Kivinen, and P. Vainikainen, "**Comparison of MIMO antenna configurations in picocell and microcell environments**," IEEE J. Sel. Areas Commun., Vol. 21, pp. 703–712, June 2003.

[9] P. Kyritsi, D. C. Cox, R. A. Valenzuela, and P. W. Wolniansky, "**Effect of antenna polarization on the capacity of a multiple element system in an indoor environment**," IEEE J. Sel. Areas Commun., Vol. 20, pp. 1227–1239, Aug. 2002.

[10] R. U. Nabar, H. Bolcskei, V. Erceg, D. Gesbert, and A. J. Paulraj, "**Performance of multiantenna signaling techniques in the presence of polarization diversity**," IEEE Trans. Signal Process., Vol. 50, pp. 2553–2561, Oct. 2002.

[11] J. P. Kermoal, L. Schumacher, F. Frederiksen, and P. E. Mogensen, "**Polarization diversity in the MIMO radio channels: Experimental validation of a stochastic model and performance assessment**," IEEE 54th Veh. Technol. Conf. 2001, Vol. 1, pp. 22–26, Oct. 2001.

[12] J. W. Wallace, M. A. Jensen, A. L. Swindlehurst, and B. D. Jeffs, "**Experimental characterization of the MIMO wireless channel: Data acquisition and analysis,**" IEEE Trans. Wireless Commun., Vol. 2, pp. 335–343, Mar. 2003.

[13] C. Waldschmidt, S. Schulteis, and W. Wiesbeck, "**Complete RF system model for analysis of compact MIMO arrays,**" IEEE Trans. Veh. Technol., Vol. 53, pp. 579–586, May 2004.

[14] B. N. Getu and J. B. Andersen, "**The MIMO cube–a compact MIMO antenna,**" IEEE Trans. Wireless Commun. , Vol. 4, pp. 1136–1141, May 2005.

[15] L. Dong, H. Choo, R. W. Heath, Jr., and H. Ling, "**Simulation of MIMO channel capacity with antenna polarization diversity,**" IEEE Trans. Wireless Commun. , Vol. 4, pp. 1869–1873, July 2005.

[16] J. B. Andersen, "**Array gain and capacity for known random channels with multiple element arrays at both ends,**" IEEE J. Sel. Areas Commun., Vol. 18, pp. 2172–2178, Nov. 2000.

[17] B. Alister, "**Evaluation of capacity of indoor wireless MIMO channel using ray tracing,**" Int. Zurich Seminar on Broadband Communications Access-Transmission-Networking 2002, pp. 28-1–28-6, 2002.

[18] M. S. Elnaggar, S. Safavi-Naeini, and S. K. Chaudhuri, "**Simulation of the achievable indoor MIMO capacity by using and adaptive phased-array,**" Radio and Wireless Conference 2004, pp. 155–158, 2004.

[19] A. A. M. Saleh and R. A. Valenzuela, "**A statistical model for indoor multipath propagation,**" IEEE J. Sel. Areas Commun., Vol. SAC-5, pp. 128–137, Feb. 1987.

[20] J.-G. Wang, A. S. Mohan, and T. A. Aubrey, "**Angles-of-arrival of multipath signals in indoor environments,**" IEEE Spring Veh. Technol. Conf. 1996, Vol. 1, pp. 155–159, 1996.

[21] M. Steinbauer, A. F. Molisch, and E. Bonek, "**The double-directional radio channel,**" IEEE Antennas Propag. Mag., Vol. 43, pp. 51–63, Aug. 2001.

[22] http://www.channelsounder.de, accessed November 2006.

[23] K. L. Wong, A. C. Chen, Y. L. Kuo, "**Diversity metal-plate planar inverted-F antenna for WLAN operation,**" Electron Lett, Vol. 4 pp. 590–591, Apr. 2003.

[24] A. Kalis, T. Antonakopoulos, C. Soras, and V. Makios, "**A switched dual antenna array for mobile computing networks**," International Journal of Electronics, Vol. 89, pp. 325–335, Aug. 2002.

[25] S. Kosulvit, M. Krairiksh, C. Phongcharoenpanich and T. Wakabayashi, "**Simple and cost-effective bidirectional antenna using a probe excited circular ring**," IEICE Trans. Electron., Vol. E84-C, pp. 443–450, April 2001.

[26] C. Waldschmidt and W. Wiesbeck, "**Compact wide-band multimode antennas for MIMO and diversity**," IEEE Trans. Antennas Propag., Vol. 52, pp. 1963–1969, Aug. 2004.

[27] B. K. Lau, S. M. S. Ow, G. Kristensson, and A. F. Molisch, "**Capacity analysis for compact MIMO systems**," IEEE 61st Veh. Technol. Conf. 2001, vol. 1, pp. 165–170, 2001.

[28] C. T. P. Song, A. Mak, B. Wong, D. George, R. D. Murch, "**Compact low cost dual polarized adaptive planar phased array for WLAN**," IEEE Trans Antennas Propag, Vol. 8 pp. 2406–16, Aug. 2005.

[29] R. S. Thomä, M. Landman, and A. Richter, "**RIMAX-a maximum likelihood framework channel parameter estimation in multidimensional channel sounding**," Int. Symp. on Antennas and Propag. 2004, pp. 53–56, 2004.

[30] T. Taga, "**Analysis for mean effective gain of mobile antennas**," IEEE Trans. Veh. Technol., Vol. 39, pp. 117–131, 1999.

[31] M. Landmann, K. Sivasondhivat, J. Takada, I. Ida, and R. Thoma, "**Polarization behavior of discrete multipath and diffuse scattering in urban environments at 4.5 GHz**," EURASIP Journal on wireless communications and networking, Vol 2007, pp. 1–16.

[32] C. A. Balanis, **Antenna Theory: Analysis and Design**, 2nd ed. New York: Wiley, 1997.

[33] N. Marcuvitz, **Waveguide Handbook**, London: Peter Peregrinus, 1986.

[34] C. A. Balanis, **Advanced Engineering Electromagnetics**, New York: John Wiley, 1989

[35] S. C. Chapra and R. P. Canale, **Numerical Methods for Engineers**, New York: McGraw-Hill, 1990.

[36] R. F. Harrington, **Time-Harmonic Electromagnetic Fields**, New York: McGraw-Hill, 1961.

[37] R. S. Elliott, **An Introduction to Guided Waves and Microwave Circuits,** London: Prentice-Hall, Inc, 1993.

[38] R. Ludwig, and P. Bretchko, **RF Circuit Design**, Upper Saddle River, NJ: Prentice-Hall, 2000.

[39] G. J. Burke and A. J. Poggio, **Numerical Electromagnetics Code (NEC) –Method of Moments, Parts I–III**, Lawrence Livermore Nat. Lab., Livermore, CA, 1981.

[40] E. K. Miller, "**PCs for AP and other EM reflections: wire-grid approximations to solid surfaces,**" IEEE Antennas Propag. Mag., Vol. 39, pp. 94–97, Feb. 1997.

[41] P. Keowsawat, C. Phongcharoenpanich, S. Kosulvit, and M. Krairiksh, "**Achievable diversity performance and range improvement from polarization diversity bi-directional antenna using two-probe excited circular ring,**" TENCON IEEE Region 10 Conf. 2004, vol. C, pp. 208–211, Nov. 2004.

[42] J. Winters, "**On the capacity of radio communication systems with diversity in a Rayleigh fading environment,**" IEEE J. Sel. Areas Commun., pp. 871–878, June 1987.

[43] A. Goldsmith, **Wireless Communications**, New York, NY: Cambridge University Press, 2005.

[44] **Part11: Wireless LAN Medium Access Control (MAC) and Physical Layer (PHY) specifications**, IEEE Std 802.11a-1999, 1999.

[45] A. F. Molisch, M. Steinbauer, M. Toeltsch, E. Bonek, and R. S. Thomä, "**Mutual information of MIMO systems based on measured wireless channels,**" IEEE J. Sel. Areas Commun., Vol. 20, pp. 561–569, Apr. 2002.

[46] J. Medbo, "**Channel model parameters for the office environment,**" COST 273 TD(05)050, Bologna, Italy, January 2005.

[47] S. Haykin and M. Moher, **Modern Wireless Communications**, Pearson Prentice Hall, Upper Saddle River, NJ 2005.

[48] J. P. Kermoal, P. E. Mogensen, S. H. Jensen, J. B. Andersen, F. Frederiksen, T. B. SØrensen, and K. I. Pedersen, "**Experimental investigation of multipath richness for multi-element transmit and receive antenna arrays,**" IEEE 51th Veh. Technol. Conf. 2000, pp. 2004–2008, 2000.

[49] S. Kriengthanasarn, S. Lamultree, C. Phongcharoenpanich, S. Kosulvit, and M.

Krairiksh, **"Design and experiment of a corner reflector antenna excited by a probe inside circular ring,"** 26th Electrical Engineering Conf. 2003, pp. 1801-1806, 2003.

APPENDIX

APPENDIX A

Electric fields and magnetic fields inside the circular ring antenna

The electric fields and magnetic fields inside this antenna can be derived by using the Green function. The fields can be expressed, cited from Kriengthanasarn's article [49], as follows:

$$E_\rho(\rho,\phi,z) = -j\omega\mu_0 \sum_{m=0}^{\infty}\sum_{n=1}^{\infty}\left[\begin{array}{l} c_\zeta m^2 \dfrac{J_m(\zeta\rho)}{\rho}\cos\left[m(\phi-\phi')\right]E_{a,TE}\begin{cases} e^{-jk_\zeta(z-z')} \\ e^{-jk_\zeta(z'-z)} \end{cases} \\ +c_\xi \dfrac{k_\xi^2}{\kappa_\xi^2}\dfrac{\partial J_m(\xi\rho)}{\partial\rho}\cos\left[m(\phi-\phi')\right]E_{a,TM}\begin{cases} e^{-jk_\xi(z-z')} \\ e^{-jk_\xi(z'-z)} \end{cases} \end{array}\right], z_<^> z' \tag{A1}$$

$$E_\phi(\rho,\phi,z) = -j\omega\mu_0 \sum_{m=0}^{\infty}\sum_{n=1}^{\infty}\left[\begin{array}{l} c_\zeta m \dfrac{\partial J_m(\zeta\rho)}{\partial\rho}\sin\left[m(\phi-\phi')\right]E_{a,TE}\begin{cases} e^{-jk_\zeta(z-z')} \\ e^{-jk_\zeta(z'-z)} \end{cases} \\ +c_\xi m \dfrac{k_\xi^2}{\kappa_\xi^2}\dfrac{J_m(\xi\rho)}{\rho}\sin\left[m(\phi-\phi')\right]E_{a,TM}\begin{cases} e^{-jk_\xi(z-z')} \\ e^{-jk_\xi(z'-z)} \end{cases} \end{array}\right], z_<^> z' \tag{A2}$$

$$H_\rho(\rho,\phi,z) = \sum_{m=0}^{\infty}\sum_{n=1}^{\infty}\left[\begin{array}{l} c_\zeta \dfrac{k_\zeta}{\kappa_\zeta}(jmk)\dfrac{\partial J_m(\zeta\rho)}{\partial\rho}\sin\left[m(\phi-\phi')\right]H_{a,TE}\begin{cases} -e^{-jk_\zeta(z-z')} \\ +e^{-jk_\zeta(z'-z)} \end{cases} \\ +c_\xi \dfrac{k_\xi}{\kappa_\xi}(jmk)\dfrac{J_m(\xi\rho)}{\rho}\sin\left[m(\phi-\phi')\right]H_{a,TM}\begin{cases} -e^{-jk_\xi(z-z')} \\ +e^{-jk_\xi(z'-z)} \end{cases} \end{array}\right], z_<^> z' \tag{A3}$$

$$H_\phi(\rho,\phi,z) = \sum_{m=0}^{\infty}\sum_{n=1}^{\infty}\left[\begin{array}{l} c_\zeta \dfrac{k_\zeta}{\kappa_\zeta}\left(jm^2k\right)\dfrac{J_m(\zeta\rho)}{\rho}\cos\left[m(\phi-\phi')\right]H_{a,TE}\begin{cases} -e^{-jk_\zeta(z-z')} \\ +e^{-jk_\zeta(z'-z)} \end{cases} \\ +c_\xi \dfrac{k_\xi}{\kappa_\xi}(jk)\dfrac{\partial J_m(\xi\rho)}{\partial\rho}\cos\left[m(\phi-\phi')\right]H_{a,TM}\begin{cases} -e^{-jk_\xi(z-z')} \\ +e^{-jk_\xi(z'-z)} \end{cases} \end{array}\right], z_<^> z' \tag{A4}$$

where

$$E_{a,TE} = H_{a,TE} = \int_{a-l}^{a}\frac{J_m(\zeta\rho')}{\rho'}\sin\left[k(\rho'-a+l)\right]d\rho'$$

$$E_{a,TM} = H_{a,TM} = \int_{a-l}^{a}\frac{\partial J_m(\xi\rho')}{\partial\rho'}\sin\left[k(\rho'-a+l)\right]d\rho'$$

$$c_\zeta = \frac{-j(2-\delta_0)}{4\pi^2\zeta^2 I_\zeta k_\zeta}$$

$$c_\xi = \frac{-j(2-\delta_0)}{4\pi^2\xi^2 I_\xi k_\xi}$$

$$I_\zeta = \frac{a^2}{2\zeta^2}\left(\zeta^2 - \frac{m^2}{a^2}\right)J_m^2(\zeta a)$$

$$I_\xi = \frac{a^2}{2\xi^2}\left[\frac{\partial J_m(\xi\rho)}{\partial\rho}\right]^2\Bigg|_{\rho=a}$$

$$k_\zeta = \begin{cases} \sqrt{k^2-\zeta^2} & \text{if } k > \zeta \\ -j\sqrt{\zeta^2-k^2} & \text{if } k < \zeta \end{cases}$$

$$k_\xi = \begin{cases} \sqrt{k^2-\xi^2} & \text{if } k > \xi \\ -j\sqrt{\xi^2-k^2} & \text{if } k < \xi \end{cases}$$

$$\kappa_\xi = \sqrt{\xi^2+k_\xi^2}$$

$$\delta_0 = \begin{cases} 0 & \text{if } m > 1 \\ 1 & \text{if } m < 1 \end{cases}$$

APPENDIX B

MIMO measurement and mutual information calculation

According to the direct field test measurement in Chapter 4, the complex S_{21} parameters from the network analyzer are used to form the channel matrix **H**. For example, when transmitting switch selected the transmitting antenna 1 and receiving switch selected the receiving antenna 1 (as shown in Fig. 4.11), this measured S_{21} is the h_{11} element for the matrix **H** and so on for the different transmitting and receiving antenna pairs. Finally, the channel matrix **H** can be obtained as follow for the 2×2 MIMO communication,

$$\mathbf{H} = \begin{bmatrix} h_{11} & h_{12} \\ h_{21} & h_{22} \end{bmatrix}. \tag{B1}$$

To evaluate the independent channel of this **H**, the Singular Value Decomposition (SVD) approach was used according to (4.2). Finally, the singular value for each channel can be obtained. In this thesis, the two different singular values can be achieved for 2×2 MIMO system.

The mutual information of the MIMO system can be calculated by using (4.10) when multiply the singular value of each channel with the power in each channel and noise figure. Lastly, the total mutual information can be summed up from the mutual information in each channel.

RELATED PUBLICATIONS

1. P. Keowsawat, K. Meksamoot, C. Phongcharoenpanich, S. Kosulvit, and M. Krairiksh, "Characteristics of Polarization Diveristy Bi-directional Antenna in Expressway Environment," in *Proc. of the 2004 IEEE International Symposium on Antennas and Propagation and USNC/URSI National Radio Science Meeting*, Monterey, California, USA, June 20–26, 2004, pp. 3199–3202.

2. P. Keowsawat, C. Phongcharoenpanich, S. Kosulvit, and M. Krairiksh, "Design of a Polarizaion Diversity Bi-directional Antenna using Two-probe Excited Circular Ring for 5 GHz WLAN," in *Proc. 2004 International Symposium on Antennas and Propagation*, Sendai, Japan, Aug. 17–21, 2004, pp. 1333–1336.

3. P. Keowsawat, C. Phongcharoenpanich, S. Kosulvit, and M. Krairiksh, "Achievable Diversity Performance and Range Improvement from Polarization Diversity Bi-directional Antenna using Two-probe Excited Circular Ring," in *Proc. TENCON 2004 IEEE Region 10 Conf.*, Vol. C, Chiangmai, Thailand, Nov. 21–24, 2004, pp. 208–211.

4. P. Keowsawat, C. Phongcharoenpanich, S. Kosulvit, J. Takada, and M. Krairiksh, "Mutual Information of MIMO System in a Corridor Environment Based on Double Directional Channel Measurement," in *Journal of Electromagnetic Waves and Applications*, Vol. 23, pp. 1221–1233, June 2009.

AUTHOR BIOGRAPHY

Panisa Keowsawat was born on July 28, 1977 in Phetchaburi, Thailand. She received the B. Eng. (Hons.) degree in Telecommunication Engineering and the M. Eng. Degree in Electrical Engineering from King Mongkut's Institute of Technology Ladkrabang, Bangkok, Thailand, in 1999 and 2001, respectively. Between 2002 to 2009 she was a Ph.D. student supported by a scholarship from the Thailand Research Fund through The Royal Golden Jubilee (RGJ) program. During the time period between October 2004 to March 2005, she was a short term research student in the Department of International Development Engineering, Graduate School of Engineering, Tokyo Institute of Technology, Tokyo, Japan under the support from RGJ and National Information and Communication Technology (NICT), Japan. Since 2001, she is a lecturer in Faculty of Industrial Technology, Phetchaburi Rajabhat University. Her research interests are antennas and propagation for wireless communications.

J. of Electromagn. Waves and Appl., Vol. 23, 1221–1233, 2009

MUTUAL INFORMATION OF MIMO SYSTEM IN A CORRIDOR ENVIRONMENT BASED ON DOUBLE DIRECTIONAL CHANNEL MEASUREMENT

P. Keowsawat, C. Phongcharoenpanich, and S. Kosulvit

Faculty of Engineering
King Mongkut's Institute of Technology Ladkrabang
Bangkok 10520, Thailand

J. Takada

Department of International Development Engineering
Graduate School of Science and Engineering
Tokyo Institute of Technology
Tokyo 152–8550, Japan

M. Krairiksh

Faculty of Engineering
King Mongkut's Institute of Technology Ladkrabang
Bangkok 10520, Thailand

Abstract—Double directional channel measurements were made in a corridor environment with a channel sounder. A multidimensional high resolution algorithm was used to extract channel parameters for calculating the mutual information of a special Multiple-Input Multiple-Output (MIMO) system. This system utilized bidirectional dual-polarized antennas at both ends of the communication. In a corridor environment, the mutual information of this system was 12 b/s/Hz higher than that of the other MIMO system equipped with traditional 1λ horizontally-spaced vertically-polarized dipole array antennas. Depolarization of the vertical polarization transmission degraded the mutual information of the dipole array antennas in this environment. The angular spread of the incoming signals at the receiver ranged from 0.9° to 3.8° depending on the distance between the transmitter and the receiver.

Corresponding author: C. Phongcharoenpanich (kpchuwon@kmitl.ac.th).

1. INTRODUCTION

Multiple-Input Multiple-Output (MIMO) systems play an important role in high speed wireless communications since it can increase data rate without increasing the frequency spectrum or transmitted power [1–5]. They usually use spatially separated antennas with single polarization, but large separation between antennas is needed to achieve uncorrelated channels. When space is limited, small, spatially separated antennas can not provide significant independent channels; hence, polarization diversity antennas are introduced to solve the problem [6, 7]. Additionally, as far as radiation pattern is concerned, dipole antennas with omnidirectional radiation pattern are used successfully in many wireless communication systems. However, for certain types of area such as in a corridor, where it is desirable to be able to communicate effectively along its maximum distance, omnidirectional radiation pattern does not give satisfactory result. Therefore, the use of transmitting antennas with bidirectional radiation pattern is proposed.

To assess the performance of MIMO systems in real propagation channel, accurate characteristics of the channel are required. A number of research studies have tried to explain the behavior of corridor channel. Most of them used ray optical models based on electromagnetic simulation [8, 9]. However, since the real propagation environments can not be completely modeled by electromagnetic simulation, the environment can be modeled by propagation measurement. The double directional channel measurement was proposed which the properties of the propagation channel were independent of the measurement antennas [10]. The parameters of multipath can be accurately estimated by parametric estimation algorithms. The results of corridor channel characteristics by double directional measurements were reported in [11] where the number of multipath clusters, angular and delay spreads in the environment were presented. Since the application of polarization diversity antennas in MIMO system design proves to be useful, it is necessary to study its polarization behavior in a corridor environment.

In this paper, we present a double directional channel measurement in a corridor. Multipath parameters including polarimetric path weight matrix, Direction of Departure (DoD) at the transmitting site, Direction of Arrival (DoA) at the receiving site, and path delay are extracted from the sounding measurement data. Depolarization of signal was studied in terms of cross polarization power ratio (XPR) [12, 13]. Angular power spectrum and angular spread of incoming signal in a corridor environment

were also investigated. The extracted multipath parameters can be used in combination with the directivity of any assessed antennas to create a complete channel model like the evaluation approach in [14]. Consequently, the mutual information that corresponds to these channel responses can be obtained. Here, the mutual information of a MIMO system with 0°/90° dual-polarized bidirectional antenna and 1λ horizontally-spaced vertically-polarized dipole array antennas are compared with each other.

2. MATERIAL AND METHOD

2.1. Double Directional Channel Measurement

The channel measurement was conducted in a corridor. The layout and photograph are shown in Fig. 1(a) and Fig. 1(b), respectively. The width of the corridor is 2 m and the length is 64 m, with lecture rooms along both sides. The walls along the corridor and between the rooms were made of reinforced concrete with wooden office doors. The floor was rubber sheets on concrete and the ceiling was covered with metal grid (approximately 50 cm gap between the metal grid and the concrete layer). The height of the corridor was 2.45 cm. There were metal pipes beneath the metal grid. A wideband measurement was performed in the 5 GHz band using the Medav RUSK-Fujitsu MIMO channel sounder [15]. The periodic multi-frequency test signal used in the measurement had a repetition period of 0.8 μs and a bandwidth of 120 MHz. The measurement was based on MIMO channel with a polarimetric rectangular array antenna as the transmitting antenna (Tx) and a stacked uniform polarimetric circular patch array antenna as the receiving antenna (Rx). For every position in the measurements, the transmitting antenna height is 180 cm and the receiving antenna height is 115 cm. The transmitted power in all measurements was fixed at 30 dBm and the time interval of the MIMO switch was 1 ms. Because the transmitting power was restricted by the transmission license, the Tx and Rx were separated only at a maximum distance of 26 m. All of the locations measured represented the Line-of-Sight (LoS) scenarios where the Tx-Rx separation varied from 26 m to 16 m. These separations corresponded to Rx1 to Rx4 in Fig. 1. The Tx was fixed at the location marked as "Tx" in Fig. 1. It should be noted that there was an emergency door 5 m behind the Tx. The Rx azimuth equals 0° was pointing at the Tx at all locations. For all measurements, dual-polarized elements were used in both transmitting and receiving array antennas to obtain a polarization matrix of the environment. The complex frequency responses were computed on-line and stored into the sounder's hard disk for subsequent off-line post-

processing. At each point in the measurement, 500 snapshots were taken. During the measurement, people were not allowed to move around in order to keep the channel static. The Tx and Rx antennas were de-embedded from the channel response for estimation of the parameters. In order to obtain a correct extraction of the multipath parameters, the Tx and Rx had to be properly synchronized in time and frequency. This was done by connecting the Tx and Rx units via optical fibers. Moreover, the effect of signal propagation through the cable and the signal processing delays were eliminated by doing back-to-back calibration. The complex frequency response data from the sounding measurement was processed off-line by using the RIMAX algorithm [16], a multi-dimensional maximum likelihood algorithm, to extract the multipath parameters.

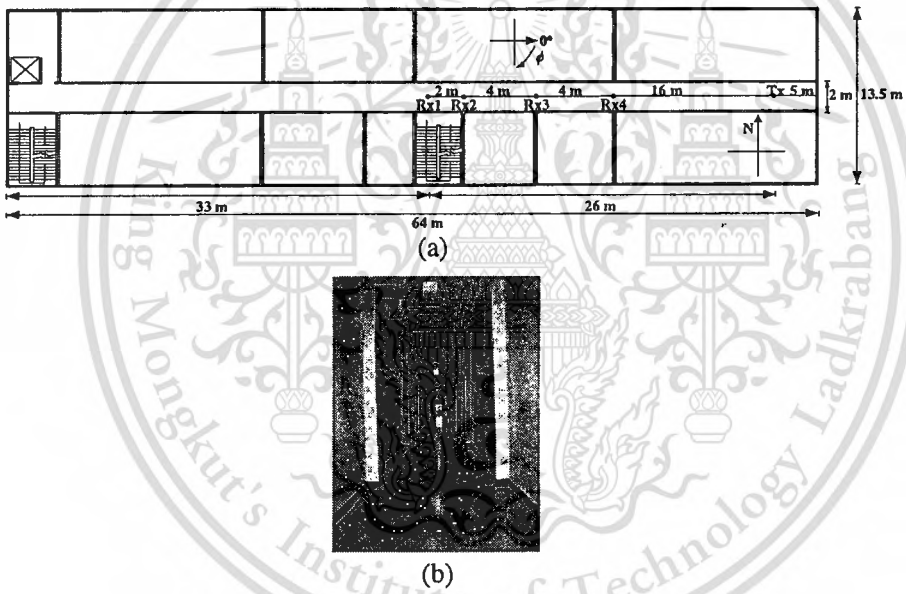

Figure 1. Location of sounding measurements. (a) Layout. (b) Photograph.

2.2. Mutual Information Calculation

Since mutual information is a random variable that depends on instantaneous channel, the Cumulative Distribution Function (CDF) of mutual information can be obtained from measurements with slightly displaced arrays or with temporally varied scatterer arrangement. However, these complex measurement techniques can be replaced by

a simple evaluation method that requires only a single measurement (single snapshot) of the channel [14]. This method uses the fact that different realizations of the channel are generated as the phases of multipath components change. These phases are uniformly distributed random variables that occur when the transmitter, receiver, or scatterers move in the channel. The transfer function of a 2×2 MIMO system with single polarization is shown in [14]. However, for a 2×2 MIMO system with dual-polarized antennas at both ends, the different realizations of the transfer function of the different polarized transmitting and receiving antennas are

$$\begin{aligned}\mathbf{H}(t,\tau) &= \iiiint \overline{\mathbf{E}}_R(\Omega_R) \times \overline{\overline{\Gamma}}(t,\tau,\Omega_R,\Omega_T) \times \overline{\mathbf{E}}_T^H(\Omega_T) d\Omega_R d\Omega_T \\ &= \sum_{l=1}^{L} \begin{bmatrix} e_{R\theta 1}(\Omega_{Rl}) & e_{R\varphi 1}(\Omega_{Rl}) \\ e_{R\theta 2}(\Omega_{Rl}) & e_{R\varphi 2}(\Omega_{Rl}) \\ \vdots & \vdots \\ e_{R\theta N}(\Omega_{Rl}) & e_{R\varphi N}(\Omega_{Rl}) \end{bmatrix} \begin{bmatrix} \gamma_l^{pp} & \gamma_l^{pq} \\ \gamma_l^{qp} & \gamma_l^{qq} \end{bmatrix} \\ &\quad \cdot \begin{bmatrix} e_{T\theta 1}^*(\Omega_{Tl}) & e_{T\theta 2}^*(\Omega_{Tl}) & \cdots & e_{T\theta N}^*(\Omega_{Tl}) \\ e_{T\varphi 1}^*(\Omega_{Tl}) & e_{T\varphi 2}^*(\Omega_{Tl}) & \cdots & e_{T\varphi M}^*(\Omega_{Tl}) \end{bmatrix}. \end{aligned} \tag{1}$$

l is the index of estimated paths and L is the total number of estimated paths. $\overline{\overline{\Gamma}}$ is the different path weights which are complex polarimetric path weights γ^{pp}, γ^{pq}, γ^{qp}, and γ^{qq} for the different transmitting and receiving polarizations. The first and second subscripts indicate the polarization at the receiver and transmitter ends, respectively, where p and q are the vertical and horizontal polarizations. $\overline{\mathbf{E}}_R$ and $\overline{\mathbf{E}}_T$ are the complex radiation patterns of the receiving and transmitting antennas, respectively. $\Omega = (\theta, \varphi)$ where θ and φ are the azimuth and elevation directions. τ is the delay different multipath number k. Referring to [2, 17], the uncorrelated channels for the MIMO system can be found by using the Singular Value Decomposition (SVD) of the channel matrix $\mathbf{H}$. It should be noted that water filling was not used to calculate the uncorrelated channels of the channel matrix $\mathbf{H}$ since power assigned to the channel remains unaltered whether channel conditions are favorable or not. From Shannon's theorem [18], the mutual information of a uniform power transmission per unit frequency or the spectral efficiency measured in b/s/Hz of parallel channels can be calculated [1, 2, 17].

3. RESULTS

3.1. Channel Characteristics

To investigate the depolarization of the signal in the corridor environment, we used the cross polarization power ratio (XPR) [12, 13] term of each detected path. The centroid of the cross polarization power ratio ($XPRC$) and the spread of the cross polarization power ratio ($XPRS$) were calculated at each measured point and used to evaluate the depolarization of the environment.

The $XPRC$ and $XPRS$ results are shown in Table 1. The $XPRC_V$ results of vertical polarization were mainly positive except at Rx1 where there was depolarization. As for the results of the $XPRC_H$ of horizontal polarizations, depolarizations could be observed at Rx1 and Rx2 but there were no depolarizations at Rx3 and Rx4. The $XPRS$ of 2 to 7 dB could be observed in both polarizations. The angular spreads at the front of the receiver in the corridor environment, shown in Table 1, varied from 0.9° to 3.8°. This result agreed well with the measurement reported in [11]. These $XPRC$ and angular spread had an influence on the mutual information of the investigated antennas. The discrete azimuth angular power spectrums at Rx1 for vertical and horizontal polarizations are shown in Figs. 2(a) and 2(b), respectively. They have bidirectional patterns which were similar to the shape of the corridor. Hence, it can be concluded that a bidirectional radiation pattern antenna is suitable for this environment. The directions of significant paths, i.e., paths with high path gain, were in the azimuth direction of 0° and 180°. The nearly 180° path was the transmission path whose signals passed over the receiver and then reflected back from the wall behind it. As shown in Table 1, the result on F/B, which are the ratios of the incoming signal in the 0° direction to the incoming signal in the 180° direction, shows that the signal strength in the front direction was significantly strong at all points measured.

Table 1. Angular spread, $XPRC$, $XPRS$, and Front-to-Back ratio (F/B).

Rx	$XPRC_V$ [dB]	$XPRC_H$ [dB]	$XPRS_V$ [dB]	$XPRS_H$ [dB]	Angular Spread		F/B [dB]
					Front	Back	
Rx1	−0.3	−1.8	6.7	7.2	3.8°	4.2°	30.0
Rx2	2.6	−0.9	4.8	5.5	1.2°	3.2°	31.3
Rx3	5.7	2.3	3.4	3.8	1.1°	2.9°	37.8
Rx4	7.2	6.5	2.3	2.1	0.9°	2.7°	42.5

The measured discrete angular power spectrums at Rx2, Rx3, and Rx4 were similar to those in Fig. 2 and so not illustrated.

3.2. Bidirectional Dual-Polarized Antenna

A bidirectional dual-polarized antenna was used for evaluation in this corridor environment. The antenna parameters were the ring radius (a), ring width (d), and probe length (l) which was the same for both excited probes as shown in Fig. 3. The angle between the two probes was fixed at 90°. The maximum gain, return loss, and isolation of the antenna were adjusted by varying the antenna parameters to achieve the desired antenna characteristics [19]. The antenna was equipped with probe 1 on the $+z$-axis to provide vertical polarization and probe 2 on the $-y$-axis to provide horizontal polarization. Both probes were of the same length (l) of 0.25λ, following the design in [20]. These two probes excited the two apertures perpendicular to the x-axis and provided a bidirectional radiation pattern along the $+x$-axis and the $-x$-axis. When the antenna was placed on the ceiling of the corridor, its bidirectional radiation pattern covered the length of the corridor along the x-axis. Maximum gains were required in the directions $\phi = 0°$ and $\phi = 180°$ to provide maximum coverage distance of the area. Ring radius of 0.30λ (1.73 cm) and ring width of 0.40λ (2.31 cm) were used to fabricate the prototype antenna.

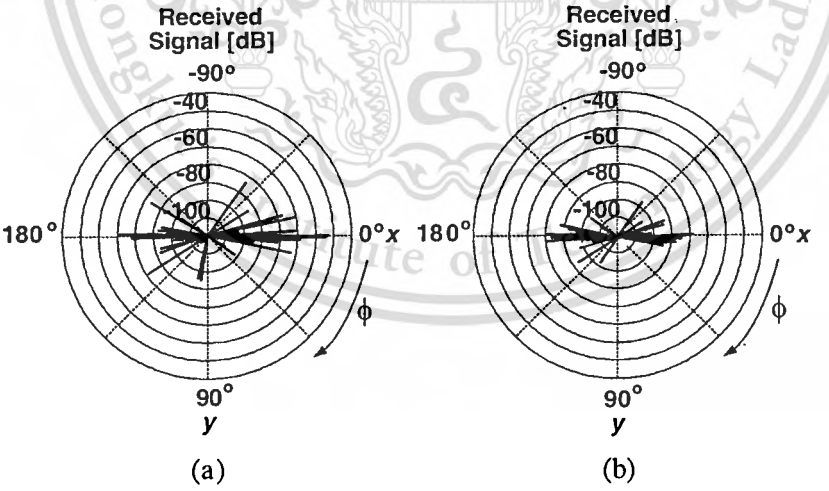

Figure 2. Received angular power spectrums at Rx1. (a) Vertical polarization. (b) Horizontal polarization.

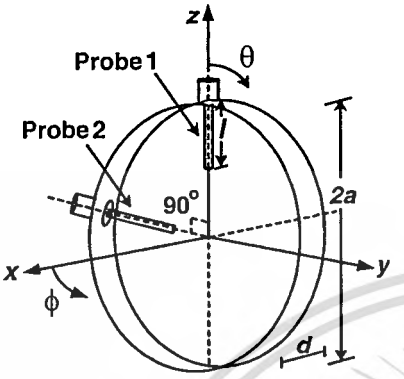

Figure 3. Configuration of a bidirectional dual-polarized antenna.

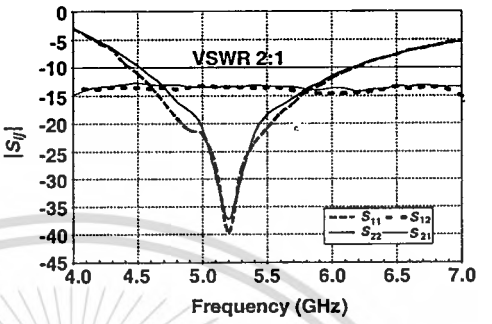

Figure 4. Measured S-parameters of the bidirectional dual-polarized antenna.

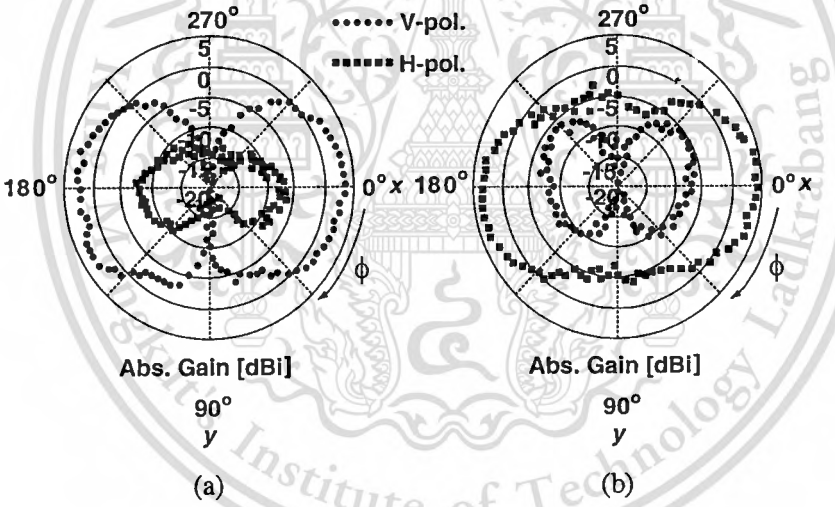

Figure 5. Radiation patterns in the xy-plane of the bidirectional dual-polarized antenna. (a) Probe 1 was excited, probe 2 was terminated. (b) Probe 2 was excited, probe 1 was terminated.

Figure 4 shows the S-parameters of the antennas over the 4–7 GHz band. The bandwidth, with VSWR at less than 2 : 1, was 1600 MHz for this proposed antenna and, consequently, the impedance bandwidth was wide. Specifically, over the operating bandwidth of 5.15–5.25 GHz, the antenna yielded return loss and isolation of more than 40 dB

and 10 dB, respectively. Figs. 5(a) and 5(b) show the measured and simulated radiation patterns in the xy-plane of the antenna when probe 1 and probe 2 were excited, respectively. The antenna possessed a bidirectional pattern with cross polarization of less than 10 dB.

3.3. Mutual Information

Two sets of Tx-Rx antennas are compared in this section, namely, the bidirectional dual-polarized antennas and the dipole array antennas at both the Tx and Rx ends. Uncorrelated paths were obtained from the eigenvalues of the SVD approach. Usually, the MIMO channel mutual information reported by most of the existing studies was investigated under a constant received power condition [1, 6, 17]. However, in order to evaluate the effect of antenna gain on mutual information, power allocation was not used in this calculation. Power in each channel and noise power were calculated from the transmitted power levels and the noise floor of the receiver according to IEEE Std 802.11a [21]. For the 5.15 to 5.25 GHz band, the total maximum output power was equal to 40 mW. Since each transmitter transmitted an independent data stream of power, we have power in each channel equals 20 mW or 13 dBm. According to IEEE Std 802.11a, the noise figure of the receiver was equal to 10 dB, noise power was equal to -91 dBm over the 20 MHz bandwidth. Finally, by using power in each channel, noise power and eigenvalues, mutual information was obtained. From the value of above power in each channel and noise power, the calculated Signal to Noise Ratio (SNR) was 104 dB which was rather high from the SNR used in an optimal power allocation system. However, these power in each channel and noise power are actually used in WLAN IEEE 802.11a. In the calculation of mutual information of the bidirectional dual-polarized antenna and the dipole array antennas, the same values of power in each channel and noise power were used.

Table 2. Comparison of 10% outage mutual information (b/s/Hz) of the antennas.

Rx	Mutual information [b/s/Hz]	
	Bidirectional Antenna	Dipole Array Antennas
Rx1	30.2	18.0
Rx2	31.2	18.3
Rx3	32.1	18.7
Rx4	36.0	19.2

The mutual information of the bidirectional dual-polarized antenna and the dipole array antennas at 10% outage probability and at all measurement points are shown in Table 2. At Rx1, the bidirectional dual-polarized antenna provided higher mutual information than the dipole array antennas did due to the corresponding radiation pattern with the angular power spectrums. In addition, there was the depolarization of the vertical polarization at Rx1 where the transmitted vertical polarization signals turned into a horizontal polarization in this corridor environment. Hence, the receiving vertical polarization dipole array antennas received cross polarization. At other Rx positions (Rx2, Rx3 and Rx4) the mutual information from the dual-polarized antenna was higher than that from the dipole array antennas since the average angular spread at these Rx positions was very small. The performance of spatially-spaced MIMO systems degrade when their incoming signal angular spread is small such as in a line-of-sight environment [22, 23]. Mutual information increases as the distance between the transmitter and the receiver decreases due to stronger received signal as the receiver approaches the transmitter. It should be pointed out that bidirectional dual-polarized antenna is suitable for a corridor environment where the angular spread is small and depolarization exists.

4. CONCLUSION

This paper presents the results of double directional channel measurements in a corridor environment by channel sounder. Channel properties, especially polarization, in a corridor are determined from *XPRC*, *XPRS*, angular spread and angular power spectrum. The obtained channel multipath parameters, i.e., DoA, DoD, TDoA and polarimetric path weight are calculated with antenna directivity to produce MIMO channel model of arbitrary antenna. Then, mutual information of arbitrary antenna in a corridor environment can be investigated. It can be observed that the reflection along the corridor established the small spread of the incoming signal. Measurement results exhibit the bidirectional shape of the received angular power spectrum. It was found that depolarization of both vertical and horizontal polarizations should be concerned in installing the antenna in the corridor. For instance, traditional dipole antenna may be installed with tilt angle to achieve good communication performance when distance between Tx and Rx is in excess of 20 m. A dual polarized antenna is a good candidate to resolve depolarization of vertical polarization in the corridor environment. Furthermore, the bidirectional antenna is suitable for the bidirectional angular power

spectrum in the corridor environment. It was illustrated that the bidirectional dual-polarized antenna provides 66.67% higher mutual information than the dipole array antennas over the same SNR value. It is noted that this result is for 2×2 array antenna; however, the result maybe different for larger array. This increased mutual information enhances data rate in high-speed modern wireless communications.

ACKNOWLEDGMENT

The authors would like to thank Dr. I. Ida of Fujitsu Ltd., Japan for his assistance and also thank members of Takada Laboratory, Tokyo Institute of Technology, Japan for their supports in channel measurement. The work of P. Keowsawat was supported by the Thailand Research Fund (TRF) through the Royal Golden Jubilee Ph.D. Program under Grant No. PHD/0067/2546. The work of M. Krairiksh was supported by the TRF through the Senior Research Scholar Program under Grant No. RTA 5180002.

REFERENCES

1. Foschini, G. J. and M. J. Gans, "On limits of wireless communications in a fading environment when using multiple antennas," *Wireless Pers. Commun.*, Vol. 6, No. 3, 311–335, Mar. 1998.
2. Teletar, I. E., "Capacity of multi-antenna Gaussian channels," *Eur. Trans. Telecommun.*, Vol. 10, No. 6, 585–595, Nov./Dec. 1999.
3. Roozbahani, M. G., E. Jedari, and A. A. Shishegar, "A new link-level simulation procedure of wideband MIMO radio channel for performance evaluation of indoor WLANs," *Progress In Eletromagnetics Research*, PIER 83, 13–24, 2008.
4. Noori, N. and H. Oraizi, "Evaluation of mimo channel capacity in indoor environment using vector parabolic equation method," *Progress In Electromagnetics Research B*, Vol. 4, 13–25, 2008.
5. Chou, H.-T., H.-C. Cheng, H.-T. Hsu, and L. R. Kuo, "Investigations of isolation improvement techniques for multiple input multiple output (MIMO) WLAN portable terminal applications," *Progress In Electromagnetics Research*, PIER 85, 349–366, 2008.
6. Kyritsi, P., D. C. Cox, R. A. Valenzuela, and P. W. Wolniansky, "Effect of antenna polarization on the capacity of a multiple

element system in an indoor environment," *IEEE J. Sel. Areas Commun.*, Vol. 20, No. 6, 1227–1239, Aug. 2002.

7. Sulonen, K., P. Suvikunnas, L. Yuokko, J. Kivinen, and P. Vaunikainen, "Comparison of MIMO antenna configurations in picocell and microcell environments," *IEEE J. Sel. Areas Commun.*, Vol. 21, No. 5, 703–712, Jun. 2003.
8. Burr, A., "Evaluation of capacity of indoor wireless MIMO channel using ray tracing," *Proc. 2002 Int. Zurich Seminar on Broadband Communications Access-Transmission-Networking*, 28-1–28-6, 2002.
9. Elnaggar, M. S., S. Safavi-Naeini, and S. K. Chaudhuri, "Simulation of the achievable indoor MIMO capacity by using an adaptive phased-array," *Proc. 2004 Radio and Wireless Conf.*, 155–158, 2004.
10. Steinbauer, M., A. F. Molisch, and E. Bonek, "The double directional radio channel," *IEEE Antennas Propag. Mag.*, Vol. 43, No. 4, 51–63, Aug. 2001.
11. Medbo, J., "Channel model parameters for the office environment," COST 273 TD(05)050, Bologna, Italy, Jan.:2005.
12. Taga, T., "Analysis for mean effective gain of mobile antennas," *IEEE Trans. Veh. Technol.*, Vol. 39, No. 2, 117–131, 1999.
13. Landmann, M., K. Sivasondhivat, J. Takada, I. Ida, and R. Thoma, "Polarization behavior of discrete multipath and diffuse scattering in urban environments at 4.5 GHz," *EURASIP Journal on Wireless Communications and Networking*, Vol. 2007, 1–16, 2007.
14. Molisch, A. F., M. Steinbauer, M. Toeltsch, E. Bonek, and R. S. Thomä, "Capacity of MIMO systems based on measured wireless channels," *IEEE J. Sel. Areas Commun.*, Vol. 20, No. 3, 561–569, Apr. 2002.
15. http://www.channelsounder.de, accessed Apr. 2009.
16. Thomä, R. S., M. Landman, and A. Richter, "RIMAX — A maximum likelihood framework channel parameter estimation in multidimensional channel sounding," *Proc. 2004 Int. Symp. on Antennas and Propag.*, 53–56, 2004.
17. Andersen, J. B., "Array gain and capacity for known random channels with multiple element arrays at both ends," *IEEE J. Sel. Areas Commun.*, Vol. 18, No. 11, 2172–2178, Nov. 2000.
18. Shannon, C. E., "A mathematical theory of communication," *Bell Syst. Tech. J.*, Vol. 27, 379–423, 623–656, Oct. 1948.
19. Keowsawat, P., C. Phongcharoenpanich, S. Kosulvit, and

M. Krairiksh, "Analysis and design of a two-probe excited circular ring antenna for MIMO application," *International Journal of Electronics*, submitted.

20. Kosulvit, S., M. Krairiksh, C. Phongcharoenpanich, and T. Wakabayashi, "Simple and cost-effective bidirectional antenna using a probe excited circular ring," *IEICE Trans. Electron.*, Vol. E84-C, No. 4, 443–450, Apr. 2001.
21. IEEE Std 802.11a-1999, *Part11: Wireless LAN Medium Access Control (MAC) and Physical Layer (PHY) Specifications*, 1999.
22. Haykin, S. and M. Moher, *Modern Wireless Communications*, Pearson Prentice Hall, Upper Saddle River, NJ, 2005.
23. Kermoal, J. P., P. E. Mogensen, S. H. Jensen, J. B. Andersen, F. Frederiksen, T. B. Sørensen, and K. I. Pedersen, "Experimental investigation of multipath richness for multi-element transmit and receive antenna arrays," *Proc. IEEE 51th Veh. Technol. Conf.*, 2004–2008, 2000.

2004 IEEE Antennas and Propogation Society International Symposium

IEEE

Volume 3

2004 Digest

June 20-25, 2004

Monterey, California

Characteristics of Polarization Diversity Bi-directional Antenna in Expressway Environment

Panisa Keowsawat[1], Komsak Meksamoot[2], Chuwong Phongcharoenpanich[1], Sompol Kosulvit[1] and Monai Krairiksh[1]

[1]Faculty of Engineering and Research Center for Communications and Information Technology, King Mongkut's Institute of Technology Ladkrabang, Bangkok 10520, Thailand.
Phone: (662) 7373000 Ext. 3327 Fax: (662) 7392429 E-mail: s5160310@kmitl.ac.th

[2]R&D Department, Antennas Division, Alan Dick(Thailand) Co., Ltd., Nakhon Pathom, Thailand

1. Introduction

In the longitudinal service areas of wireless communications where the height of the antennas at the cell station are not much higher than the mobile users (such as on the street, in the tunnel, on the expressway or in the corridor of the building), the bi-directional antenna is usually used [1]. Moreover, the multi-path fading that reduces the performance of wireless communication is inevitable. The way to mitigate this fading problem is to use the antenna diversity at the cell station for the uplink reception [1]. This paper introduced a simple and cost-effective bi-directional polarization diversity antenna which is used as cell station antenna in the expressway. The proposed antenna, which is adopted from [2], consists of a two-perpendicular-probe excited circular ring and is called Polarization Diversity Bi-directional Antenna (PDBA) hereafter. The antenna characteristics such as gain pattern and impedance characteristics are simulated by NEC-2 [3] based on the Method of Moments (MoM) and are compared with the experimental results. The isolation result between two ports of the PDBA is also determined. The angular power density function for the antenna that is particularly used in the expressway is also proposed. Subsequently, the diversity characteristics of the PDBA, mean effective gain (MEG) [4], correlation coefficient (ρ_e), diversity gain (G_{div}) and DAG on Selection Combining (SC) and Maximum Ratio Combining (MRC), are calculated.

2. Antenna Configuration and Modeling

The PDBA structure is composed of a circular ring of the radius a excited by two-perpendicular linear electric probes of the same length l aligned in $+x$-axis and $-y$-axis as shown in Fig. 1(a). When the PDBA is installed beside the expressway, the direction of beams are along the $+x$-axis and $-x$-axis. For vertical polarization reception, the probe on $+z$-axis is active (branch 1) whereas the probe on $-y$-axis is terminated circuit. ("terminated circuit" is just "terminated", hereafter.) Also, for horizontal polarization reception, the probe on $-y$-axis is active (branch 2) whereas the probe on $+z$-axis is terminated. The ring length is equal to d with two circular apertures in $x=d/2$ and $x=-d/2$ planes. The PDBA is modeled by conductive wire-grid structure which are loaded with conductivity 2.56×10^7 S/m (Brass) as shown in Fig.1(b). The selection of wire radius is based on the equivalent surface area assumption [3]. The wires are divided into small segments about 0.01λ to 0.03λ in length that is efficiently small to achieve reliable impedance characteristics as well as radiation patterns [3]. The excitation at probes is modeled by delta-gap voltage source between the probe base and the ring strip. At each probe base, two diagonal wires are added to support the high current density from the excitation. To confirm the validity of the proposed antenna design method and the PDBA usefulness, the PDBA is fabricated at 1.9 GHz band. The dimension of the PDBA at 1.9 GHz has ring radius $a = 0.32\lambda$ (5.10 cm), ring length $d = 0.15\lambda$ (2.40 cm) and a feed probe $l = 0.25\lambda$ (3.95 cm) [2], [5]. The prototype of the PDBA is shown in Fig.1(c) where branch 2 is used and branch 1 is terminated.

Financial support from the Thailand Research Fund through the Royal Golden Jubilee Ph.D. Program (Grant No. PHD/0067/2546) to P. Keowsawat and M. Krairiksh is acknowledged.

0-7803-8302-8/04/$20.00 ©2004 IEEE

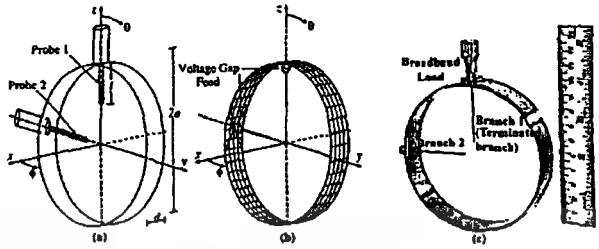

Fig.1 Configuration of PDBA (a) real model (b) wire-grid model (c) prototype antenna

3. Antenna Characteristics

The comparison between theoretical and experimental component gain patterns (G_θ and G_ϕ) in *xy*-plane of each branch is illustrated in Fig. 2. The good agreement of the theoretical and experimental bi-directional patterns can confirm the accuracy of the simulation. The SWR is also measured and found that the resonant frequency of the PDBA is at 1.9 GHz which coincides with the simulation. The experimental bandwidth of the PDBA with SWR less than 2.0 is 420 MHz. The isolation between two branches of the PDBA is better than 12 dB that is rather low. However the isolation can be improved by varying the angle between two probes at the expense of the higher SWR.

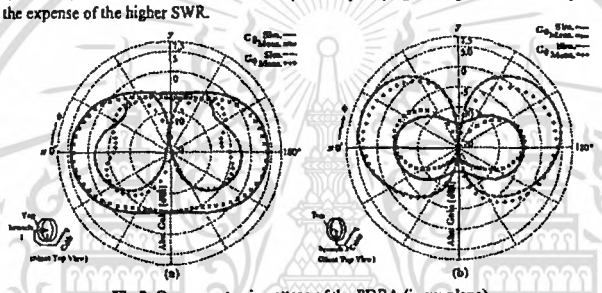

Fig.2. Component gain pattern of the PDBA (in xy-plane)
(a) branch 1 (vertical) is active and branch 2 is terminated
(b) branch 2 (horizontal) is active and branch 1 is terminated

4. Diversity Characteristics

The new angular power density function for the expressway environment is proposed in this paper. We assume that P_θ (vertical polarization) and P_ϕ (horizontal polarization) are identical in the expressway environment. The incident waves at the base station can be assumed to come from only at the elevation plane which $\theta = 90^\circ$ (measure from +z-axis) because the slightly different height between base station antenna and mobile users [6]. Therefore the only azimuth angle (ϕ) can be used to describe the angular power density function [6]. In order to obtain the angular power density function, the model of the expressway is illustrated in Fig. 3(a) and Fig. 3(b). The width and the length of the expressway are w_e and $2d$, respectively. The antenna is installed beside the expressway as shown in Fig. 3(a). In this model, the distribution of the users along the expressway is assumed to be uniform. From Fig. 3(a), it can be seen that the expressway area can be divided into two symmetrical quadrants of the dimension $w_e \times d$.

Thus, only one quadrant noted by no.1 is considered as illustrated in Fig. 3(b). This rectangular area will be subdivided into N small triangles by the azimuth angle (ϕ) as shown in the black region in Fig. 3(b). The azimuth angle of the diagonal of the expressway is ϕ_e. The angular power density function of each azimuth angle can be realized by the numerical values of the area covered by that azimuth angle ϕ_i and its previous azimuth angle ϕ_{i-1}. The resultant expression of the angular power density function after some mathematical manipulations can be expressed as

$$P_{\theta,\phi}(\phi)=\begin{cases}\dfrac{1}{2}Ad^2\left(\tan\phi_i-\tan\phi_{i-1}\right), & 0<\phi_i\le\phi_e,\ \phi_0=0\\ \dfrac{1}{2}Aw_e^2\left(\cot\phi_i-\cot\phi_{i-1}\right), & \phi_e<\phi_i\le\dfrac{\pi}{2}\end{cases} \tag{1}$$

The angle ϕ_e can be calculated using the geometry in Fig. 3(b) and it can be written by $\phi_e=\arctan w_e/d$. The constant A can be determined from the condition of $\sum_{\phi=0}^{\pi/2}P_{\theta,\phi}(\phi)=1/2$.

The angular power density function of the other quadrant can be derived by the same procedure as in quadrant no. 1. To cover the area of the outdoor cell, the practical parameters will be used in the model. The overall parameters for the model in Fig. 3(b) are $w_e=25$ m, $d=250$ m, $N=90$ and $\phi_e=5.71^\circ$. The normalized angular power density function is shown in Fig. 3(c). This resultant angular power density function will be used to calculate the MEG and envelope correlation coefficient.

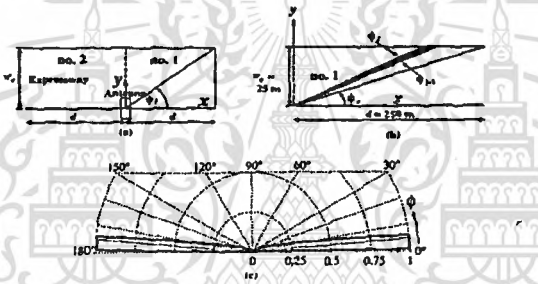

Fig.3 Angular power density function on the expressway

The MEG (G_e) which can be calculated from gain patterns, angular power density function and cross-polarization power ratio (XPR) that is equal to 0 dB is expressed in [4]. In Table 1, the MEG of branch 1 and branch 2 of PDBA are 1.18 and 2.05, recpectively. The antenna that has higher MEG means its gain pattern is better fits to the angular power density function than the other. The envelope correlation coefficient (ρ_e) of two-branch diversity is given in [7]. For the base station antenna, the ρ_e lower than 0.7 is allowed [8]. ρ_e can be calculated from complex radiation patterns that are the results from NEC-2, angular power density function and XPR (0 dB). In Table 1, ρ_e of the PDBA equals 0.06. The diversity gain (G_{div}) is defined as the difference of the average CNR at a certain value of the bit-error rate (BER) (usually at 10^{-3}). The average BER of the two-branch diversity antenna for $\pi/4$ shifted Quadrature Phase Shift Keying (QPSK) modulation in Additive White Gaussian Noise (AWGN) for SC and MRC is expressed in [9]. The diversity gains of the PDBA in Fig.3 are

equal to 9.85 and 9.30 dB for SC and MRC, respectively. The DAG of the antenna is the most effective parameter to evaluate the performance. It is defined as a product of MEG and diversity gain of a diversity antenna in [9]. In Table 1, DAG of the PDBA are equal to 11.90 and 11.35 for SC and MRC, respectively.

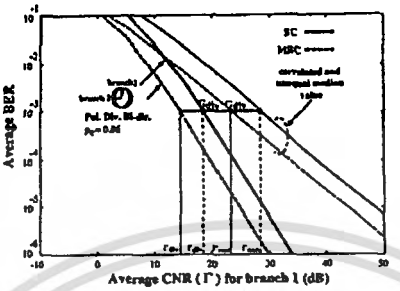

Fig.4 Diversity gain of the PDBA

Table 1 Diversity parameters of PDBA

Antenna		MEG (dBi)	ρ_e	G_{div} (dB)		DAG (dB)	
				SC	MRC	SC	MRC
PDBA	1	1.18	0.06	9.85	9.30	11.90	11.35
branch	2	2.05					

5. Conclusion

The polarization diversity bi-directional antenna is proposed to be used as the cell station antenna in the expressway environment. The gain patterns are simulated by wire-grid modeling. The experimental radiation pattern and SWR agree reasonably with the simulated results which validates the accuracy of the wire-grid modeling. The bi-directional pattern and good diversity performance of this proposed antenna ensure that this antenna is a promising candidate for the cell station antennas in the expressway environment.

Reference

[1] H. Arai and K. Cho, "Cellular and PHS base station antenna systems," *IEICE Trans. Commun.*, vol.E86-B, no.3, pp.980-992, March 2003.

[2] S. Kosulvit, M. Krairiksh, C. Phongcharoenpanich and T. Wakabayashi, "A simple and cost-effective bidirectional antenna using a probe excited circular ring," *IEICE Trans. Electron.*, vol.E84-C, no.4, pp.443-450, Apr. 2001.

[3] G.J. Burke and A.J. Poggio, *Numerical Electromagnetics Code (NEC)—Method of Moments, Parts I-III*, Lawrence Livermore Nat. Lab., Livermore, CA, 1981.

[4] T. Taga, "Analysis for mean effective gain of mobile antennas in land mobile radio environments," *IEEE Trans. Veh. Technol.*, vol.39, no.2, pp.117-131, May 1990.

[5] P. Keowsawai, A bi-directional antenna using two-perpendicular-probe excited ring for polarization diversity, Master Thesis, Faculty of Engineering, King Mongkut's Institute of Technology Ladkrabang, Thailand, 2001 (in Thai).

[6] J.C. Liberti and T.S. Rappaport, "A geometrically based model for line-of-sight multipath radio channels," *Proc. 46th IEEE Veh. Technol. Conf.*, vol.1, pp.844-848, Apr. 1996.

[7] K. Ogawa and J. Takada, "An analysis of the effective performance of a handset diversity antenna influenced by head, hand and shoulder effects-A proposal for the diversity antenna gain based on a signal bit-error rate and the analytical results for the PDC system," *IEICE Trans.*, vol.J83-B, no.6, pp.852-865, June 2000.

[8] W.C.Y. Lee, *Mobile Communications Engineering*, 2nd ed., pp.572-573, McGraw-Hill Book Company, Singapore, 1998.

[9] K. Ogawa and J. Takada, "An analysis of the diversity antenna gain of handset diversity antenna close to the human operator," *Proc. 2000 Int. Sym. Antennas and Propagat.*, pp.1059-1062, 2000.

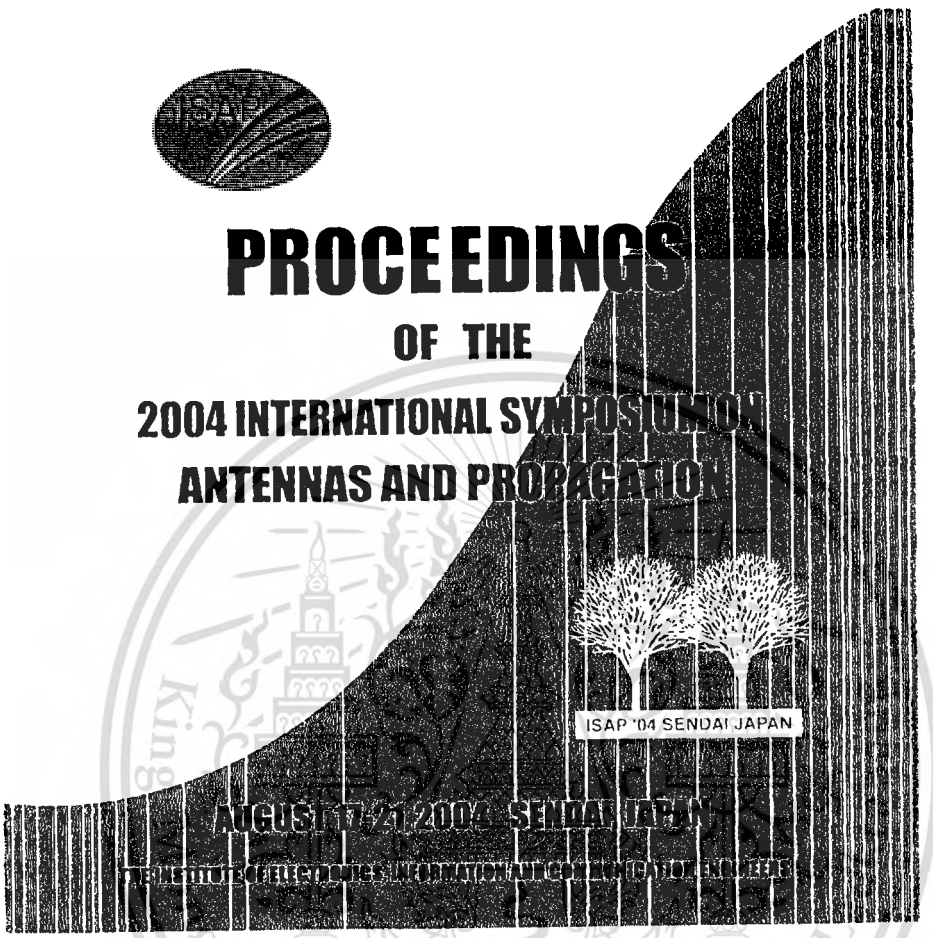

4D3-4

DESIGN OF A POLARIZATION DIVERSITY BI-DIRECIONAL ANTENNA USING TWO-PROBE EXCITED CIRCULAR RING FOR 5 GHZ WLAN

Panisa KEOWSAWAT, Chuwong PHONGCHAROENPANICH, Sompol KOSULVIT and Monai KRAIRIKSH
Faculty of Engineering and Research Center for Communications and Information Technology, King Mongkut's Institute of Technology Ladkrabang, Bangkok 10520, Thailand.
E-mail: s5160310@kmitl.ac.th

1. Introduction

In the indoor propagation channel which transmitter and receiver are surrounded by the various objects, the multipath signal can be received at the receiving antenna and the receiver. One possible way to mitigate multipath fading is to implement a diversity combining technique [1]. The horizontal space diversity is traditionally used to reduce the fading problems at the base station. In recent years, the polarization diversity is one of the most promising techniques to reduce multipath with compact antenna configuration requiring only one antenna location [2]. In cases where the radio unit will be applied in the long and narrow areas, such as in the corridor or long rows of objects, a uni- or bi-directional antenna may provide better coverage area than a conventional omni-directional antenna. There are a number of research works dealing with uni- and bi-directional antenna proposed for polarization diversity [3]. Nevertheless, the dual polarization can be achieved at the expense of complicated configuration with an expensive material. In this paper, to mitigate effectively the multipath influence to the indoor communications, we proposed the simple and cost-effective polarization diversity with bi-directional antenna using a circular ring with two probes. Since the antenna is used under the multipath environment, the radiation patterns have no direct meaning of the antenna performance [4]. Then, the diversity characteristics of the antenna are necessarily investigated. In this paper, the critical issues in the design for 5 GHz are determined, and both simulated and experimental results are presented.

2. Antenna Configuration and Design

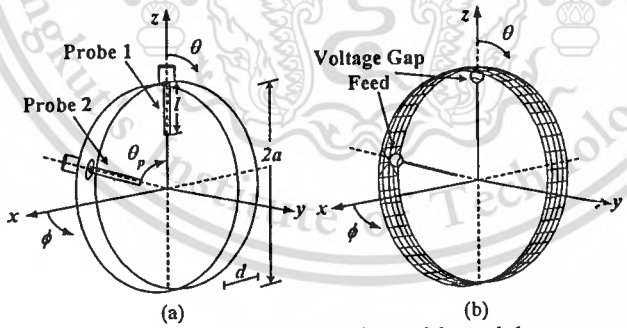

Fig.1 Configuration of the antenna (a) real model (b) wire-grid model

Figure 1(a) shows the structure of the presented polarization diversity bi-directional antenna [5]. The antenna consists of a circular ring of the radius a excited by two linear electric probes of the same length l which the angle between two-probe is θ_p. The ring width is equal to d with two circular apertures in $x = d/2$ and $x = -d/2$ planes. The probe 1 will be active while probe 2 is terminated with 50 Ω load resulting in vertical polarization, and vice versa resulting in horizontal polarization. The direction of beams of the antenna are along $+x$-axis and $-x$-axis for both polarizations. The optimization for design is carried out through the simulations using the Numerical Electromagnetics Code 2 [6] based on Method of Moment (MoM) by changing the dimension of radius a, width of ring d and length of probe l. The conductivity of the wire-grid antenna structure is 2.56×10^7 S/m as Brass. The selection of the wire radius is based on the equivalent surface area assumption [7]. The wires are

ISBN: 4-88552-207-2 C3055©IEICE

divided into small segments about 0.01λ to 0.03λ in length that is efficiently small to achieve reliable impedance characteristics as well as radiation patterns [6]. The excitation at probes is modeled by delta-gap voltage source between the probe base and the ring strip. At each probe base, two diagonal wires are added to support the high current density from the excitation as shown in Fig. 1(b). The design resonant frequency is chosen as 5.25 GHz for wireless LAN. The variation in gain and return loss (S_{11}) with a and d are plotted in Fig. 2(a) and (b), respectively. In this case, the probe length is fixed and θ_p is 90°. The gain of branch 1 and 2 at $\phi = 0°$ and 180° is considered. The antenna that has the highest gain with $S_{11} \leq$ -14 dB (SWR $\leq$ 1.5:1) is selected. As a result, the optimum parameters were finally selected as $a = 0.32\lambda$ (1.83 cm), $d = 0.27\lambda$ (1.54 cm) and $l = 0.23\lambda$ (1.31 cm). The isolation (S_{21}) can be considered in term of θ_p. The maximum S_{21} (14.32 dB) is obtained when the angle between two probes is 120° with sacrificed gain and S_{11} as shown in Fig 3.

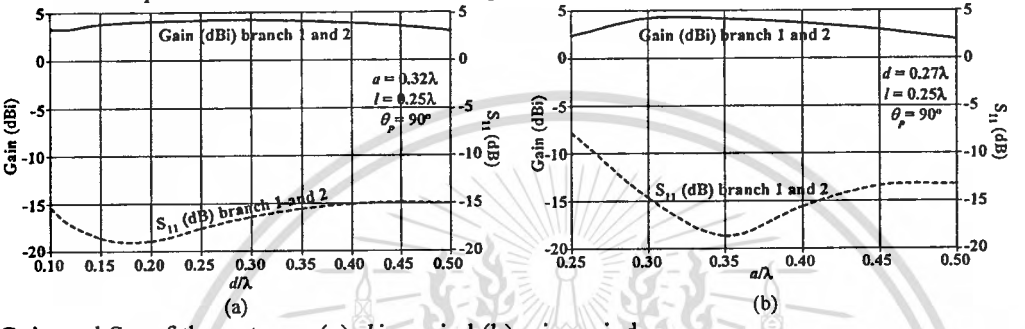

Fig. 2 Gain and S_{11} of the antenna (a) d is varied (b) a is varied

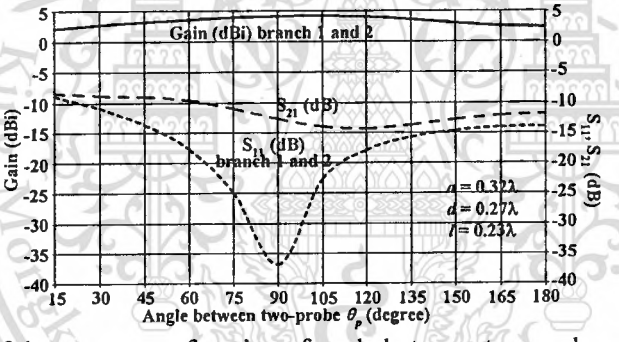

Fig.3 Gain, S_{11} and S_{21} of the antenna as function of angle between two probes

The variation of the angle between two-probe not only influences to the gain, S_{11} and S_{21} but also to the diversity performance of the antenna as shown in Fig. 4(a) – (d). In Fig. 4(a), The Mean Effective Gain (MEG) that can be expressed in [4] of the antenna in the indoor picocell angular power density function which the portion of line-of-sight is significant on the order of 40 % follow the measurement performed by Kalliola [8] is illustrated. The maximum MEG of branch 1 (G_{e1}) is 0.17 dBi when the angle between two probes is 105° while the minimum G_{e1} is -7.95 dBi when the angle between two probes is 180°. The maximum MEG of branch 2 (G_{e2}) is -5.45 dBi when the angle between two probes is 60° while the minimum G_{e2} is -7.95 dBi when the angle between two probes is 180°. The G_{e2} are changed over narrow interval of -5 to -7 dBi because the position of branch 2 is fixed while the position of branch 1 is altered in the simulation. This condition causes the various results of G_{e1} (removable probe) while the results of G_{e2} are almost uniform (fixed probe). The envelope correlation coefficient (ρ_e) [9] result is changed as shown in Fig. 4(b). The maximum result is 0.53 when the angle between two probes is 45°. The minimum result is 0.03 when the angle between two probes is 135°. The ρ_e are lower than 0.7 for any angles between two probes which the uncorrelated signal between two branches is obtained [10]. In Fig. 4(c) the diversity gain (G_{div}) [11] of the antenna for Binary Phase Shift Keying (BPSK) modulation on Maximum Ratio Combining (MRC) technique [12] is shown. The maximum result is 8.72 dB when the angle between two probes is 180° because the ratio of the MEG for each branch (r) is equal to 1. The minimum G_{div} of the antenna is 6.1 dB when

the angle between two probes is 60° and 75°. The G_{div} result is not a sufficient parameter for determining the performance of the antenna. Then we use these G_{div} to calculate the effective parameter i.e., Diversity Antenna Gain (DAG) [11]. The maximum DAG is 6.61 dB when the angle between two probes is 120°. Furthermore from the above result, when the angle between two probes is 120°, the antenna yields the best isolation. The minimum DAG is 0.77 dB when the angle between two probes is 180°. Although the antenna that has the angle of 180° between two probes provides the maximum G_{div}, its DAG is the lowest result. When the angle between two probes is 90°, the DAG of the antenna is 6.15 dB which is 0.46 dB lower than the highest DAG.

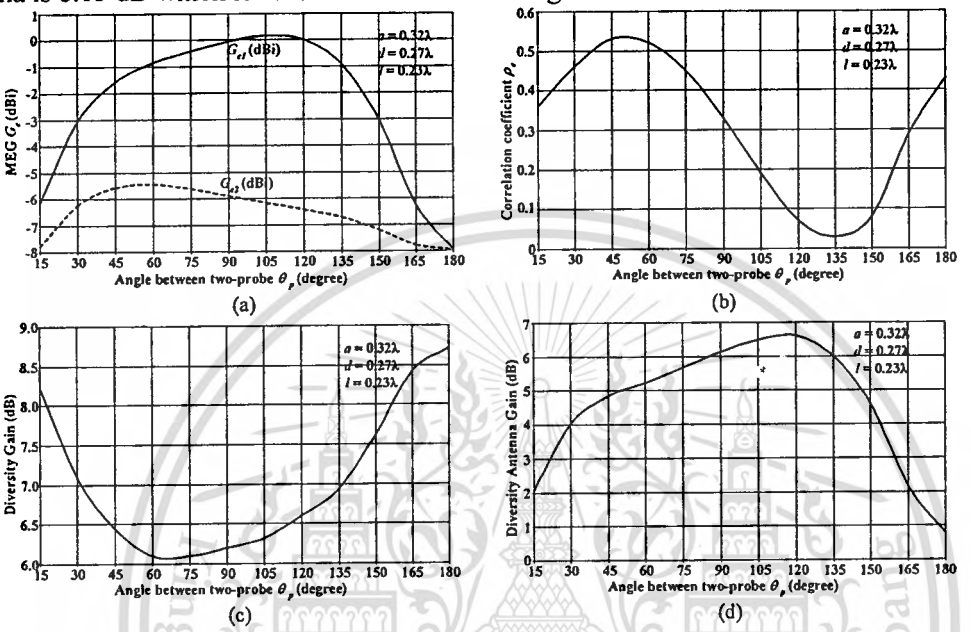

Fig. 4 Diversity performance of the antenna as function of angle between two probes (a) MEG (b) ρ_e (c) G_{div} (d) DAG

3. Simulation and Experimental Results

The prototype antenna is fabricated for validation. In Fig. 5, the simulation and experimental S_{11} and S_{21} of the antenna that has the angle of 120° between two probes are illustrated. The measured S_{11} of branch 1 and 2 at the design frequency is around -19 dB while S_{21} is approximately -13 dB. The -14 dB S_{11} bandwidth is 400 MHz (7.6%) at the center frequency of 5.25 GHz. The discrepancy which may be due to the error of fabrication can be found. The error of the fabrication can be avoided by using a superior process. The difference of the measured and the simulated S_{21} results is about 1 dB, however the graph is in the same trend. The S_{21} results are not high because the antenna has two probes in the same ring. Fig. 6 shows the *xy*-plane radiation pattern at 5.25 GHz when the angle between two probes is 120°. The result shows the bi-directional pattern of the experimental and simulation G_θ (vertical polarization), and G_ϕ (horizontal polarization) in *x*-direction for each branch of the antenna. When branch 1 is used, the major component is G_θ and vice versa when branch 2 is used. The radiation patterns are measured by using a linearly polarized monopole antenna in an anechoic chamber. The good agreement is found between simulated and measured results. The gain of branch 1 and 2 at $\phi = 0°$ and 180° are approximately 4 dBi for both the simulated and measured results.

4. Conclusion

This paper presents the design of a polarization diversity bi-directional antenna using two-probe excited circular ring. Both simulated and measured results are mentioned. The gain and return loss of the antenna are investigated when the radius (a) and the width (d) of the circular ring are varied. The dimension of $a = 0.32\lambda$ (1.83 cm), $d = 0.27\lambda$ (1.54 cm) and $l = 0.23\lambda$ (1.31 cm) gives the maximum gain with return loss ≤ -14 dB. The isolation of the antenna can be improved by changing the angle between two probes. The maximum isolation and DAG is obtained when the antenna has the angle of

120° between two probes. The antenna possesses a gain of 4 dBi with the 400 MHz bandwidth at the center frequency of 5.25 GHz. The simulated and measured radiation patterns of each branch are bi-directional pattern that are suitable for the long and narrow service area. The results of simulation and experiment almost agree with each other.

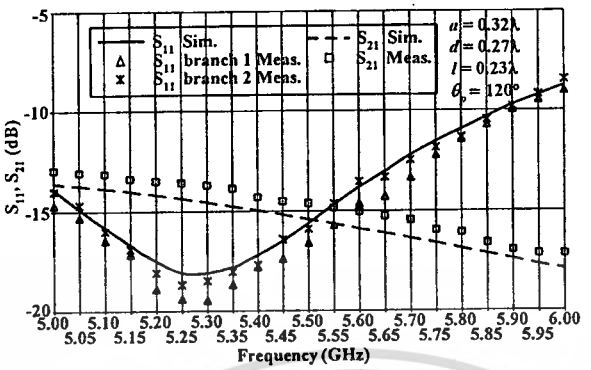

Fig. 5 S_{11} and S_{21} of the antenna that has the angle of 120° between two probes

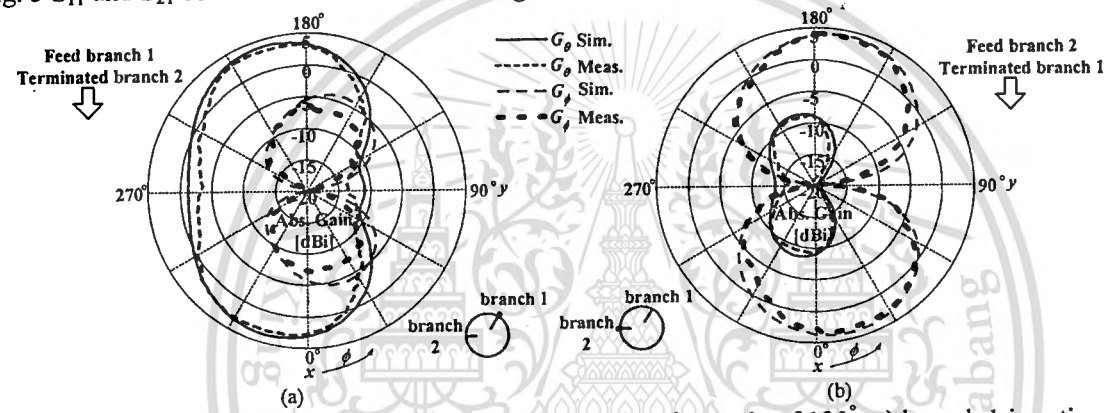

Fig. 6 The *xy*-plane radiation pattern of the antenna that has the angle of 120° (a) branch 1 is active and branch 2 is terminated (b) branch 2 is active and branch 1 is terminated

5. Acknowledgement

Financial support from the Thailand Research Fund through the Royal Golden Jubilee Ph.D. Program (Grant No. PHD/0067/2546) to P. Keowsawat and M. Krairiksh is acknowledged.

References

[1] K. Fujimoto and J.R. James, Mobile Antenna Systems Handbook, ch.2, Artech House, Norwood, MA, 1994.

[2] R.G. Vaughan, "Polarization diversity in mobile communications," IEEE Trans. Veh. Technol., vol.39, no.3, pp.177–186, Aug. 1990.

[3] S.H. Hong, Y.S. Lee, M.S. Choi and Y.J. Yoon, "Polarization diversity with directional antennas for indoor environments," Proc. 1999 Asia Pacific Microwave Conf., vol.3, pp. 785–788, 1999.

[4] T. Taga, "Analysis for mean effective gain of mobile antennas in land mobile radio environments," IEEE Trans. Veh. Technol. vol. 39, no. 2, pp.117–131, May 1990.

[5] P. Keowsawat, A Bi-directional Antenna Using Two-perpendicular-probe Excited Ring for Polarization Diversity, Master Thesis (in Thai), Faculty of Engineering, King Mongkut's Institute of Technology Ladkrabang, Thailand, 2001.

[6] G.J. Burke and A.J. Poggio, Numerical Electromagnetics Code (NEC) –Method of Moments, Parts I–III, Lawrence Livermore Nat. Lab., Livermore, CA, 1981.

[7] E.K. Miller, "PCs for AP and other EM reflections: Wire-grid approximations to solid surfaces," IEEE Antennas and Propagat. Mag., vol.39, no.1, pp.94–97, Feb. 1997.

[8] K. Kalliola, K. Sulonen, H. Laitinen., O. Kivekas, J. Krogerus and P. Vainikainen, "Angular power distribution and mean effective gain of mobile antenna in different propagation environments," IEEE Trans. Veh. Technol., vol.51, no.5, pp.823–838, Sept. 2002.

[9] R.H. Clarke, "A statistical theory of mobile-radio reception," Bell System Technical J., vol.47, no.6, pp.957–1000, July–Aug. 1968.

[10] W. C. Y. Lee, Mobile Communications Engineering. 2nd ed., McGraw-Hill, Singapore, 1998.

[11] K. Ogawa and J. Takada, "An analysis of the effective performance of a handset diversity antenna influenced by head, hand and shoulder effects–A proposal for the diversity antenna gain based on a signal bit-error rate and the analytical results for the PDC system," IEICE Trans. Commun., vol.J83-B, no.6, pp.852–865, June 2000.

[12] K. Ogawa and J. Takada, "An analysis of the diversity antenna gain of a handset diversity antenna close to the human operator," Proc. 2000 Int. Symp. on Antennas and Propagat., pp. 1059–21062, Fukuoka, Japan, Aug. 2000.